https://www.mdc-berlin.de/de/veroeffentlichungstypen/clinical-journal-club

Als gemeinsame Einrichtung von MDC und Charité fördert das Experimental and Clinical Research Center die Zusammenarbeit zwischen Grundlagenwissenschaftlern und klinischen Forschern. Hier werden neue Ansätze für Diagnose, Prävention und Therapie von Herz-Kreislauf- und Stoffwechselerkrankungen, Krebs sowie neurologischen Erkrankungen entwickelt und zeitnah am Patienten eingesetzt. Sie sind eingeladen, uns beizutreten. Bewerben Sie sich!

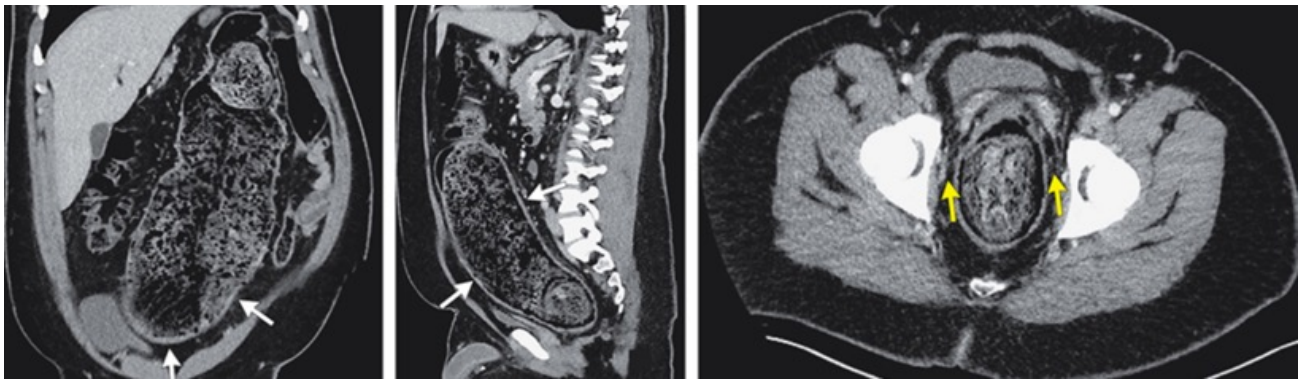

A 23-year-old man with autism spectrum disorder and chronic constipation presented to the emergency department with a 1-week history of abdominal pain on his left side, nausea, and vomiting. Physical examination was notable for abdominal distention and mild tenderness to palpation on the left side of the abdomen. Computed tomography of the abdomen and pelvis is shown. What is the most likely diagnosis?

Hirschsprung‘s disease

Simple fecal impaction

Stercoral colitis

Toxic megacolon

Ulcerative colitis

The CT scan revealed distention of the colon by a large stool burden, mural thickening, and perirectal fat stranding. A diagnosis of stercoral colitis was made. In stercoral colitis, chronically impacted feces distend the colon, resulting in inflammation. In some cases, the fecaloma may lead to focal-pressure necrosis or perforation. Treatment includes an aggressive bowel regimen and, in some cases, fecal disimpaction.

Stercoral-Kolitis ist eine seltene, lebensbedrohliche Entzündung des Dickdarms, die durch chronische Verstopfung und die Ansammlung von hartem Stuhl verursacht wird. Die Fäkalmasse führt zu erhöhtem Druck und Entzündungen, die Geschwüre, Ischämie (Minderdurchblutung), Perforation (Darmdurchbruch) und Sepsis (Blutvergiftung) auslösen können. Die Diagnose erfolgt meist mittels bildgebender Verfahren wie CT, und die Behandlung umfasst die Beseitigung der Verstopfung und die Behandlung der Grunderkrankung.

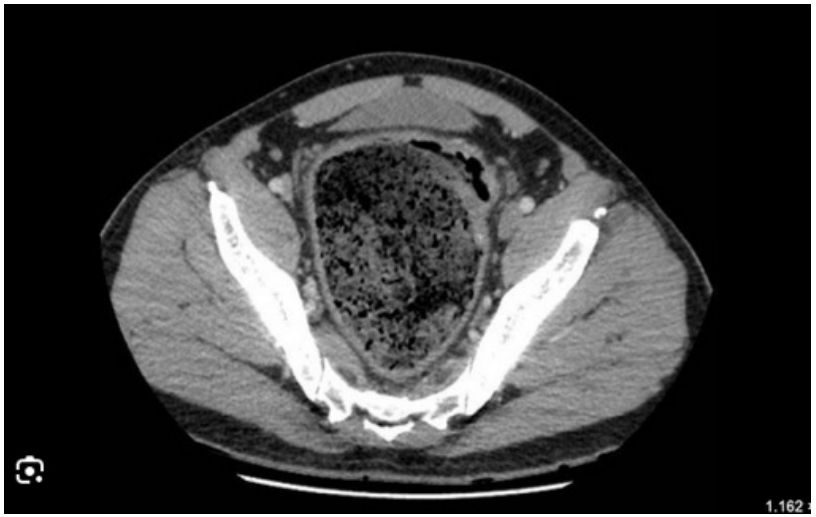

Stercoral Colitis

Occurs when chronic constipation leads to fecal impaction, increased intraluminal pressure, compression of the vasculature, and resultant bowel wall ischemia

Clinical
- Abdominal pain or distention
- Constipation
- Nausea and vomiting
- Generalized weakness and fatigue (symptoms may be vague)

Diagnosis
- CT scan of the abdomen and pelvis with IV contrast
  - Thickened bowel wall with fat stranding
  - Fecal impaction with colonic distention
  - Perforation and abscess formation can be seen

Management
- Manual disimpaction
- Enemas
- If perforated, IV antibiotics and surgical consultation

Aldosterone synthesis is a multi-step process that occurs in the zona glomerulosa of the adrenal glands, starting with cholesterol and proceeding through several intermediate steroid precursors using a series of enzymes, including aldosterone synthase (also known as CYP11B2). Key enzymes involved are 3-beta-hydroxysteroid dehydrogenase, 21-alpha-hydroxylase, and 11-beta-hydroxylase, which convert cholesterol into aldosterone. The rate of synthesis is primarily stimulated by Angiotensin II and to a lesser extent by high extracellular potassium and low sodium levels, while atrial natriuretic peptide inhibits it.

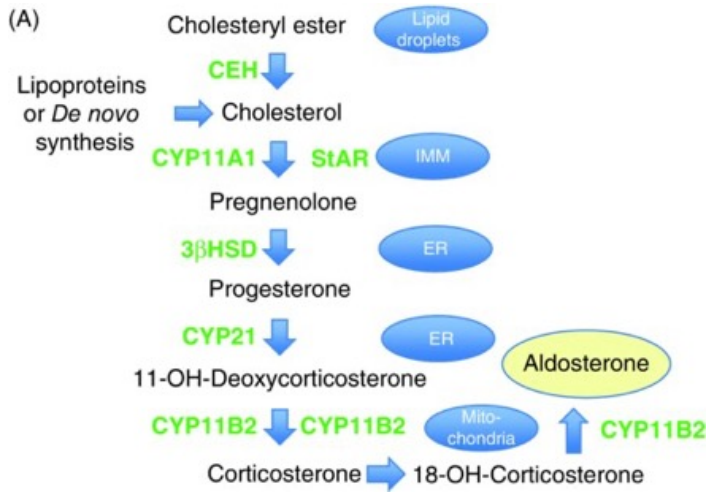

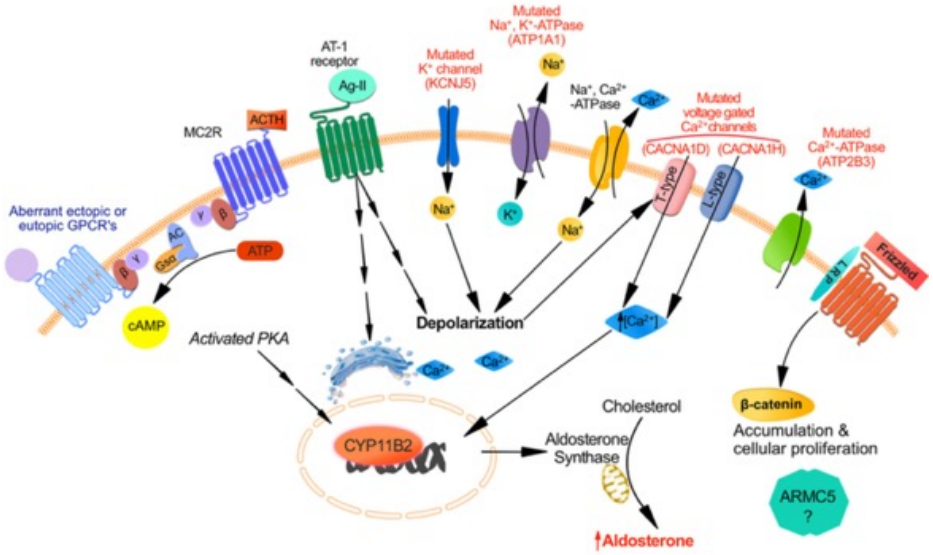

Baxdrostat senkt den Blutdruck, indem es die Aldosteron-Synthase (ein Enzym, das Aldosteron produziert) hemmt. Aldosteron ist ein Hormon, das den Blutdruck steigert, und durch die Blockade seiner Bildung in der Nebenniere wird der Blutdruck effektiv gesenkt, insbesondere bei Patienten mit therapieresistenter Hypertonie.

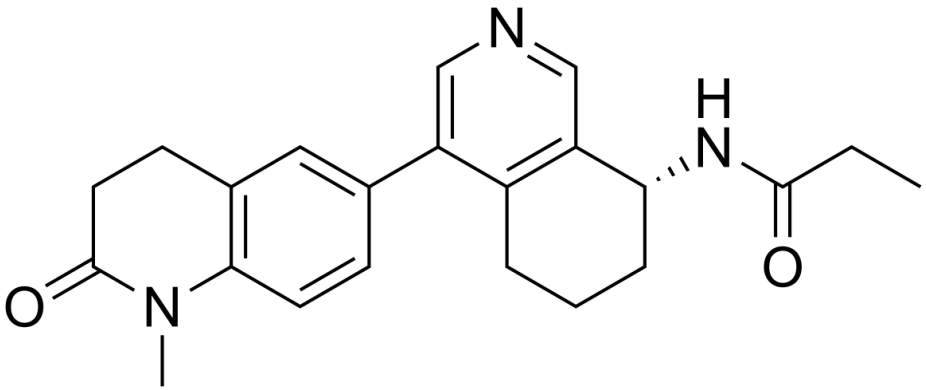

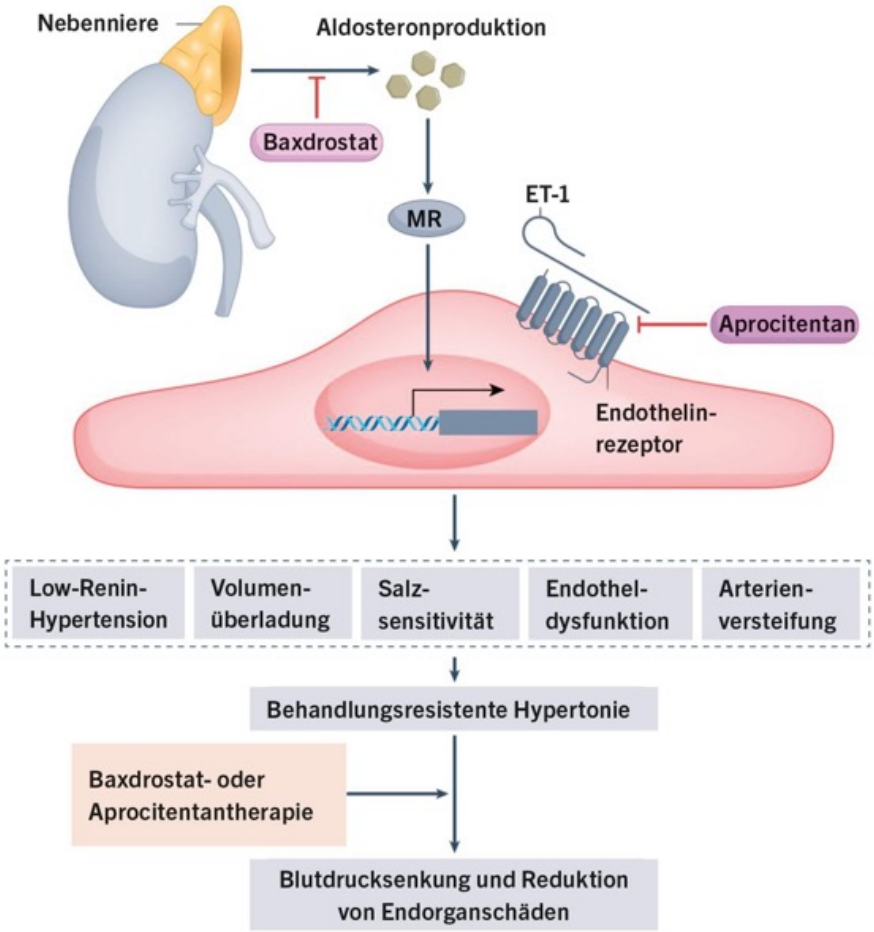

Efficacy and Safety of Baxdrostat in Uncontrolled and Resistant Hypertension

Aldosterone dysregulation plays an important pathogenic role in hard-to-control hypertension. In several studies, baxdrostat, an aldosterone synthase inhibitor, reduced the seated systolic blood pressure of patients with uncontrolled or resistant hypertension.

In this phase 3, multinational, double-blind, randomized, placebo-controlled trial, we recruited patients with a seated systolic blood pressure of between 140 mm Hg and less than 170 mm Hg despite the receipt of stable treatment with two antihypertensive medications (uncontrolled hypertension) or three or more such medications (resistant hypertension), including a diuretic. After a 2-week placebo run-in period, we randomly assigned patients with a seated systolic blood pressure of 135 mm Hg or more in a 1:1:1 ratio to receive baxdrostat at a dose of 1 mg, baxdrostat at a dose of 2 mg, or placebo once daily for 12 weeks. The primary end point was the change in seated systolic blood pressure from baseline to week 12.

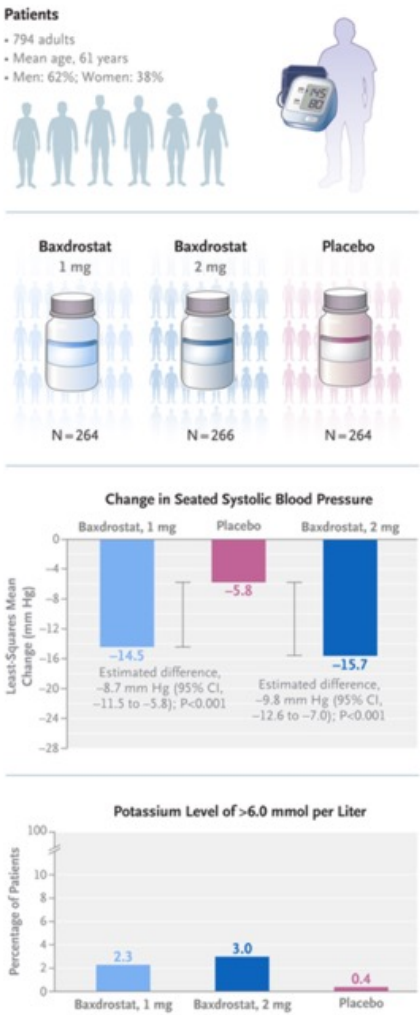

Inappropriately elevated aldosterone production relative to patient sodium status is a key driver of hard-to-control (uncontrolled or resistant) hypertension and hypertension-mediated organ damage. Mineralocorticoid receptor antagonists (MRAs) can block the mineralocorticoid receptor–mediated pathophysiological effects of aldosterone but are underused because of dose-dependent adverse effects. Moreover, MRAs induce dose-related counter-regulatory increases in renin and circulating aldosterone levels that may stimulate MR-independent effects of aldosterone.

Eligible Patients and Run-In Period

The trial enrolled men and women who were at least 18 years of age and who had hard-to-control hypertension, which was defined as a mean seated systolic blood pressure of 140 mm Hg to less than 170 mm Hg, as measured during an office visit, despite treatment with maximally tolerated doses of either two antihypertensive medications (for uncontrolled hypertension) or three or more such medications (for resistant hypertension), including a diuretic, for at least 4 weeks before screening.

End Points

The primary efficacy end point was the change in the seated systolic blood pressure from baseline to week 12, as assessed for each baxdrostat group as compared with placebo.

Demographic and Clinical Characteristics

Characteristic	Baxdrostat, 1 mg (N=264)	Baxdrostat, 2 mg (N=266)	Placebo (N=264)
Age — yr	59.8±11.8	61.8±11.7	61.9±11.6
Male sex — no. (%)	169 (64.0)	163 (61.3)	162 (61.4)
Race or ethnic group — no. (%)†			
White	165 (62.5)	168 (63.2)	167 (63.3)
Black	23 (8.7)	21 (7.9)	15 (5.7)
Asian	65 (24.6)	72 (27.1)	72 (27.3)
Other	10 (3.8)	2 (0.8)	8 (3.0)
Hispanic or Latino	27 (10.2)	39 (14.7)	38 (14.4)
Missing data	1 (0.4)	3 (1.1)	2 (0.8)
Seated blood pressure — mm Hg			
Systolic	149.7±10.1	149.1±9.1	149.0±8.7
Diastolic	88.0±10.5	85.8±10.5	85.8±10.5
Body-mass index‡	31.5±6.4	31.2±6.2	31.1±6.0
Estimated glomerular filtration rate — ml/min/1.73 m^2§	86.6±18.5	84.3±17.9	84.1±18.0
Diabetes — no. (%)	83 (31.4)	110 (41.4)	110 (41.7)
Serum sodium — mmol/liter			
Mean	139.9±2.6	139.8±2.5	139.6±2.5
Median (IQR)	140 (138–141)	140 (138–141)	140 (138–141)
Serum potassium — mmol/liter			
Mean	4.2±0.4	4.2±0.4	4.2±0.5
Median (IQR)	4.2 (3.9–4.4)	4.2 (3.9–4.5)	4.2 (3.9–4.5)
Hypertension — no. (%)¶			
Uncontrolled	77 (29.2)	67 (25.2)	71 (26.9)
Resistant	187 (70.8)	199 (74.8)	193 (73.1)

Changes in Blood Pressure, According to Hierarchical Order.

End Point	Baxdrostat, 1 mg	Baxdrostat, 2 mg	Placebo
Primary end point: change in seated SBP from baseline to 12 wk†			
No. of patients	264	266	263
Least-squares mean placebo-corrected difference (95% CI) — mm Hg	−8.7 (−11.5 to −5.8)	−9.8 (−12.6 to −7.0)	—
P value	<0.001	<0.001	—
Secondary end points			
Change in seated SBP during randomized-withdrawal period: wk 24 to 32‡			
No. of patients	NA	172	85
Least-squares mean placebo-corrected difference (95% CI) — mm Hg	NA	−5.1 (−8.3 to −1.9)	—
P value	NA	0.002	—
Change from baseline in seated SBP up to wk 12 in the resistant-hypertension subpopulation§			
No. of patients	187	199	192
Least-squares mean placebo-corrected difference (95% CI) — mm Hg	−9.1 (−12.6 to −5.7)	−9.8 (−13.1 to −6.4)	—
P value	<0.001	<0.001	—
Change from baseline in seated diastolic blood pressure up to wk 12¶			
No. of patients	264	266	263
Least-squares mean placebo-corrected difference (95% CI) — mm Hg	−3.3 (−5.2 to −1.4)	−3.9 (−5.7 to −2.0)	—
P value	0.001	<0.001	—

Adverse Events during the 12-Week Double-Blind Treatment Period.

Adverse Events	Baxdrostat, 1 mg (N=264)	Baxdrostat, 2 mg (N=266)	Placebo (N=264)
Any serious adverse event — no. (%)*	5 (1.9)	9 (3.4)	7 (2.7)
Death — no. (%)	0	0	1 (0.4)
Any adverse event — no. (%)	125 (47.3)	119 (44.7)	109 (41.3)
Moderate or severe event	27 (10.2)	37 (13.9)	23 (8.7)
Severe event	3 (1.1)	7 (2.6)	5 (1.9)
Adverse event leading to discontinuation — no. (%)			
Any	7 (2.7)	12 (4.5)	5 (1.9)
Hyperkalemia	2 (0.8)	4 (1.5)	0
Adverse event of special interest — no. (%)†			
Hyperkalemia	7 (2.7)	21 (7.9)	0
Hyponatremia	2 (0.8)	6 (2.3)	1 (0.4)
Hypotension	5 (1.9)	6 (2.3)	2 (0.8)
Serum potassium — no./total no. (%)‡			
>5.5 mmol/liter	16/262 (6.1)	29/261 (11.1)	1/260 (0.4)
>6.0 mmol/liter	6/262 (2.3)	8/263 (3.0)	1/262 (0.4)
>6.5 mmol/liter	5/262 (1.9)	1/263 (0.4)	1/263 (0.4)

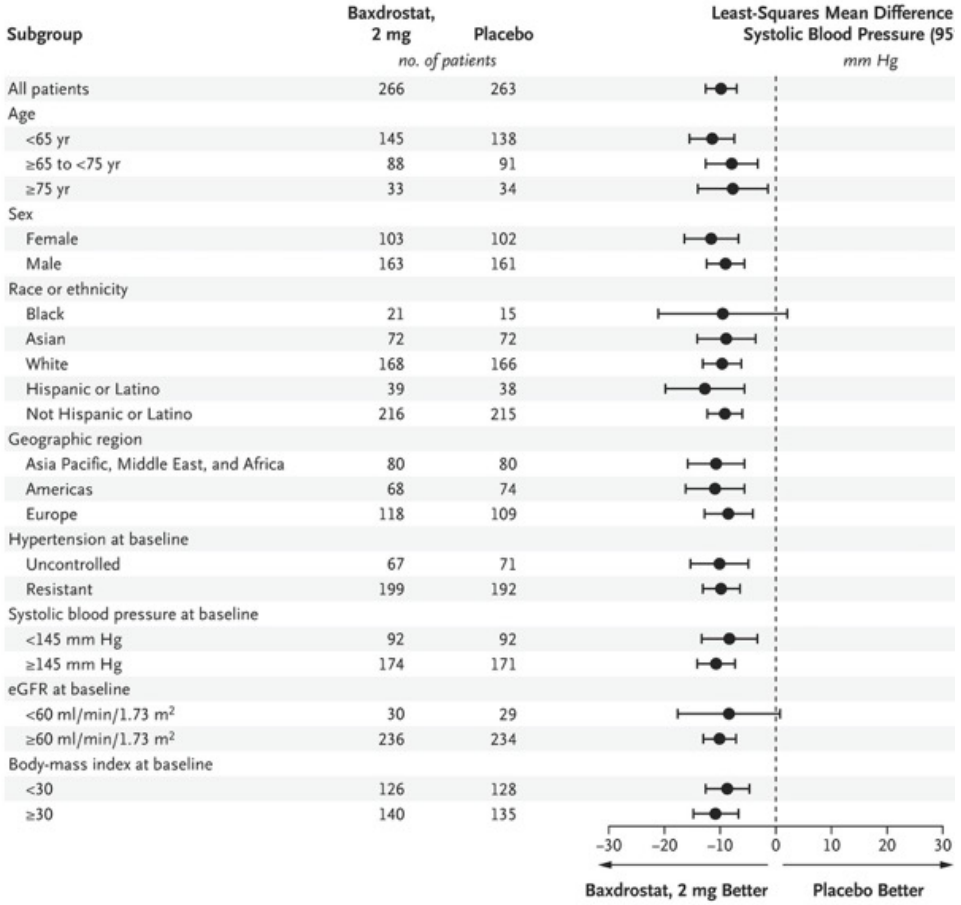

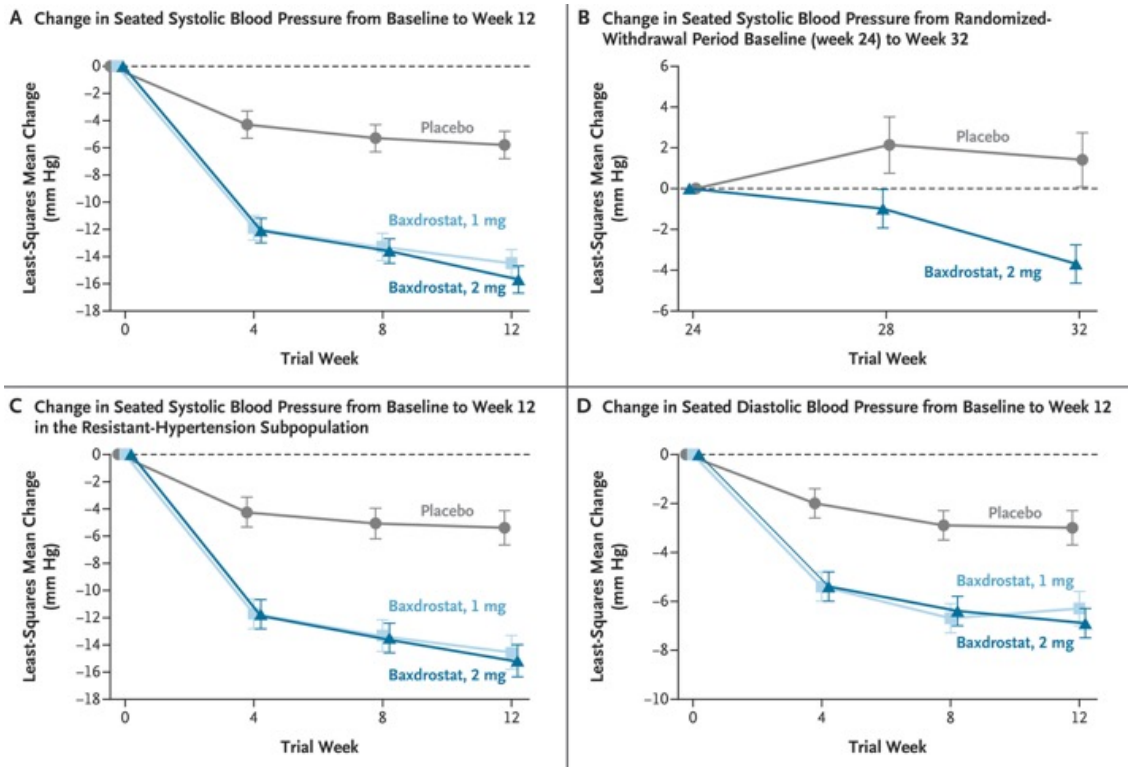

Change in Blood Pressure in Patients with Uncontrolled or Resistant Hypertension.

The line graphs show the time course for least-squares mean changes from baseline in the seated systolic blood pressure up to week 12 (Panel A), the change from the randomized-withdrawal baseline (week 24) in the seated systolic blood pressure up to week 32 (Panel B), the change from baseline in the seated systolic blood pressure up to week 12 in the resistant-hypertension subpopulation (Panel C), and the change from baseline in the seated diastolic blood pressure up to week 12 (Panel D). I bars on the line graphs indicate standard errors.

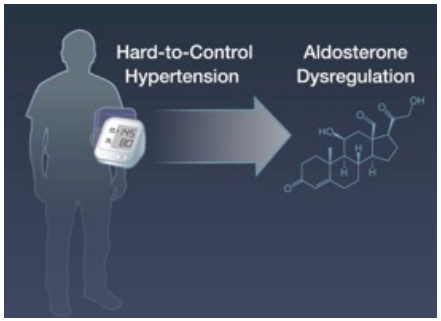
Hard-to-Control Hypertension
Aldosterone Dysregulation


New Phase 3 Trial
794 Adults
Seated systolic blood pressure of ≥135 mm Hg
Baxdrostat
Baxdrostat
Placebo
1 mg
2 mg
Once daily

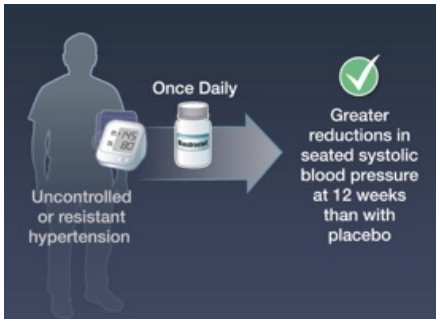
Once Daily
Uncontrolled or resistant hypertension
Greater reductions in seated systolic blood pressure at 12 weeks than with placebo


Baxdrostat
Mixed Results
?
Baxdrostat

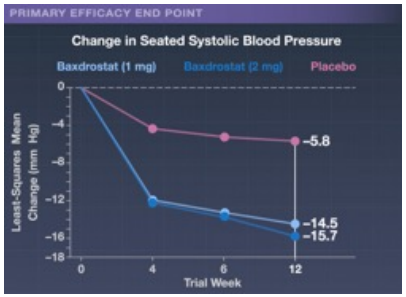
PRIMARY EFFICACY END POINT
Change in Seated Systolic Blood Pressure
Baxdrostat (1 mg)
Baxdrostat (2 mg)
Placebo
Least-Squares Mean Change (mm Hg)
0
−4
−8
−12
−16
−18
−5.8
−14.5
−15.7
0
4
6
12
Trial Week

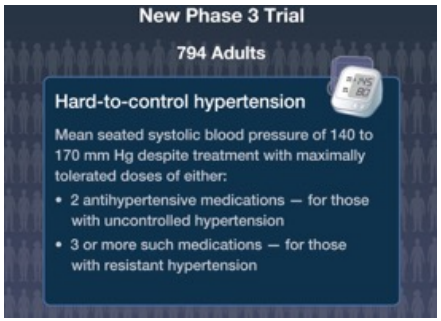
New Phase 3 Trial
794 Adults
Hard-to-control hypertension
Mean seated systolic blood pressure of 140 to 170 mm Hg despite treatment with maximally tolerated doses of either:
• 2 antihypertensive medications — for those with uncontrolled hypertension
• 3 or more such medications — for those with resistant hypertension

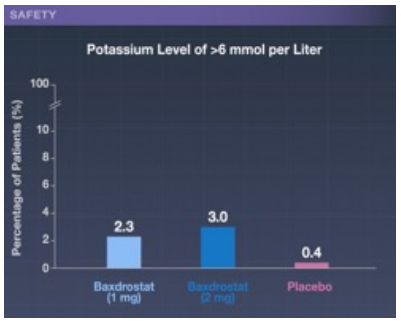
SAFETY
Potassium Level of >6 mmol per Liter
Percentage of Patients (%)
100
10
8
6
4
2
0
2.3
3.0
0.4
Baxdrostat (1 mg)
Baxdrostat (2 mg)
Placebo

Transthyretin (TTR) primarily functions as a transport protein, carrying thyroid hormones (thyroxine) and vitamin A (retinol) throughout the body. It is produced mainly in the liver and choroid plexus, and it plays a critical role in nerve and brain health by moving hormones and potentially protecting against neurodegenerative diseases.

Key functions:

Hormone transport:

TTR transports thyroxine, a thyroid hormone, from the blood into the brain and the rest of the body.

Vitamin A transport:

TTR binds to retinol-binding protein (RBP) to transport vitamin A (retinol) throughout the body.

Brain and nerve health:

TTR may have neuroprotective properties and has been shown to help clear harmful protein aggregates, such as those associated with Alzheimer's disease.

How it works:

TTR is a tetramer, meaning it is made of four identical protein units that bind together to transport its cargo.

The liver is the main producer of TTR, but a small amount is also made in the choroid plexus of the brain and the retina

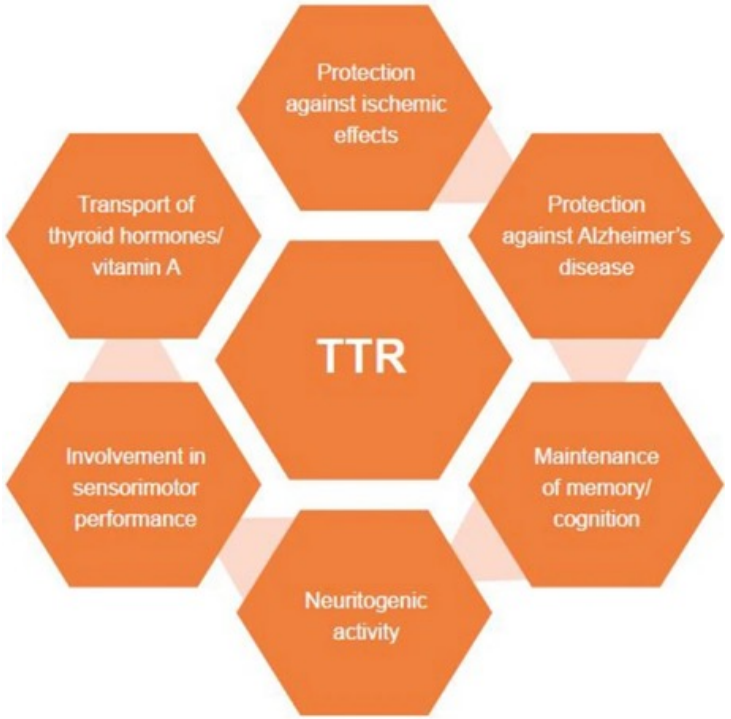

ATTR ist die Abkürzung für die Transthyretin-Amyloidose, eine seltene, fortschreitende und lebensbedrohliche Erkrankung, die durch die Ablagerung von Amyloid-Transthyretin-Protein in verschiedenen Organen verursacht wird. Diese Ablagerungen, die aus fehlgefaltetem Transthyretin (TTR) entstehen, das normalerweise von der Leber produziert wird, können das Herz, das Nervensystem und andere Gewebe schädigen.

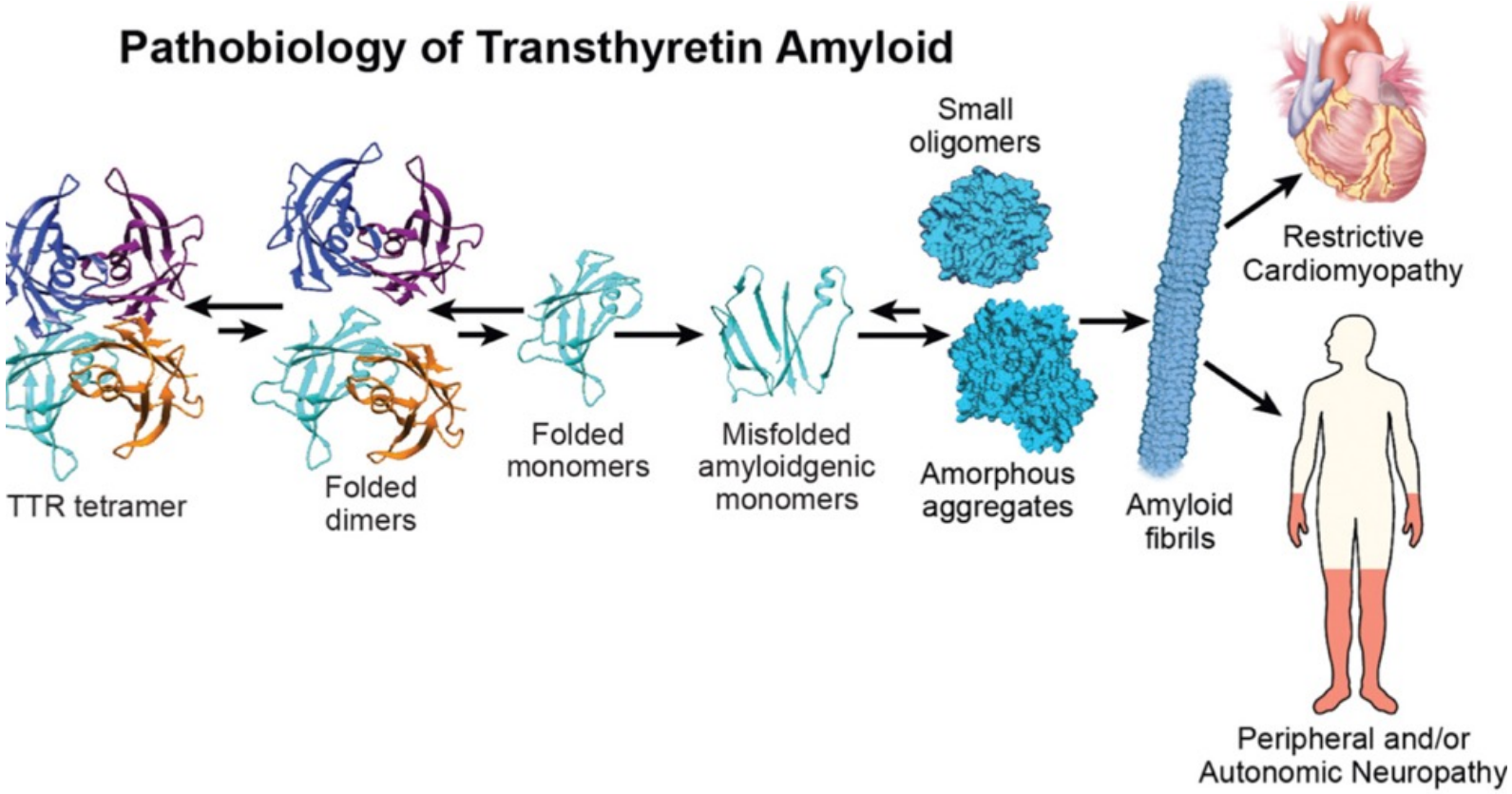

CRISPR Mechanism of Action

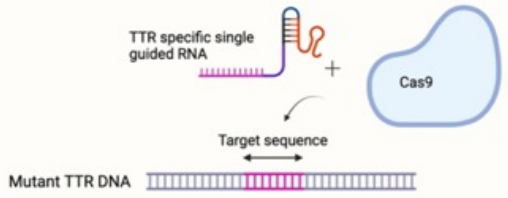

1. Target Recognition:
   - Cas9 binds to guide RNA.
   - The guide RNA hybridizes with complementary target DNA sequence in the genome.

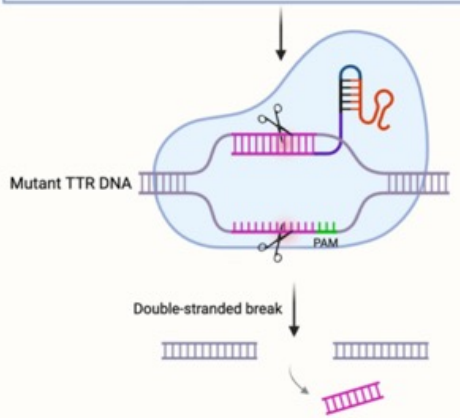

2. DNA Cleavage:
   - A specific nearby sequence, called the PAM (Protospacer Adjacent Motif), must be present for Cas9 to bind and cut.
   - Once the guide RNA binds to the complementary DNA, Cas9 introduces a double-stranded break at target site.
   - The break occurs at a specific position relative to PAM sequence.

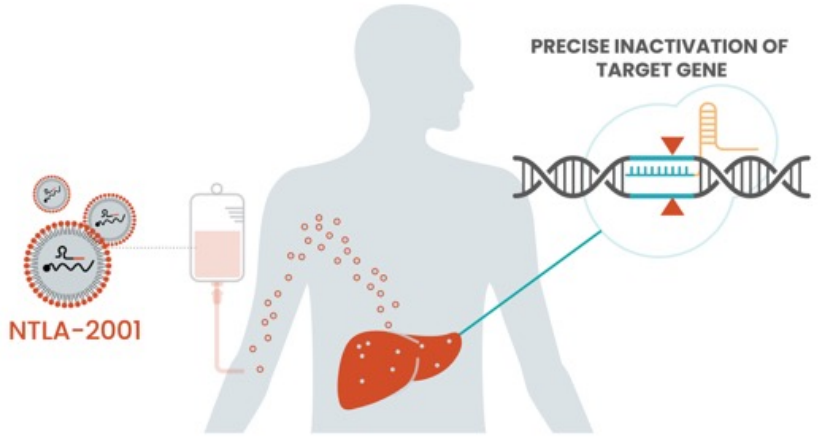

Nexiguran Ziclumeran Gene Editing in Hereditary ATTR with Polyneuropathy

Hereditary transthyretin amyloidosis with polyneuropathy (ATTRv-PN) is a rare, multisystem, progressive, debilitating, and fatal disease characterized by tissue deposition of misfolded transthyretin (TTR) in peripheral nerves. Nexiguran ziclumeran (nex-z) is an investigational in vivo therapy based on CRISPR-Cas9 (clustered regularly interspaced short palindromic repeats and associated Cas9 endonuclease) that is designed to reduce serum TTR levels through selective inactivation of TTR in the liver. In this phase 1, open-label study, we administered one infusion of nex-z to patients with ATTRv-PN. Primary objectives included assessment of the safety and pharmacodynamics of nex-z. Secondary end points included changes in the familial amyloid polyneuropathy stage, polyneuropathy disability score, serum neurofilament light chain (NfL) level, modified body-mass index (modified BMI, defined as the conventional BMI [weight in kilograms divided by square of height in meters] multiplied by the albumin level in grams per liter), and modified Neuropathy Impairment Score+7 (mNIS+7; range, 0 to 304, with higher scores indicating more impairment).

Conclusions

A single administration of nex-z in patients with ATTRv-PN was associated with rapid, deep, and durable reductions in serum TTR levels. The results support further investigation of nex-z to treat ATTRv-PN. (Funded by Intellia Therapeutics and Regeneron Pharmaceuticals; ClinicalTrials.gov number, NCT04601051.)

Transthyretin amyloidosis (ATTR) is a multisystem disease caused by the deposition of transthyretin (TTR) amyloid in various organ systems.1 TTR circulates as a tetramer,2 whereas pathogenic TTR variants potentiate dissociation into monomers, which misfold and deposit in tissues.1 Hereditary (variant) ATTR amyloidosis is frequently associated with polyneuropathy (ATTRv-PN) owing to amyloid deposition in peripheral nerves that leads to progressive disability, including worsening sensorimotor and autonomic impairment, decreased functional ability, reduced quality of life, and death. The median survival from disease onset ranges from 6 to 12 years and varies depending on age at onset, TTR variant, cardiac involvement, and promptness of treatment.

Nexiguran ziclumeran (nex-z, also known as NTLA-2001) is an investigational in vivo gene-editing therapy that is based on clustered regularly interspaced short palindromic repeats (CRISPR) and CRISPR-associated protein 9 (Cas9).

Characteristic	All Patients (N=36)
Median age (range) — yr	61 (19–75)
Male sex — no. (%)	26 (72)
Race or ethnic group — no. (%)†	
White	33 (92)
Asian	1 (3)
Native Hawaiian or Other Pacific Islander	1 (3)
Multiple	1 (3)
Median weight (range) — kg	77.0 (55.0–116.7)
Median time since diagnosis (range) — yr	2 (0–11)
TTR genotype — no. (%)	
p.Val50Met	11 (31)
Non-p.Val50Met	25 (69)
Wild-type	0
Previous medication for ATTR — no. (%)	
Tafamidis	10 (28)
Diflunisal	9 (25)
Patisiran‡	7 (19)
Inotersen	1 (3)
Doxycycline	1 (3)
Neuropathy Impairment Score§	31±27
Previous disease progression during patisiran therapy	69±18
Previous use of tafamidis	41±33
mNIS+7¶	47±33
Previous disease progression during patisiran therapy	80±17
Previous use of tafamidis	43±34
Modified BMI‖	1174±220
Norfolk QoL-DN score**	35±32
Neurofilament light chain — pg/ml	29±26)
Polyneuropathy disability score — no. (%)††	
0	0
I	23 (64)
II	7 (19)
IIIa	5 (14)
IIIb	1 (3)
IV	0
Familial amyloid polyneuropathy stage — no. (%)‡‡	
0	1 (3)
1	28 (78)
2	7 (19)
3	0
EQ-5D-5L§§	
Index score	0.78±0.23
Visual analogue scale score	69.7±18.8

Safety Summary in All Patients with ATTRv-PN Treated with Nex-z.

Event	Patients (N=36)
Phase 1 study	
At least one adverse event — no. (%)	36 (100)
Adverse events occurring in ≥15% of patients — no. (%)	
Infusion-related reaction	21 (58)
Headache	10 (28)
Diarrhea	8 (22)
Thyroxine decreased†	8 (22)
Aspartate aminotransferase increased	6 (17)
Any treatment-related adverse event — no. (%)	28 (78)
Treatment-related adverse event in ≥10% of patients — no. (%)	
Infusion-related reaction	21 (58)
Thyroxine decreased	8 (22)
Headache	4 (11)
Any serious event — no. (%)‡	11 (31)
Serious adverse event occurring in ≥5% of patients: prostate cancer — no. (%)	2 (6)
Any adverse event leading to treatment discontinuation — no. (%)	0
Any event leading to death — no. (%)	1 (3)§
Long-term follow-up study	
Any serious event — no./total no. (%)‡¶	4/31 (13)

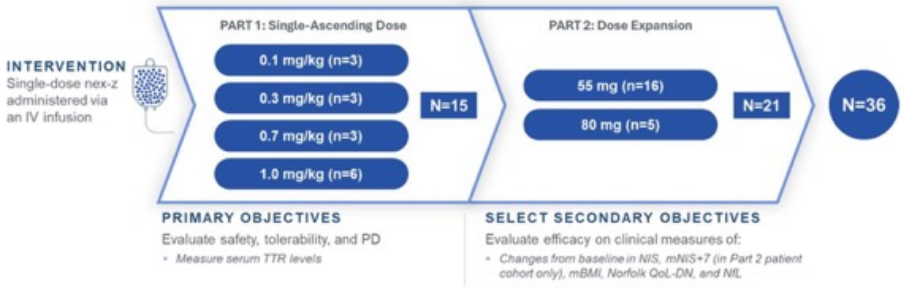

IV, intravenous; mBMI, modified body mass index; mNIS+7, modified Neuropathy Impairment Score +7; NfL, neurofilament light chain; NIS, Neuropathy Impairment Score; Norfolk QoL-DN, Norfolk Quality of Life-Diabetic Neuropathy Questionnaire; PD, pharmacodynamics; TTR, transthyretin.

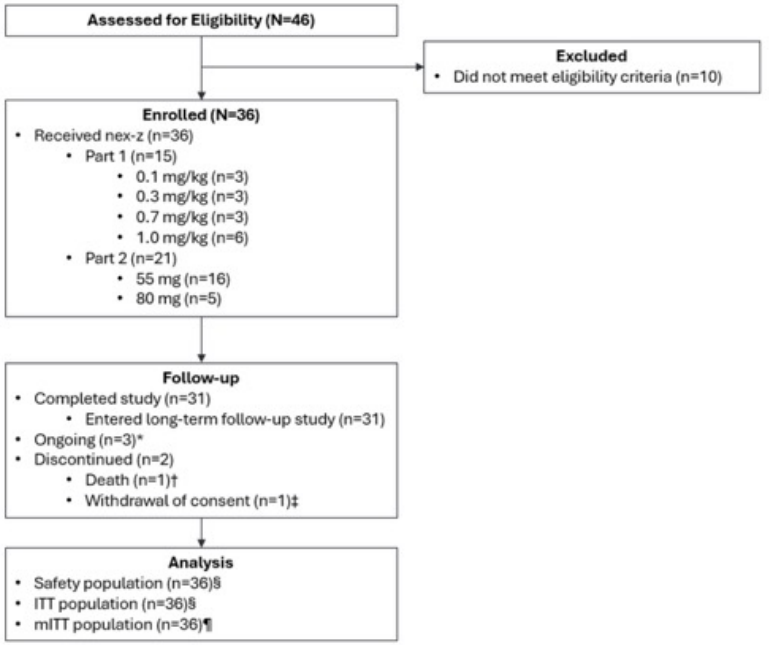

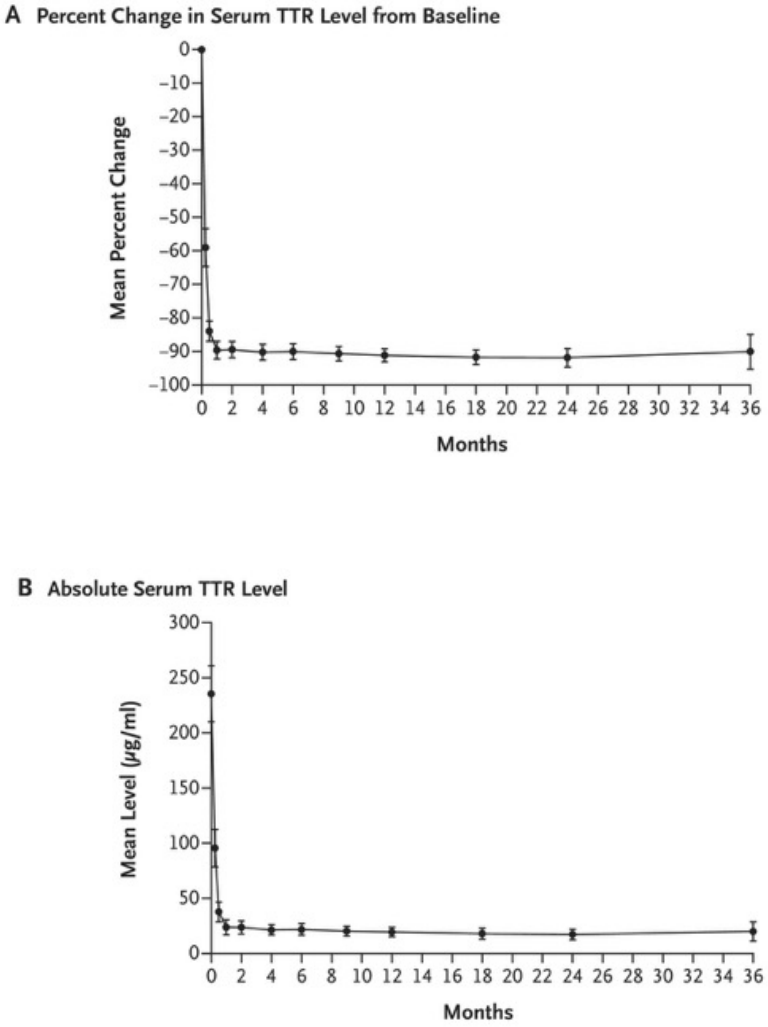

Reduction in Serum TTR Levels in Patients Who Received Nex-z at a Dose of More Than 0.1 mg per Kilogram.

Panel A shows the mean percentage change from baseline in transthyretin (TTR) levels after a single intravenous infusion of nexiguran ziclumeran (nex-z). The mean change in the transthyretin (TTR) level was −84% at day 14, −90% at day 28, −91% at month 12, −92% at month 24, and −90% at month 36. Panel B shows the corresponding mean absolute serum TTR levels, which were 37.8 μg per milliliter at day 14, 23.8 μg per milliliter at day 28, 19.5 μg per milliliter at month 12, 17.3 μg per milliliter at month 24, and 20.0 μg per milliliter at month 36. The variability in serum TTR levels was low, with the mean (±SD) maximum change in a patient's TTR levels from day 28 to month 24 of −4.1±14.8 μg per milliliter. Data regarding the serum TTR level at month 36 were collected from patients who entered the long-term follow-up safety monitoring study (data-cutoff date, April 16, 2025). In both panels, I bars indicate 95% confidence intervals.

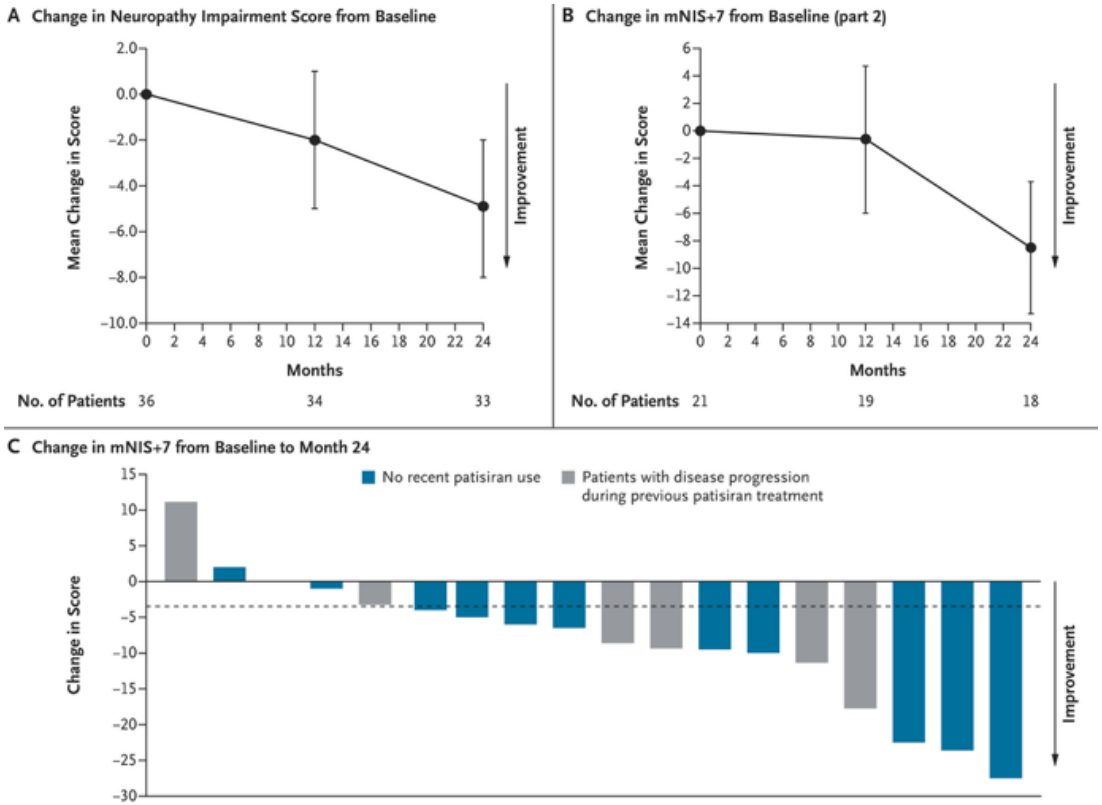

Change from Baseline in Neuropathy Impairment Score (Parts 1 and 2) and mNIS+7 (Part 2).

Panel A shows the mean change from baseline in the Neuropathy Impairment Score in all patients in parts 1 and 2 of the study; the score is assessed on a scale from 0 to 244, with higher scores indicating more impairment. The mean change in the Neuropathy Impairment Score was −2.0 at month 12 and −4.9 at month 24. Panel B shows the mean changes from baseline in the modified Neuropathy Impairment Score+7 (mNIS+7) in all patients in part 2 of the study. The mNIS+7 is assessed on a scale from 0 to 304, with higher scores indicating more impairment. The mean changes in the mNIS+7 were −0.6 at month 12 and −8.5 at month 24. In Panels A and B, I bars indicate 95% confidence intervals. Panel C shows the changes in the mNIS+7 from baseline to month 24 for each patient, according to previous receipt of patisiran (no recent use or disease progression during therapy). The dashed line provides a reference for clinically meaningful improvement (reduction of ≥4 points).[27] Of the 18 patients with data, 13 had clinically meaningful improvement.

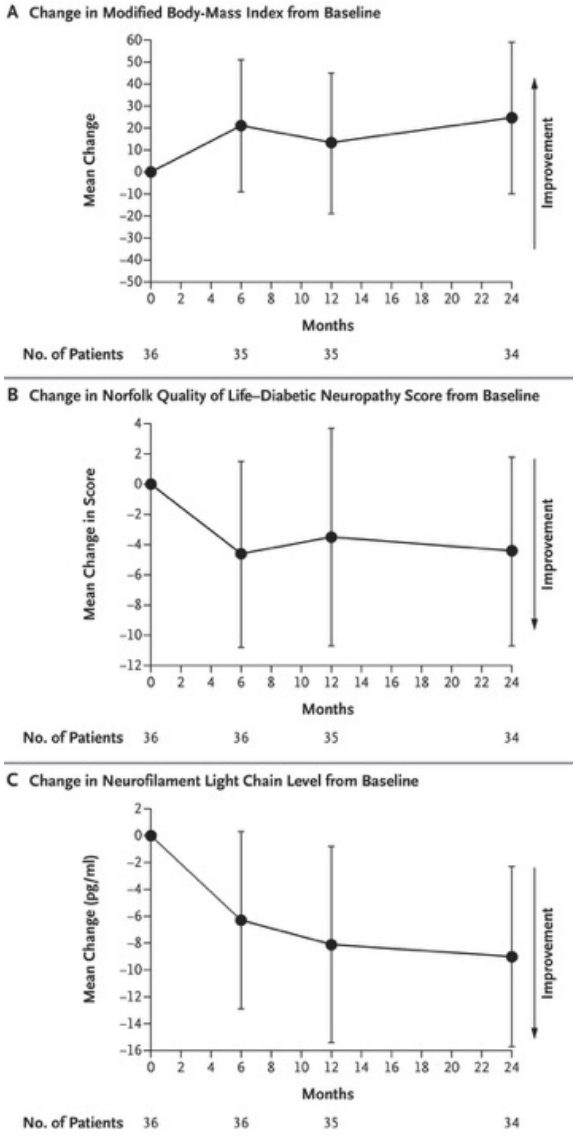

Changes from Baseline in the Modified BMI, Norfolk QoL-DN Score, and Neurofilament Light Chain Level in All Patients.

Panel A shows the mean changes from baseline to month 24 in the modified body-mass index (modified BMI, defined as the conventional BMI [weight in kilograms divided by square of height in meters] multiplied by the albumin level in grams per liter). The normal range for the modified BMI as based on the normal range for albumin at the local laboratory was 650 to 1300. The mean change in modified BMI was 13.4 at month 12 and 24.7 at month 24; a higher modified BMI indicates improvement. Panel B shows the mean changes from baseline to month 24 in the Norfolk Quality of Life–Diabetic Neuropathy (QoL-DN) scores (assessed on a scale from –4 to 136, with lower scores indicating better quality of life). The mean change in the Norfolk QoL-DN score was –3.5 at month 12 and –4.4 at month 24. Panel C shows the mean changes from baseline to month 24 in the neurofilament light chain level. The mean change in the neurofilament light chain level was –8.1 pg per milliliter at month 12 and –9.0 pg per milliliter at month 24; lower values indicate clinical improvement. In all panels, I bars indicate 95% confidence intervals.

Discussion

Patients who were treated with a single nex-z infusion had rapid, deep, and durable reductions in serum TTR levels, with a mean reduction of at least 90% from baseline that was sustained from day 28 through month 36. At month 24, a total of 94% of the patients had TTR levels below 50 µg per milliliter, including 90% who had levels below 30 µg milliliter. These near-total and sustained TTR reductions resulted in stabilization of or improvement in disease-related clinical measures through month 24. The mean change in the mNIS+7 at month 24 of −8.5 points exceeded the clinically meaningful threshold of a reduction of at least 4 points. Consistent changes were also observed in the Norfolk QoL-DN score, NfL level, and modified BMI. Conversely, data from natural history studies and from patients who have received placebo in trials indicate that ATTRv-PN is characterized by disease progression, including worsening neuropathy scores (increased NIS and mNIS+7), nutritional status (decreased modified BMI), quality of life (increased Norfolk QoL-DN score), and biomarkers (increased NfL levels).

Targeted indoor spraying agsinst mosquitoes: Is this strategy helpful or not?

Photos show all hired personnel and equipment as well as modes of TIRS application in houses.

Pirimiphos-methyl wird als Wirkstoff
in Pflanzenschutzmitteln verwendet. Es ist ein Nachernte-Insektizid, das in den USA bei eingelagertem Mais, Hirse und Saatgut verwendet wird. Es dient zur Bekämpfung verschiedener Insekten wie Wollläusen und Fliegen (bei Rindern) und Zigarettenkäfern, Reismehlkäfern, Leistenkopfplattkäfern, Motten (auf Mais und Getreide) und anderen. Das chemisch verwandte Ethyl-derivat (Pirimiphos-ethyl[9]) wird ebenfalls als Insektizid eingesetzt. Pirimiphos-methyl wurde in den USA 1978 als Insektizid zugelassen und im Jahr 2006 wurden etwa 12.000 pounds (5,4 t) verwendet. Es wirkt durch Hemmung der Acetylcholinesterase.

The moderate acute toxicity of pirimiphos-methyl is due to its inhibition of cholinesterase. After single toxic doses the onset of inhibition of cholinesterase and appearance of toxic signs were delayed for several hours and persisted for several days.

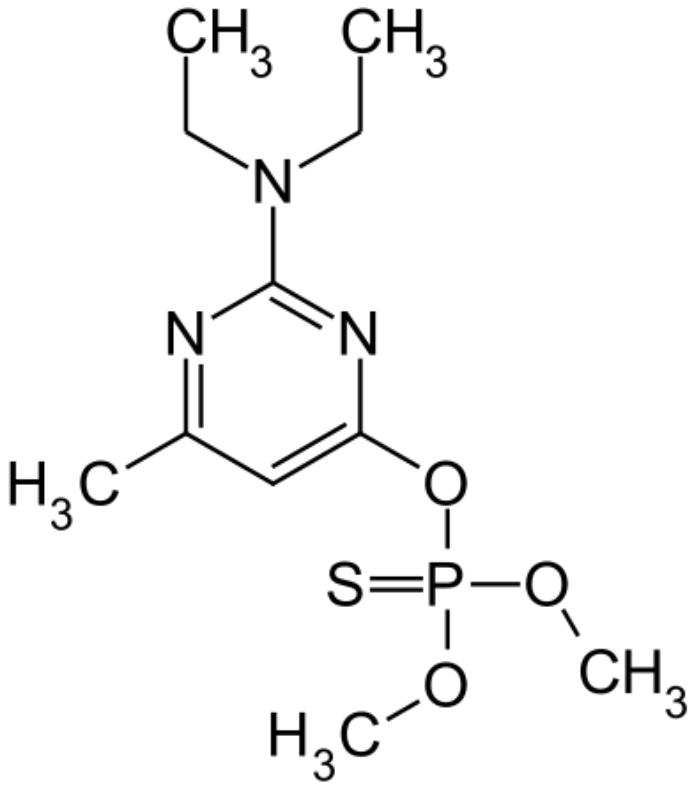

Randomized Trial of Targeted Indoor Spraying to Prevent Aedes-Borne Diseases

Targeted indoor residual spraying focuses insecticide applications on common resting surfaces of *Aedes aegypti* mosquitoes (an arboviral disease vector) in houses, such as exposed lower sections of walls and under furniture.
We conducted a two-group, parallel, unblinded, cluster-randomized trial in Merida, Mexico, to quantify the efficacy of targeted indoor residual spraying for preventing aedes-borne diseases (chikungunya, dengue, or Zika). Children 2 to 15 years of age were enrolled from households in 50 clusters of five-by-five city blocks. Households in 25 clusters received an annual application of targeted indoor residual spraying (intervention) before each season of aedes-borne disease (July through December). All clusters received routine Ministry of Health vector control. The primary end point was laboratory-confirmed, symptomatic aedes-borne disease. Community effects were assessed with the use of geolocated national surveillance data.

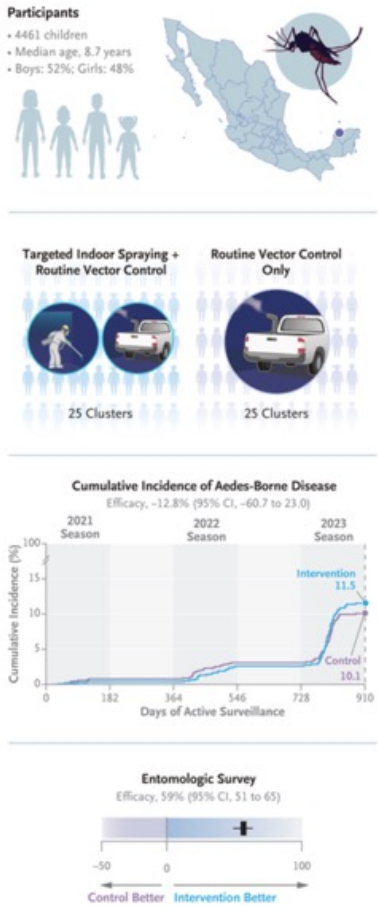

The public health effects of aedes-borne diseases, including chikungunya, dengue, and Zika, are growing. The incidence of dengue has surged to unprecedented levels, with more than 10 million suspected cases in the Americas in 2024. After a dramatic reduction in the burden of Zika since 2016, evidence of its continued presence in the Americas is mounting. The burden of chikungunya is also increasing, with outbreaks in the Americas.

In Australia, targeted indoor residual spraying that was deployed to houses during a dengue outbreak led to a risk of infection that was nearly 86% lower than that in unsprayed houses. Although most vector control is reactive, implemented during an outbreak, mathematical models predict that the effect of targeted indoor residual spraying is highest when the intervention is applied before the beginning of the season for aedes-borne diseases, before growth of the vector population.

Trial Design and Oversight

We conducted this two-group, parallel, unblinded, cluster-randomized, controlled trial of targeted indoor residual spraying in a hot spot for aedes-borne diseases in Merida, Yucatan State, Mexico.

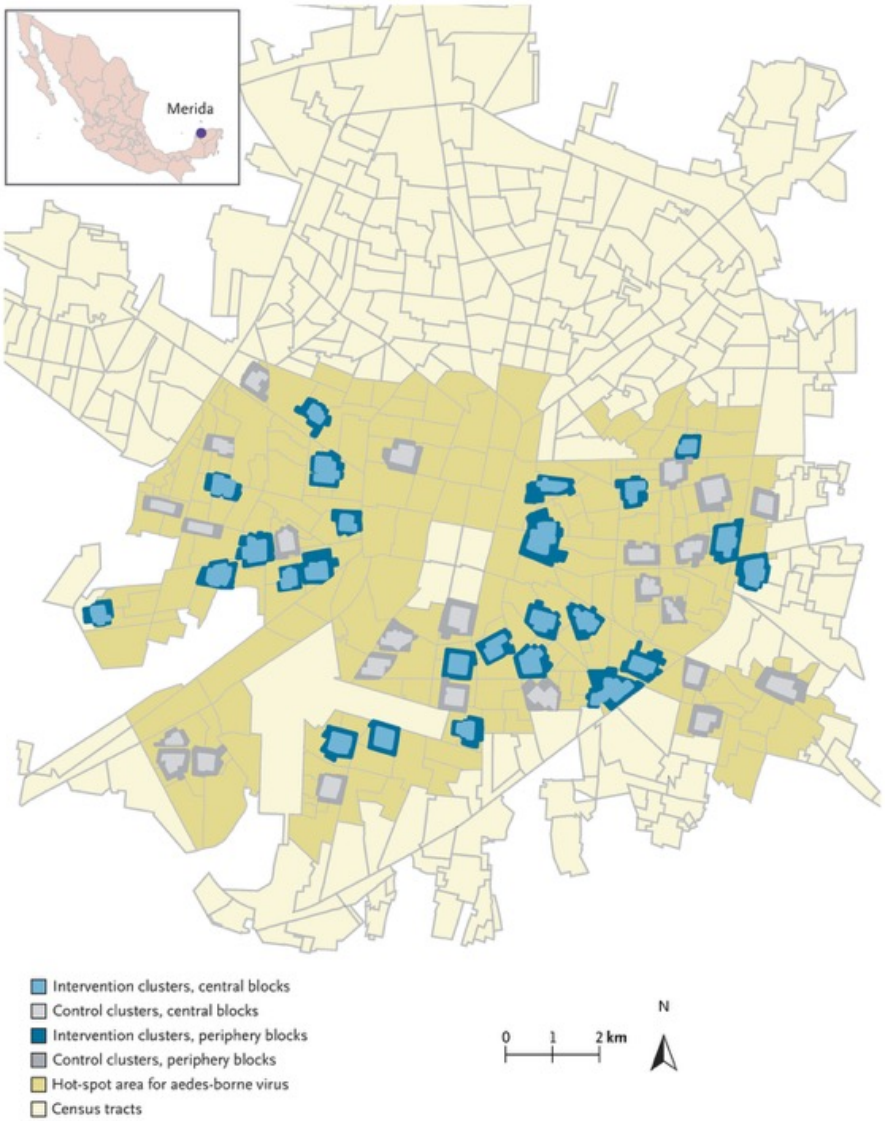

Map of Trial Area.

A total of 50 clusters (five-by-five city blocks) were selected within the aedes-borne virus hot-spot region of Merida, Mexico. Eligible hot-spot regions on the city map are indicated. The trial included 25 intervention clusters (blue) and 25 control clusters (gray). The 25 clusters in the intervention group received targeted indoor residual spraying, and all 50 clusters received Ministry of Health vector-control actions. The mean area of the clusters was 28.7 hectares (95% confidence interval [CI], 25.3 to 32.2) in the intervention group and 31.7 hectares (95% CI, 27.3 to 36.0) in the control group. Cluster-central blocks (three-by-three city blocks) are highlighted in lighter shades. The inset shows the geographic location of Merida in the state of Yucatan.

TIRS intervention

The insecticide Pirimiphos-methyl (Actellic 300CS, Syngenta) was applied at the target dose of 1 g a.i./m2 using a manual pump IK Vector Control Super (Goizper Group, Spain) in all houses that consented to the application and were available at the time of the intervention. Specifically, an insecticide bottle (833 mL) was mixed in 7.5 L of water and applied with a manual compression equipment IK-Vector Control Super® (Goizper Group, Antzuola, mouthpiece 8002EVS, and yellow control flow valve), providing an average flow rate of 580 mL/min. Three spraying rounds lasting 2 months each were conducted at the beginning of each of the three TIRS evaluation years (2020, 2021, 2022). Each round started in May and extended until July 1st (considered the start of active surveillance). On each round, the same procedures and timeline were followed: a) hiring of spraying personnel (a total of 70, half from the community and half from the Yucatan MOH); b) training of personnel and practice of TIRS in experimental houses; c) development of spraying plan, which includes cluster-ID and weekly schedule of spraying from May to July; d) active messaging through flyers, radio and street megaphone announcements, indicating the week of intervention and advertising the project; e) spraying of houses, dividing into two spraying groups: team treating houses with enrolled kids (N=10) and teams treating all other houses (N=60); f) survey of householders 30 days, 3 months, and 6 months post-spraying to assess community perception; g) health monitoring for signs of intoxication of reaction to the insecticide in the community. **Figure S1** shows images of the implementation of TIRS.

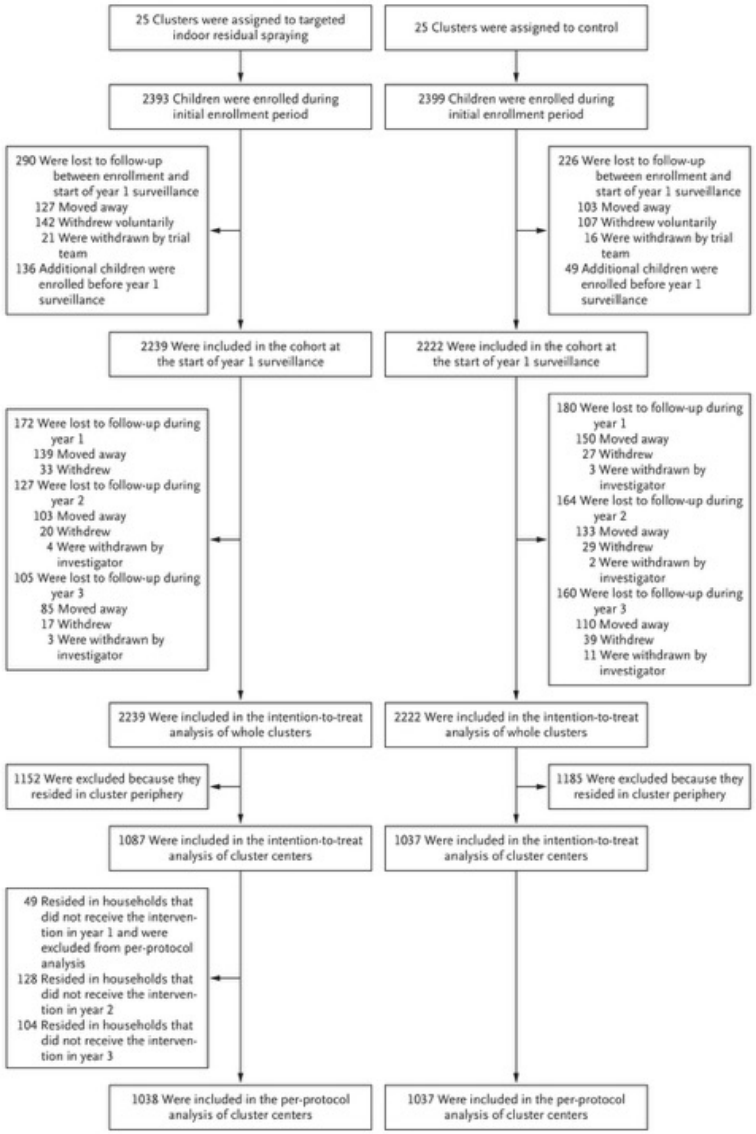

Cluster Randomization, Enrollment of Participants, and Inclusion in Analysis Datasets.

The flow diagram summarizes the data contributing to key epidemiologic analyses: the intention-to-treat analysis of the entire clusters, the intention-to-treat analysis of cluster centers, and the per-protocol analysis of cluster centers. To balance losses that occurred between initial enrollment and the start of year 1 surveillance owing to participants moving out of the trial area, voluntary withdrawal, and withdrawal by the trial team, additional enrollment was undertaken in both groups. After the start of active surveillance, participant follow-up time was censored at the time of exit from the trial. The most common reasons for exit from the trial were moving away, voluntary withdrawal, or withdrawal by the trial team. For the per-protocol analysis of the cluster center, 49 children contributed no person-time to the intervention group owing to protocol deviations (no spraying), with further data censoring at the start of years 2 and 3.

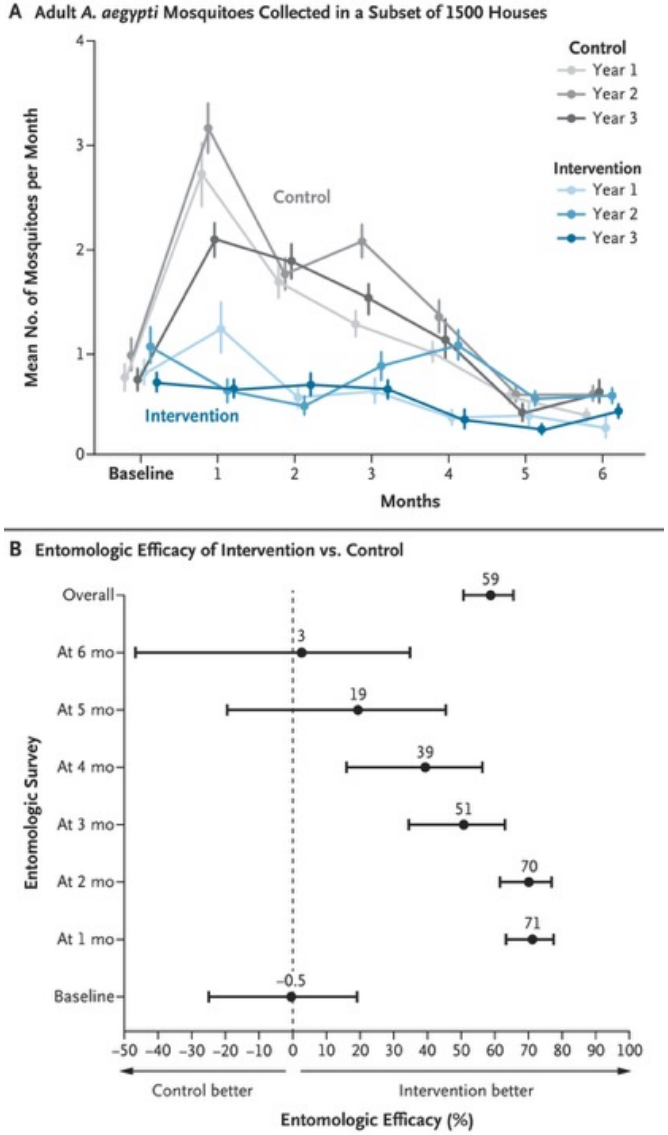

Mean Entomologic Indexes over Time and Entomologic Efficacy.

Panel A shows the mean number of *Aedes aegypti* adult mosquitoes that were collected in a subset of 1500 houses (with a 1:1 ratio between the intervention group [targeted indoor residual spraying] and the control group) monthly during the 3 years of the trial. Baseline indicates the survey that was conducted before the application of the intervention, with monthly surveys conducted throughout the peak disease season from July through December of each year. Error bars indicate the 95% confidence interval of the mean. Panel B shows the entomologic efficacy of the intervention, quantified as the overall percentage difference (point estimate) as compared with control (over all months and years) and analyzed according to baseline (before the intervention) and month after the intervention. Error bars indicate 95% confidence intervals.

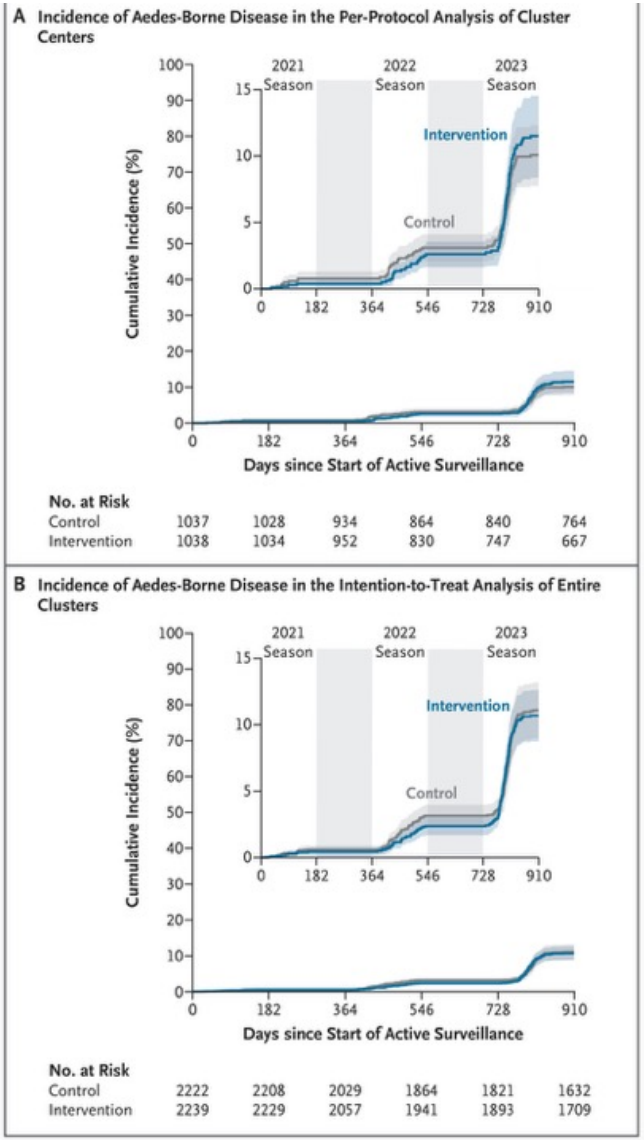

Cumulative Incidence of Aedes-Borne Disease for Key Efficacy Analyses.

Shown is the cumulative incidence of aedes-borne disease in the trial groups, as estimated with the Kaplan–Meier method. Periods between disease seasons, when active surveillance was paused, are shown in light gray on the insets, which show the same data on an expanded y axis. Shading around the graphed lines represents 95% confidence intervals. Panel A shows the per-protocol analysis of cluster centers (primary analysis). Panel B shows the intention-to-treat analysis of the entire clusters (center and periphery) (secondary analysis).

Epidemiologic Efficacy Estimates.

Analysis	Targeted Indoor Residual Spraying			Control			Efficacy*
	No. of Participants	No. of Cases	Cumulative Incidence (95% CI)†	No. of Participants	No. of Cases	Cumulative Incidence (95% CI)†	Point Estimate (95% CI)
			%			%	%
Primary analysis							
Per-protocol analysis of cluster centers	1038	91	11.5 (8.4 to 14.5)	1037	89	10.1 (7.8 to 12.3)	−12.8 (−60.7 to 23.0)
Secondary analyses							
Intention-to-treat analysis of entire clusters	2239	198	10.1 (8.4 to 11.8)	2222	199	10.5 (8.6 to 12.3)	3.9 (−28.1 to 26.7)
Community effect analysis	—	150		—	202		24.0 (6.0 to 38.6)

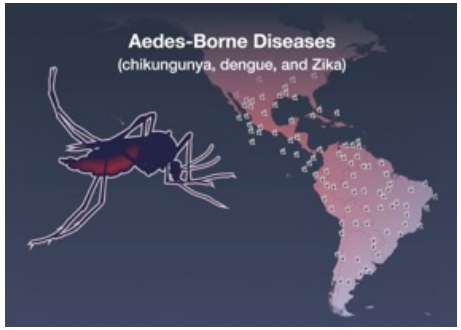
Aedes-Borne Diseases
(chikungunya, dengue, and Zika)

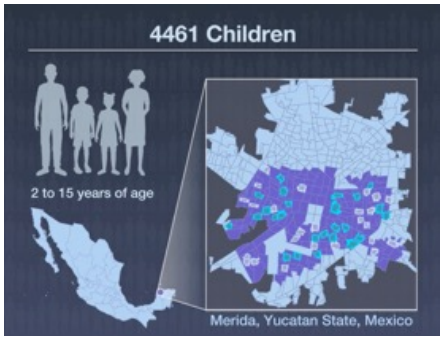
4461 Children
2 to 15 years of age
Merida, Yucatan State, Mexico


PRIMARY END POINT
Cumulative Incidence
Efficacy, −12.8% (95% CI, −60.7 to 23.0)
2021 Season
2022 Season
2023 Season
Cumulative Incidence (%)
Intervention
11.6% (95% CI, 9.4 to 14.0)
Control
10.1% (95% CI, 7.8 to 12.3)
0
182
364
546
728
910
Days since Start of Active Surveillance

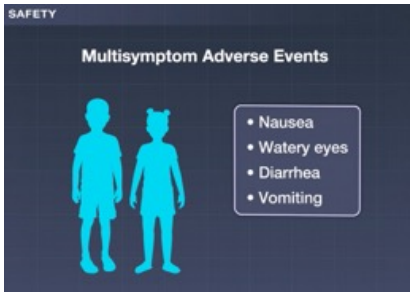
SAFETY
Multisymptom Adverse Events
• Nausea
• Watery eyes
• Diarrhea
• Vomiting

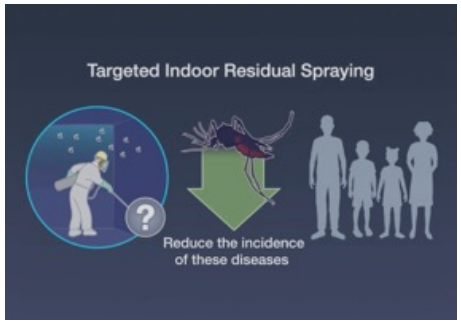
Targeted Indoor Residual Spraying
Reduce the incidence of these diseases


Targeted Indoor Residual Spraying
+
Routine Vector Control
25 clusters
Routine Vector Control Only
25 clusters

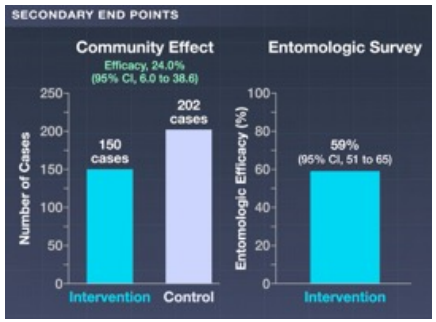
SECONDARY END POINTS
Community Effect
Efficacy, 24.0% (95% CI, 6.0 to 38.6)
Number of Cases
150 cases
202 cases
Intervention
Control
Entomologic Survey
Entomologic Efficacy (%)
59% (95% CI, 51 to 65)
Intervention

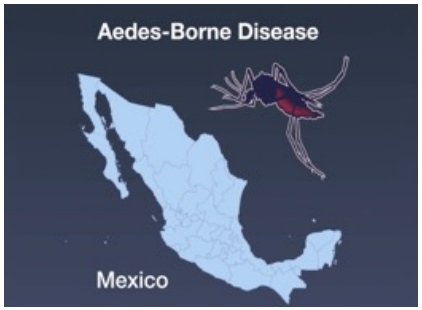
Aedes-Borne Disease
Mexico


Trial
• Two-arm
• Parallel
• Unblinded
• Cluster-randomized
• Controlled


PRIMARY END POINT
Cumulative Incidence of Laboratory-Confirmed Symptomatic Aedes-Borne Disease
July–December
July–December
July–December
Over three consecutive seasons


SAFETY
Multisymptom Adverse Events
Possibly related to the intervention


Targeted Indoor Residual Spraying
Did not reduce the incidence of aedes-borne disease among children 2 to 15 years of age, despite reduction in entomologic indexes

Anopheles auch Malaria-, Gabel-
oder Fiebermücken genannt, ist eine Gattung in der Familie der Stechmücken (Culicidae) und namensgebend für die Unterfamilie Anophelinae. Die Gattung umfasst etwa 420 Arten, wobei weltweit rund 40 Arten als Überträger von Malaria auftreten können. Malariamücken sind mit etwa sechs Millimetern relativ klein und haben einen schmächtigen Körperbau, sind aber dennoch an ihrer Körperhaltung gut erkennbar: der Körper befindet sich meistens in einem Winkel von etwa 30 bis 45° zum Untergrund. Es gibt zahlreiche Arten und Unterarten, die teilweise aufgrund ihrer großen Ähnlichkeit nur von Spezialisten zu unterscheiden sind.

Permethrin ist ein Insektizid und Akarizid und gehört zur Gruppe der Pyrethroide. Es wirkt als Kontakt- und Fraßgift. In Deutschland ist es zur Behandlung der Krätze (Scabies) zugelassen. Zudem wird es in der Therapie von Kopf- und Filzläusen eingesetzt. Permethrin wirkt auf Natriumkanäle in den Nervenzellmembranen. Zunächst werden diese sensorisch erregt, dann folgen Koordinationstsörungen und der Tod der Milben tritt durch Paralyse ein.

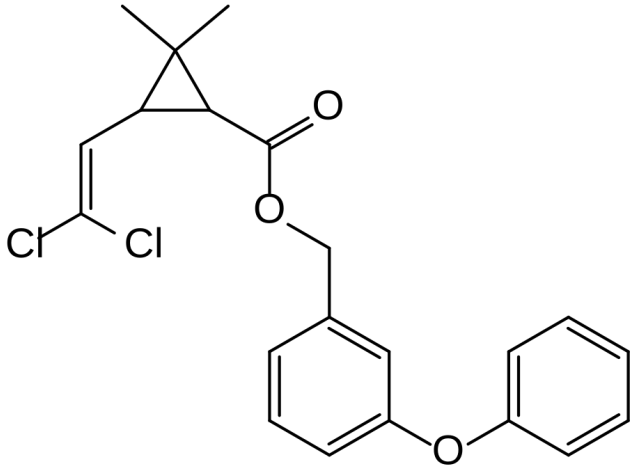

Permethrin-Treated Baby Wraps for the Prevention of Malaria

Malaria remains a major cause of childhood death in sub-Saharan Africa. We leveraged the traditional practice of mothers carrying children on their backs in cloth wraps to assess whether treating the wraps with an insect repellent might provide a layer of protection against malaria.
In a double-blind, randomized, placebo-controlled trial conducted in Uganda, we enrolled adult women with a child who was 6 to 18 months of age. The mother–child pairs were randomly assigned in a 1:1 ratio to use permethrin-treated wraps (intervention group) or sham-treated wraps (control group). The wraps underwent retreatment every 4 weeks. All the participants received a new, pyrethroid-only long-lasting insecticide-treated bed net. The participants visited the trial clinics every 2 weeks for 24 weeks and made unscheduled visits in the case of febrile illness in the children. The primary outcome was clinical malaria in the children, as defined by fever and a positive malaria rapid diagnostic test.

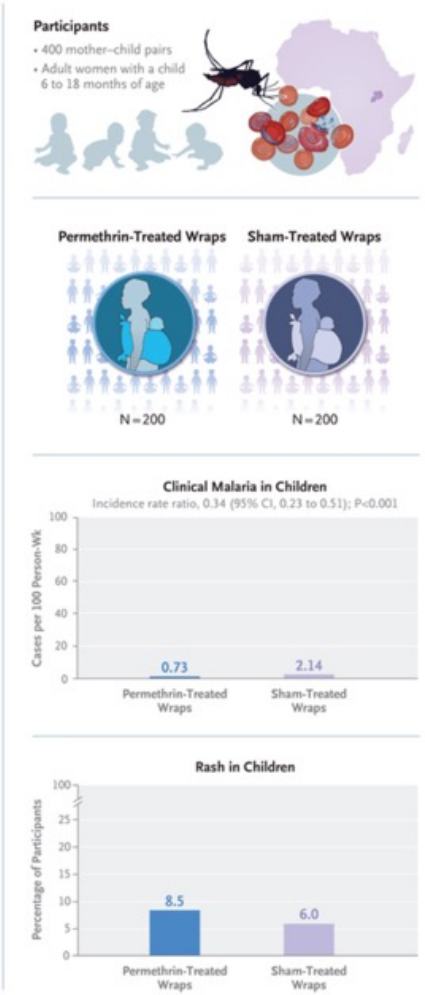

Despite gains in recent decades, progress against malaria has stalled. In 2023, nearly 600,000 deaths from malaria were reported. Approximately 95% of these deaths occurred in the World Health Organization African region, and most occurred in children younger than 5 years of age. Insecticide resistance and increases in outdoor mosquito biting during dawn and dusk hours are driving persistent transmission. Seasonal malaria chemoprevention in which children receive antimalarial medications during peak periods has proved to be effective, but its feasibility and sustainability in areas with perennial transmission is less certain. Malaria vaccines may address these gaps, but existing vaccines are characterized by waning protection and appear to be less effective in infants than in young children. Therefore, complementary innovations are needed.

Treatment and Use of Baby Wraps.

The baby wraps used in the trial were treated with a 0.5% solution of permethrin (Panel A) or underwent a sham treatment with water. Participating mothers were assigned to use either the permethrin-treated wraps or the sham-treated wraps to carry their children during the trial period (Panels B and C).

Interventions

We obtained swathes of waxed cotton cloth measuring 2 m by 1 m from a local vendor on the basis of information obtained during pilot testing. The wraps that were to be given to the intervention group were soaked in a permethrin solution diluted to 0.5% in accordance with instructions from the manufacturer (Sawyer Products) and were allowed to dry. We chose permethrin because of its demonstrated efficacy, commercial availability, and established safety record. The wraps that were to be given to the control group underwent a sham treatment by being soaked in water. There was no difference in the material or the appearance of the wraps that were distributed to the two groups. However, permethrin has a distinct odor that could not be masked. At the first clinic visit (week 0), the participants who had been assigned to the intervention group received two wraps that had been treated with permethrin, and those in the control group received two sham-treated wraps. The wraps underwent retreatment every 4 weeks during trial visits. All the participants also received a new, pyrethroid-only long-lasting insecticide-treated bed net .

Outcomes

The primary outcome was clinical malaria in the children, as defined by fever (temperature of ≥38.0°C) or reported fever within the previous 24 hours and a positive malaria rapid diagnostic test.

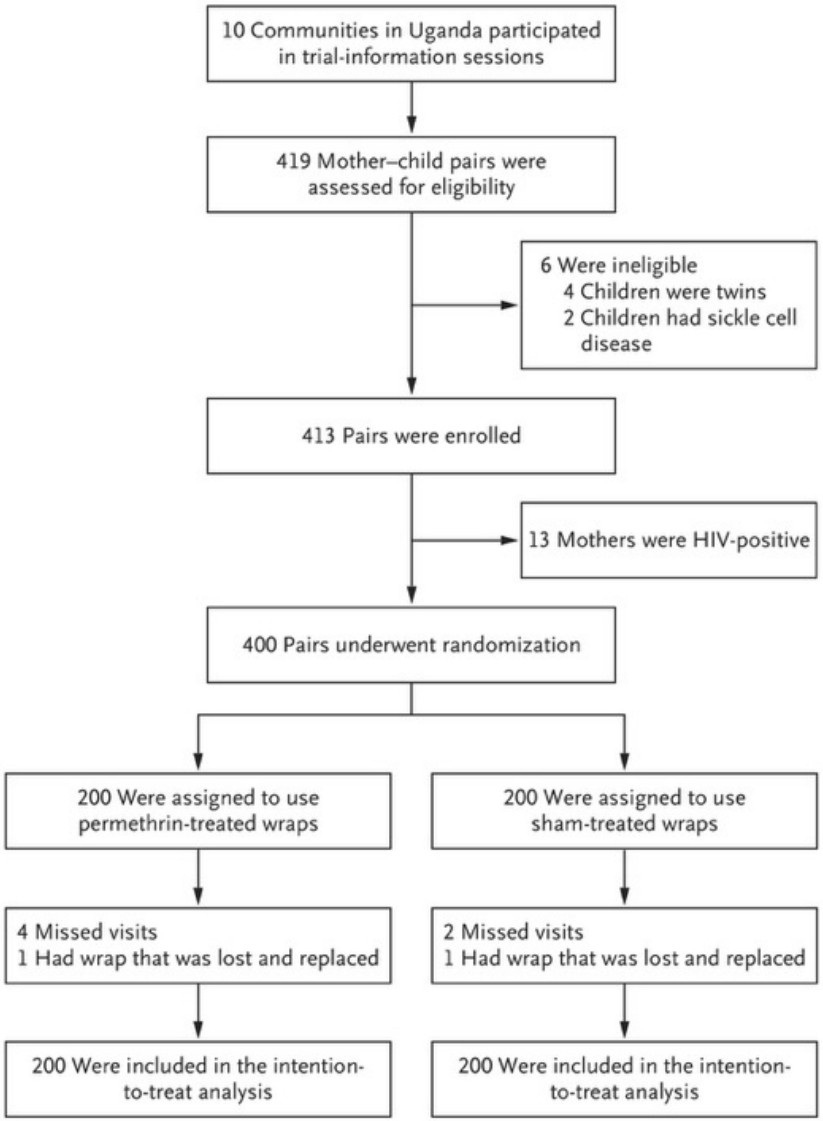

Characteristic	Permethrin-Treated Wraps (N=200)	Sham-Treated Wraps (N=200)
Children		
Female sex — no. (%)	98 (49.0)	94 (47.0)
Median age (IQR) — mo	12.0 (8.0–15.0)	11.0 (8.0–14.0)
Age group — no. (%)		
6–11 mo	98 (49.0)	103 (51.5)
12–18 mo	102 (51.0)	97 (48.5)
Place of birth — no. (%)		
Public health center	129 (64.5)	134 (67.0)
Public hospital	28 (14.0)	23 (11.5)
Private facility	34 (17.0)	28 (14.0)
Home	9 (4.5)	14 (7.0)
Other	0	1 (0.5)
Mothers		
Median age (IQR) — yr	26.5 (22.0–32.0)	25.0 (21.0–30.2)
Median maternal parity (IQR)	3.0 (1.0–5.0)	3.0 (1.0–4.0)
Highest education level — no. (%)		
Primary	117 (58.5)	122 (61.0)
Ordinary level	66 (33.0)	70 (35.0)
Advanced level	2 (1.0)	1 (0.5)
University or tertiary	10 (5.0)	5 (2.5)
Missing data	5 (2.5)	2 (1.0)
Households		
Median no. of household members (IQR)	6.0 (5.0–7.0)	6.0 (5.0–7.0)
Floor material of home — no. (%)		
Earth or sand	129 (64.5)	118 (59.0)
Concrete, cement, bricks, or tiles	70 (35.0)	82 (41.0)
Other	1 (0.5)	0
Primary source of drinking water — no. (%)		
Piped	63 (31.5)	74 (37.0)
Public tap	40 (20.0)	43 (21.5)
Well or borehole	47 (23.5)	41 (20.5)
Surface water	50 (25.0)	42 (21.0)
Owns livestock — no./total no. (%)	88/200 (44.0)	91/198 (46.0)
Electricity in home — no./total no. (%)	32/199 (16.1)	44/199 (22.1)
Malaria and care seeking		
Median no. of long-lasting insecticide-treated bed nets in household (IQR)	1.0 (1.0–2.0)	1.0 (1.0–2.0)
Median participant-reported travel time to nearest health facility (IQR) — min	24.0 (19.5–28.0)	24.0 (18.0–28.5)
Care sought in previous 2 wk for fever in child — no. (%)	59 (29.5)	61 (30.5)
Any drug given to a child for fever in previous 2 wk — no. (%)	66 (33.0)	71 (35.5)
Clinical characteristics of the children		
Median mid-upper-arm circumference (IQR) — cm	14.3 (13.6–15.2)	14.3 (13.8–15.1)
Malnutrition category — no. (%)†		
Severe acute malnutrition	0	0
Moderate acute malnutrition	37 (18.5)	30 (15.0)
Adequately nourished	163 (81.5)	170 (85.0)
Median hemoglobin level (IQR) — g/dl	12.0 (10.7–13.0)	11.9 (10.6–12.9)
Positive malaria rapid diagnostic test at household visit — no. (%)	20 (10.0)	21 (10.5)
Malaria rapid diagnostic testing performed at first clinic visit — no. (%)	27 (13.5)	35 (17.5)
Positive malaria rapid diagnostic test at first clinic visit — no./total no. (%)	3/27 (11.1)	5/35 (14.3)

Clinical Malaria in the Children.

Variable	Permethrin-Treated Wraps (N=200)	Sham-Treated Wraps (N=200)	Difference in Incidence Rates (95% CI)	Incidence Rate Ratio (95% CI)
Cases of clinical malaria	34	94	—	—
Time at risk — person-wk	4641	4395	—	—
Incidence rate — cases/100 person-wk	0.73 (0.51 to 1.02)	2.14 (1.73 to 2.62)	−1.41 (−2.03 to −0.83)	0.34 (0.23 to 0.51)†
Age 6–11 mo	0.66 (0.37 to 1.09)	2.07 (1.52 to 2.76)	−1.42 (−2.22 to −0.70)	0.32 (0.18 to 0.57)
Age 12–18 mo	0.80 (0.48 to 1.26)	2.21 (1.62 to 2.94)	−1.41 (−2.39 to −0.51)	0.36 (0.21 to 0.62)

Secondary Outcomes in the Children.

Outcome	Permethrin-Treated Wraps (N=200)	Sham-Treated Wraps (N=200)	Difference (95% CI)
Hospitalization for malaria — no. (%)	7 (3.5)	17 (8.5)	−5.0 (−10.3 to −0.2)†
Change in hemoglobin level — g/dl			
Baseline to wk 12	0.76	0.81	−0.05 (−0.34 to 0.25)
Baseline to wk 24	1.19	1.34	−0.15 (−0.51 to 0.22)
Change in mid-upper-arm circumference — cm			
Baseline to wk 12	0.65	0.60	0.05 (−0.10 to 0.20)
Baseline to wk 24	1.27	1.27	0.00 (−0.17 to 0.16)
Change in height-for-weight z score			
Baseline to wk 12	0.46	0.49	−0.03 (−0.26 to 0.20)
Baseline to wk 24	0.74	0.78	−0.04 (−0.31 to 0.23)
Change in height-for-age z score			
Baseline to wk 12	−0.02	0.03	−0.06 (−0.24 to 0.12)
Baseline to wk 24	0.09	0.18	−0.09 (−0.34 to 0.16)
Change in weight-for-age z score			
Baseline to wk 12	0.38	0.45	−0.07 (−0.22 to 0.09)
Baseline to wk 24	0.65	0.75	−0.10 (−0.29 to 0.08)

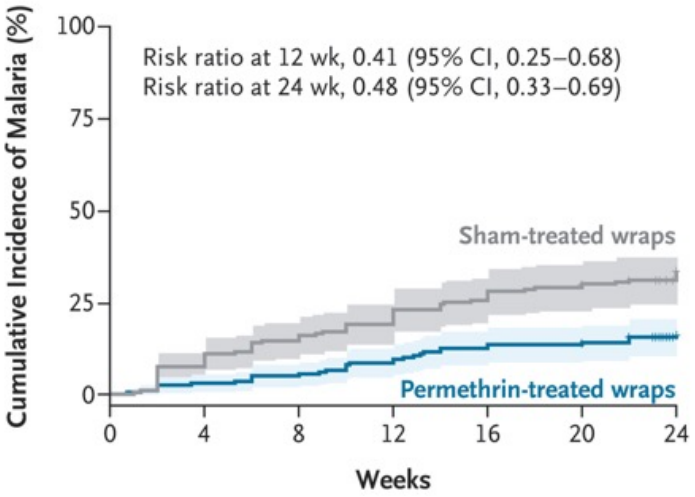

Cumulative Incidence of a First Episode of Clinical Malaria in the Children.

The shaded areas indicate 95% confidence intervals, and the tick marks indicate censored data.

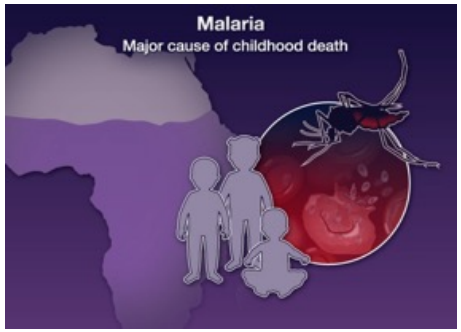
Malaria
Major cause of childhood death

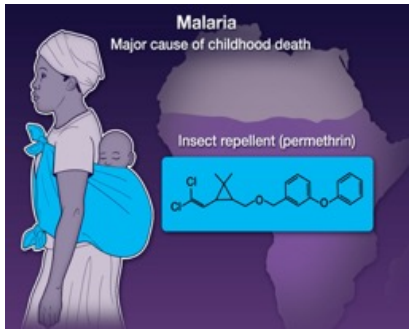
Malaria
Major cause of childhood death
Insect repellent (permethrin)


Intervention Group
Permethrin-treated wraps
+ new bed net
Control Group
Sham-treated wraps
+ new bed net
24 weeks
• Attended trial clinics every 2 weeks
• Wraps treated every 4 weeks
N=200
N=200


Women and Children in Western Uganda
With access to bed nets
Maternal use of
permethrin-treated wraps
led to lower incidence of
malaria in children

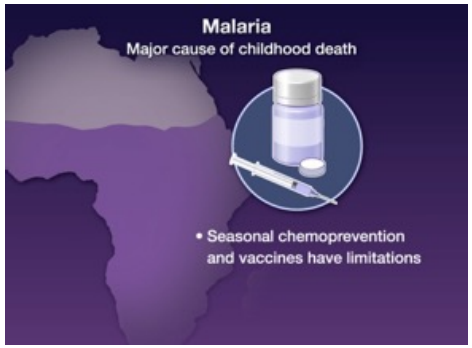
Malaria
Major cause of childhood death
• Seasonal chemoprevention
and vaccines have limitations


Trial
• Randomized
• Double-blind
• Placebo-controlled
• Western Uganda
400 women with
a child 6 to 18
months old

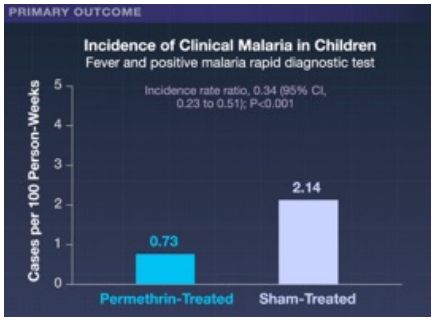
PRIMARY OUTCOME
Incidence of Clinical Malaria in Children
Fever and positive malaria rapid diagnostic test
Incidence rate ratio, 0.34 (95% CI,
0.23 to 0.51); P<0.001
Cases per 100 Person-Weeks
0
1
2
3
4
5
0.73
2.14
Permethrin-Treated
Sham-Treated


Malaria
Major cause of childhood death

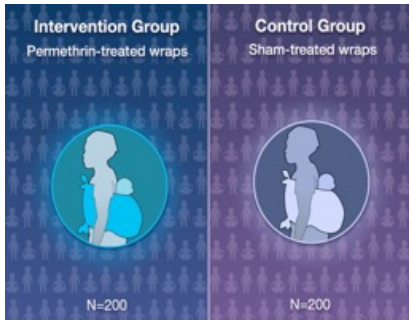
Intervention Group
Permethrin-treated wraps
Control Group
Sham-treated wraps
N=200
N=200

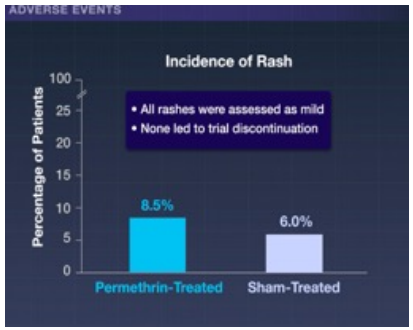
ADVERSE EVENTS
Incidence of Rash
• All rashes were assessed as mild
• None led to trial discontinuation
Percentage of Patients
0
5
10
15
20
25
100
8.5%
6.0%
Permethrin-Treated
Sham-Treated

Pseudotumor cerebri ist der früher verwendete Name für idiopathische intrakranielle Hypertension (IIH), eine Erkrankung, bei der der Hirndruck ohne erkennbare Ursache stark ansteigt. Hauptsymptome sind chronische Kopfschmerzen und Sehstörungen wie verschwommenes Sehen oder Gesichtsfeldausfälle, die bis zur Erblindung führen können. Die Behandlung umfasst Gewichtsabnahme, Medikamente wie Azetazolamid sowie bei schweren Fällen Eingriffe wie Lumbalpunktionen, Shunt-Anlagen oder die endovaskuläre Stentimplantation, um den Hirndruck zu senken.

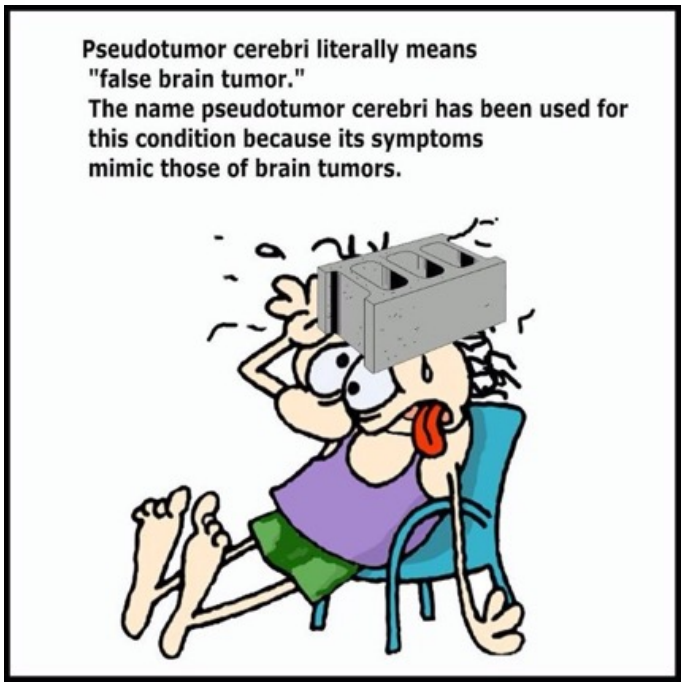

Idiopathic Intracranial Hypertension

In the early 20th century, soon after the technique of lumbar puncture was devised, Max Nonne, a German neurologist, described a syndrome of headache accompanied by swollen optic disks in patients with raised cerebrospinal fluid (CSF) pressure. He called the condition “pseudotumor cerebri,” because none of the patients proved to have a brain tumor. This name is still used, although it has largely been supplanted by the term “idiopathic intracranial hypertension.” This review explores current ideas about the disease, with emphasis on the importance of dural venous sinus stenosis and new treatment options.

Clinical Diagnosis

More than 95% of patients with idiopathic intracranial hypertension are women of childbearing age with obesity. Men are seldom affected, for unknown reasons. Even among women with obesity the disease is rare; it occurs in about 1 in 500 female persons with a body-mass index (the weight in kilograms divided by the square of the height in meters) higher than 30. The prevalence of the disease is rising, driven by surging obesity rates. A history of recent weight gain often precedes the onset of symptoms. Idiopathic intracranial hypertension can occur in children, but before puberty the association with obesity and female sex is less marked.

KEY POINTS

Idiopathic Intracranial Hypertension

- Idiopathic intracranial hypertension, also called pseudotumor cerebri, refers to elevated cerebrospinal fluid (CSF) pressure that develops most often in women of reproductive age with obesity, causing headache, neck pain, pulsatile tinnitus, and visual symptoms.
- Funduscopic examination is critical to identifying papilledema, which is present in 95% of affected patients.
- Magnetic resonance imaging rules out hydrocephalus or tumor and reveals characteristic findings that include a partially empty sella, distended optic-nerve sheaths, protrusion of the optic disks into the vitreous cavity, and stenosis of the distal transverse dural sinuses.
- Lumbar puncture shows a high opening pressure and normal CSF, but ambiguous readings can occur because of overlap in the range of pressures recorded in patients with idiopathic intracranial hypertension and in unaffected persons.
- Nearly all patients can be treated medically with acetazolamide to reduce CSF production and with agonists to glucagon-like peptide-1 or gastric inhibitory polypeptide to induce weight loss.
- Prompt surgical intervention is necessary if papilledema threatens vision.
- CSF shunting has been the standard surgical treatment; however, dural venous sinus stenting, which breaks the positive feedback cycle driving high intracranial pressure, is gaining wider acceptance.

A Severe Papilledema with Retinal Hemorrhages and Exudates

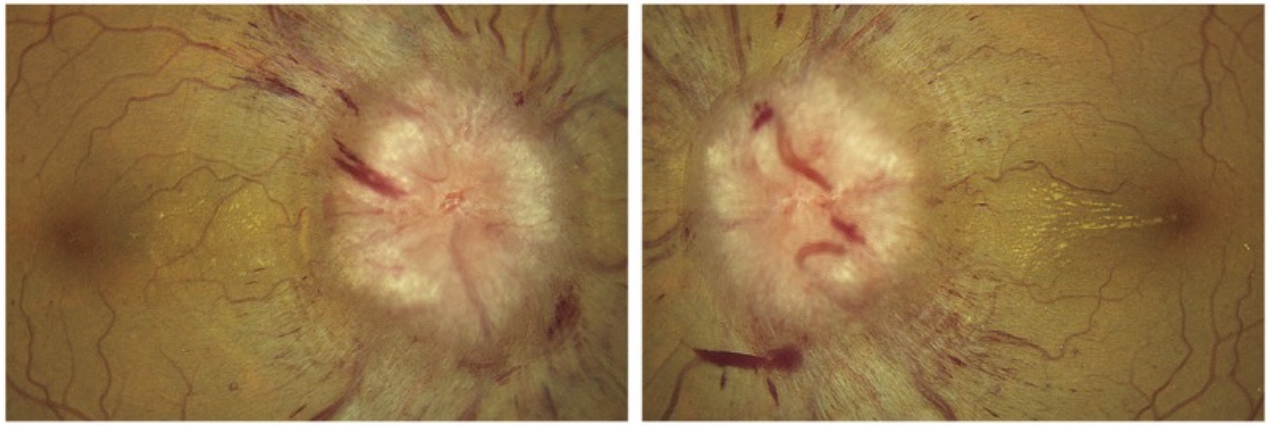

B Resolving Papilledema after ICP Reduction by Venous Sinus Stenting Followed by Shunt Repair

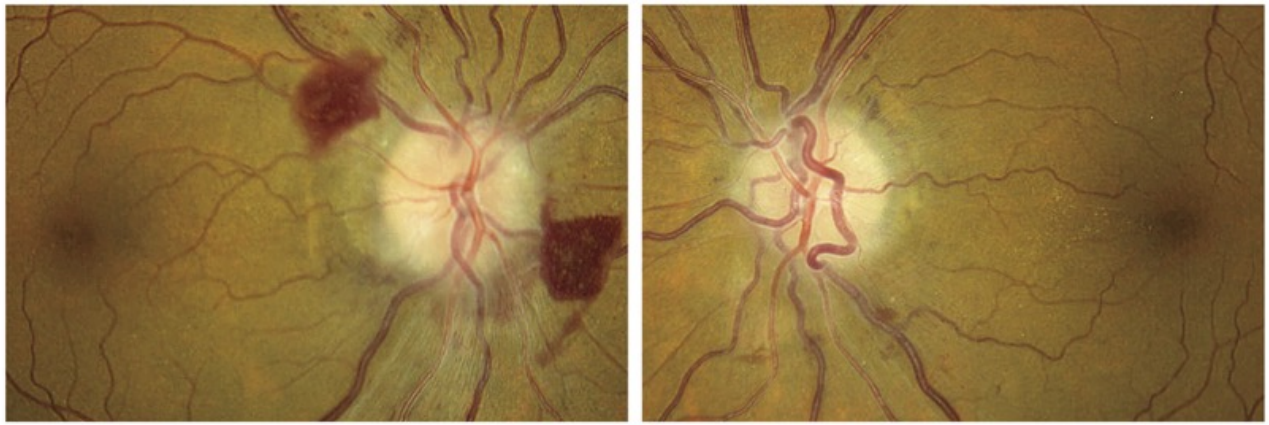

Papilledema before and after Surgical Treatment of Idiopathic Intracranial Hypertension.

A 46-year-old woman with a body-mass index of 33.7 had new onset of headaches followed by transient visual obscurations. A lumboperitoneal shunt had been implanted 20 years earlier after a diagnosis of idiopathic intracranial hypertension was made. The funduscopic images in Panel A show severe papilledema in the right and left eyes with hemorrhages and exudates. A shunt study revealed no drainage of a radioactive tracer into the abdomen, which confirmed shunt occlusion. Panel B shows the right and left fundi 3 months later, with resolving papilledema after reduction in intracranial pressure (ICP) by venous sinus stenting followed by shunt repair.

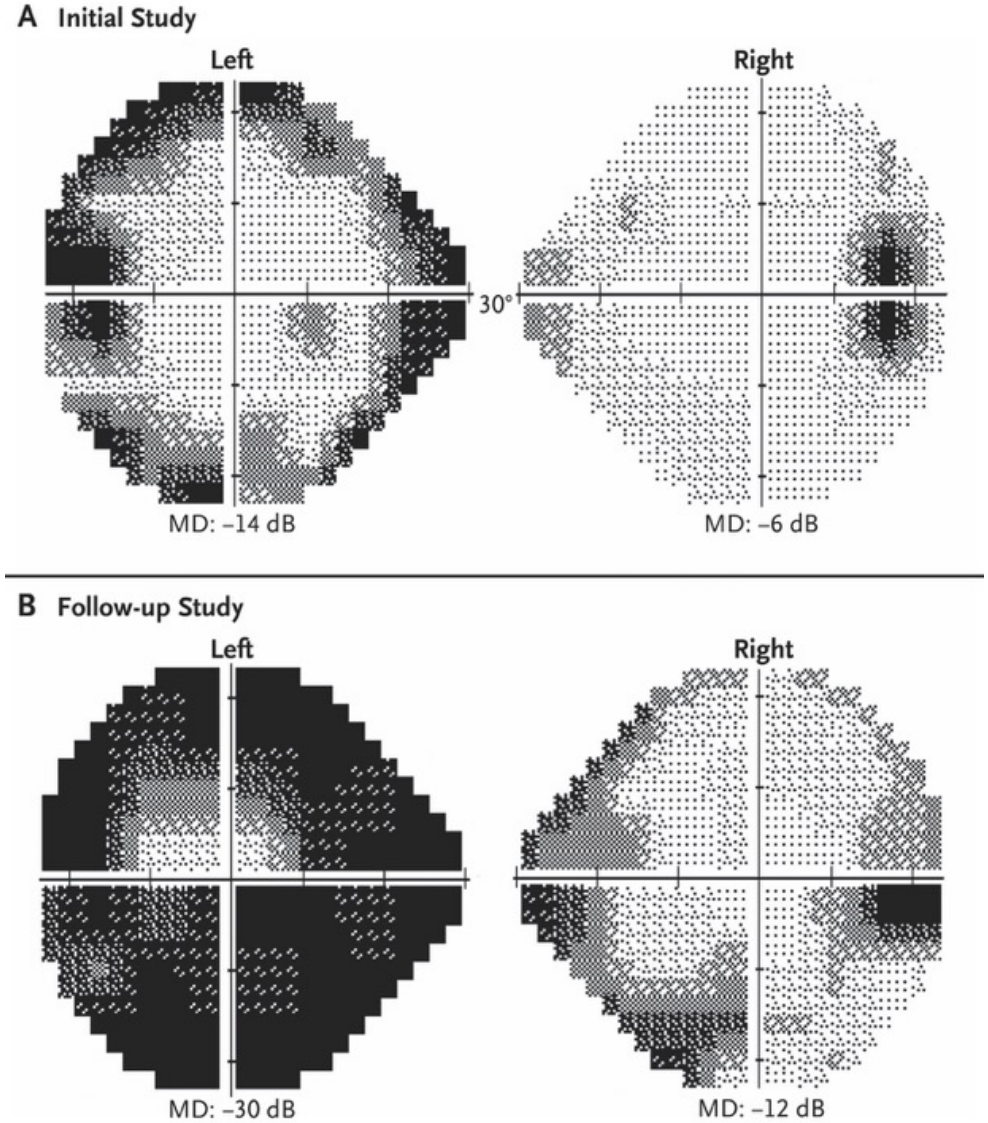

Humphrey Visual Fields.

Panel A shows the initial Humphrey visual field study in the patient from Figure 1, performed the same day as the fundus imaging, showing bilateral blind-spot enlargement and peripheral constriction of the visual field in the left eye. Acuity was 20/20 in each eye. Panel B shows the follow-up visual fields 3 months later, showing severe constriction of the field in the left eye and moderate constriction in the right eye. Acuity remained 20/20 in the right eye; however, the acuity in the left eye progressively declined to 20/800 after stenting and then recovered to 20/60 after shunt revision. Shown for each eye is the mean deviation (MD) in decibels (dB) of retinal sensitivity as compared with a normal visual field. A value of –30 dB indicates the average retinal sensitivity was reduced by 3 log units.

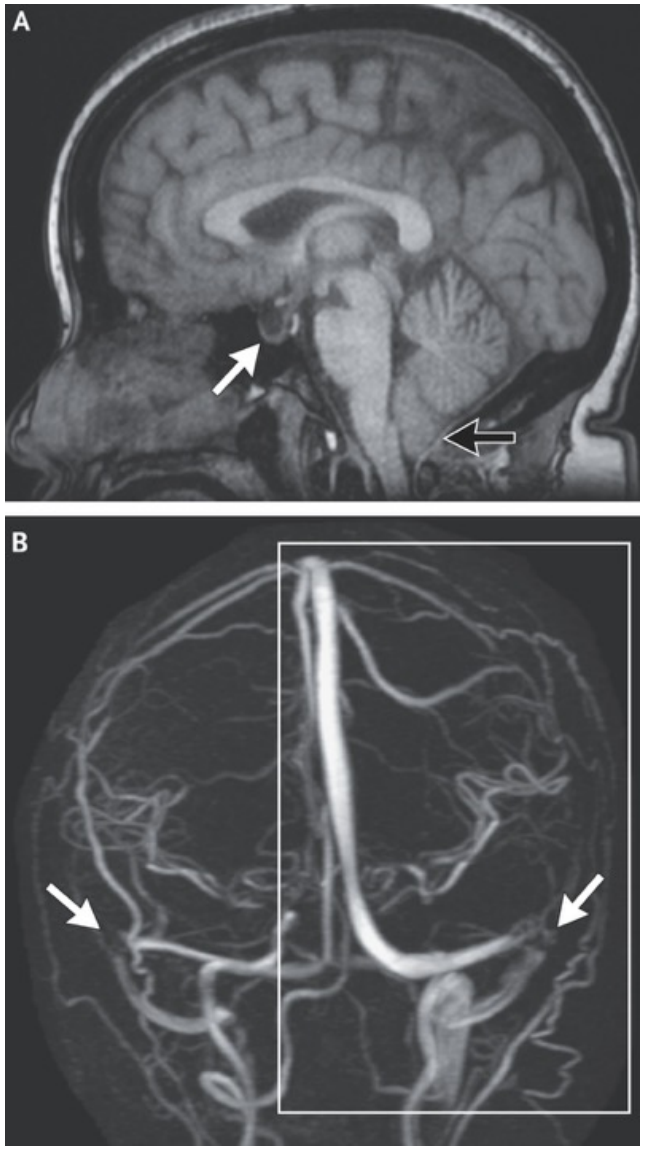

MRI Scans in Idiopathic Intracranial Hypertension.

Panel A shows an MRI (sagittal T1-weighted view without contrast) of the patient from Figure 1 showing typical findings in idiopathic intracranial hypertension: a partially empty sella (white arrow) and a 6-mm descent of the cerebellar tonsils below the foramen magnum (black arrow), possibly caused in part by a pressure gradient induced by the lumboperitoneal shunt. Panel B is a noncontrast three-dimensional phase-contrast magnetic resonance venogram image showing stenosis (arrows) in both distal transverse dural sinuses. The area inside the rectangle is the portion of the venous system shown in Figure 5.

Postulated Mechanism of Idiopathic Intracranial Hypertension.

Weight gain increases central venous pressur which increases dural venous sinus pressure and ICP. The increased ICP compresses the dural venous sinuses, worsening venous hypertension. The cause of stenosis becomin focal at the junction of the transverse and sigmoid sinuses remains unexplained. Weigh loss and acetazolamide induce remission, presumably by reversing the positive feedbac cycle that drives intracranial hypertension. CS denotes cerebrospinal fluid.

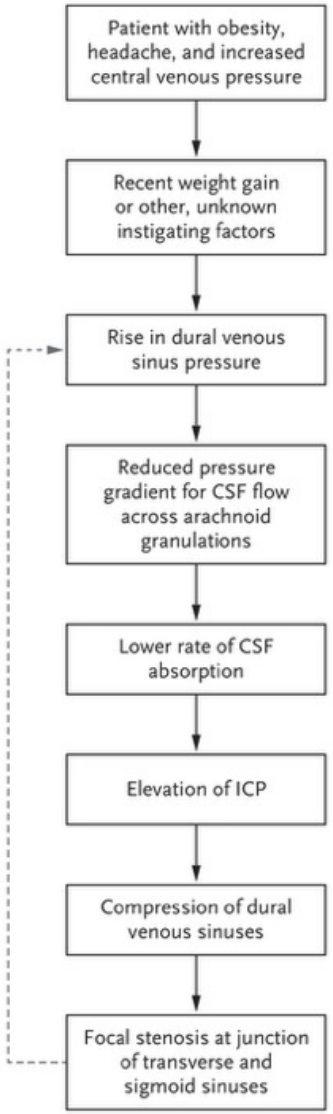

Diagnostic and Therapeutic Aspects of Measuring CSF Pressure

If neuroimaging has eliminated a mass lesion or venous thrombosis from consideration, a lumbar puncture is usually performed to measure the lumbar subarachnoid opening pressure and to sample the CSF. A manometer reading that is higher than 25 cm of water (18.4 mm Hg) when measured with the patient in the lateral decubitus position is considered to be diagnostic for idiopathic intracranial hypertension if the CSF composition is normal and the clinical circumstances are appropriate.

Treatment

Most patients with suspected idiopathic intracranial hypertension can be treated in an outpatient setting, provided the evaluation is performed expeditiously. Referral to an emergency department is appropriate if there is vision loss. Many patients with the disease have limited insurance coverage and come to emergency departments to access health care.

Medical Treatment

Weight reduction combined with oral acetazolamide have been the mainstays of treatment for idiopathic intracranial hypertension. Acetazolamide inhibits carbonic anhydrase, an enzyme that mediates CSF secretion. The usual dose is a 500-mg extended-release capsule taken two to four times per day. Escalating the dose over several days may reduce side effects such as nausea and paresthesias of the hands and feet.

Surgical Treatment

Occasionally, drastic vision loss, fulminant papilledema, and elevated ICP develop in patients who have had symptoms for only a few days or weeks. Such cases support the theory that idiopathic intracranial hypertension can smolder undetected and then erupt when dural sinus stenosis causes a sudden rise in ICP.

Fenestration of the Optic-Nerve Sheath

In fenestration of the optic-nerve sheath, an ophthalmologist creates an aperture in the optic-nerve sheath just behind the globe, relieving papilledema by allowing CSF to drain into the orbit. Sometimes, papilledema improves in the contralateral eye as well, but usually the operation must be done bilaterally.

Dural Venous Sinus Stent

To place a dural venous sinus stent, with the patient under general anesthesia, an interventional radiologist threads a stent across the stenosis affecting the dominant transverse sinus after first verifying that a sizable venous pressure gradient exists across the region. The appealing feature of this procedure is that it corrects the anatomical obstruction that is considered central to the self-reinforcing rise in ICP.

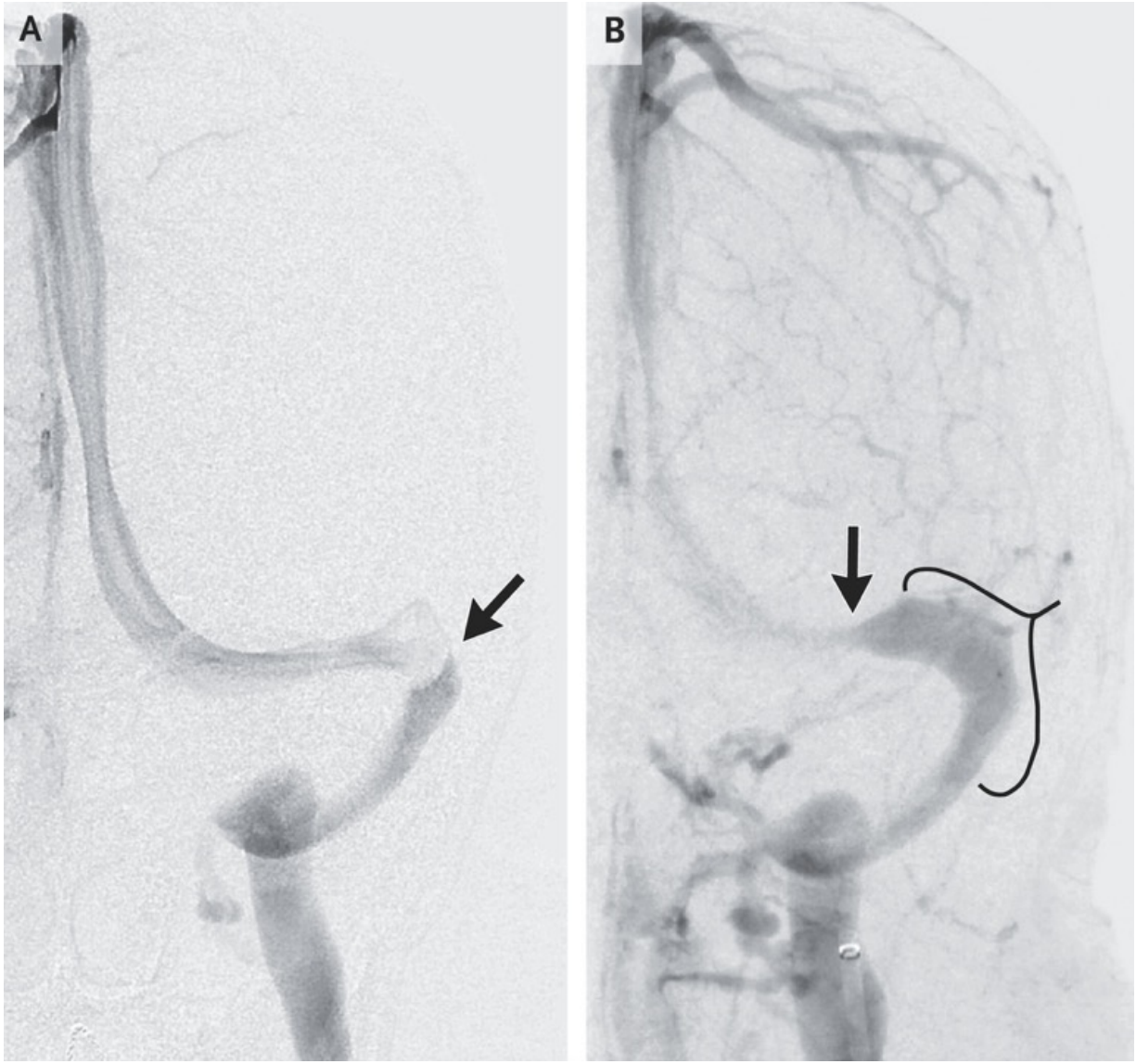

Stenting of the Dominant Transverse Sinus.

Panel A shows a catheter angiography image of the venous phase after contrast injection into the carotid artery in the patient from Figure 1, confirming stenosis of the distal left transverse sinus before treatment (arrow). A stent was placed because the patient's lumboperitoneal shunt was occluded, but her vision continued to worsen. Panel B shows a follow-up study 6 weeks later with a new stenosis (arrow) upstream from the stent (bracket). A second stent (not shown) was placed across the new stenosis, but the patient's visual acuity continued to decline. A month later, the lumboperitoneal shunt was revised, leading to partial recovery of acuity to 20/60 in the left eye, but the visual field remained severely constricted (Fig. 2B).

Conclusions and Future Directions

The rising prevalence of obesity has increased the population at risk for idiopathic intracranial hypertension. Diagnosis is challenging when papilledema is subtle or absent and ICP barely exceeds the normal range. Discovery of a noninvasive technique for accurate measurement of ICP would facilitate the evaluation of patients with headache from suspected idiopathic intracranial hypertension. Neuroimaging has furnished an important clue to the mechanism of this disease by revealing focal stenosis of the distal transverse sinuses, which activates a positive feedback cycle that drives ICP elevation. This cycle can be broken by treatment with GLP-1 or gastric inhibitory polypeptide agonists to induce weight loss and acetazolamide to reduce CSF production. When papilledema is severe enough to threaten irreversible vision loss, a surgical procedure is performed urgently to prevent blindness. Randomized trials are needed to determine which of the two most common operations — CSF shunting or venous sinus stenting — is superior. The optimal care of patients with severe idiopathic intracranial hypertension is complex, with the potential for permanent impairment of vision despite appropriate treatment.

Butterfly Vertebra

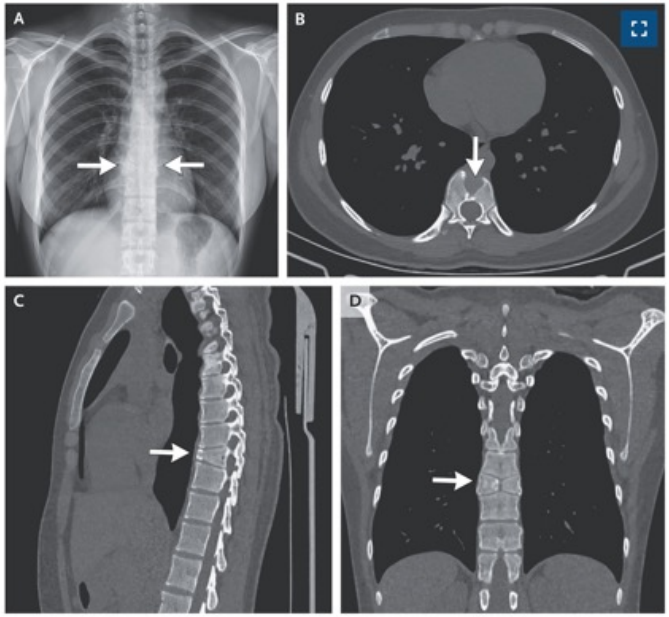

A 21-year-old woman who had presented to the pulmonary clinic with a 7-day history of sore throat and cough was noted to have a vertebral abnormality on chest radiograph. She reported no history of back pain. Physical examination was notable only for mild pharyngeal erythema. A chest radiograph showed normal lungs and two hemivertebrae (Panel A, arrows) at the ninth thoracic vertebral body (T9). Subsequent computed tomography of the chest showed a sagittal cleft (Panel B, arrow, axial view), anterior wedging (Panel C, arrow, parasagittal view), and symmetric, triangular hemivertebrae resembling the wings of a butterfly at T9 (Panel D, arrow, coronal view). A diagnosis of a butterfly vertebra was made. A butterfly vertebra is a rare congenital anomaly that results from a lack of fusion of the two lateral ossification centers during embryonic development. It is usually asymptomatic and discovered incidentally on imaging, most commonly in the thoracic and lumbar spine. A butterfly vertebra may occur in isolation or be associated with other congenital anomalies. Reassurance regarding the benign nature of the vertebral finding was provided. Supportive care was recommended for the patient's cough and sore throat, which were attributed to an upper respiratory infection.

Oral Verruciform Xanthomas

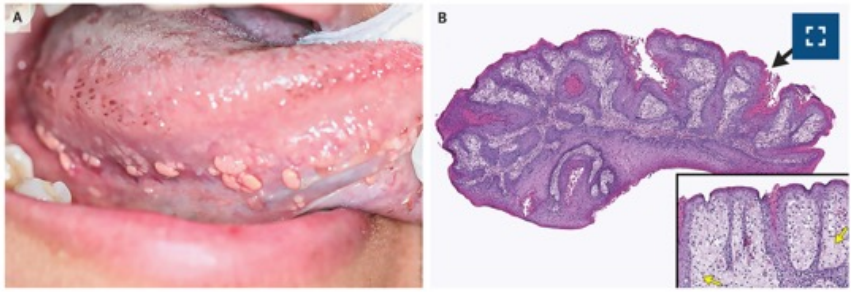

A previously healthy 22-year-old woman presented to the oral medicine clinic with a 3-month history of bumps on the right ventral surface of her tongue. She had no history of tobacco or alcohol use and was monogamous with one sexual partner. The lesions had been previously diagnosed as condyloma acuminatum. On physical examination, the bumps were observed to be pink papillomatous lesions measuring 3 to 8 mm in diameter (Panel A). Testing for human immunodeficiency virus infection and syphilis was negative. Histopathological analysis of an excised lesion revealed acanthotic, papillary, and parakeratinized epithelium (Panel B, black arrow) with an accumulation of large cells with foamy cytoplasm in the connective tissue (inset, yellow arrows). The foamy cells stained positive for CD68 on immunohistochemical analysis, which confirmed that they were macrophages. In situ hybridization for human papillomavirus infection was negative. A diagnosis of oral verruciform xanthomas — benign growths of the mucosa characterized by the presence of parakeratosis and foamy macrophages — was made. The cause of oral verruciform xanthomas is unknown, but they may result from trauma and chronic inflammation. Surgical excision is curative. In this case, surgical excision was offered, but the patient declined owing to the asymptomatic nature of the lesions. The lesions have remained stable in both number and size over 6 months of follow-up.

Case 28-2025: A 36-Year-Old Man with Abdominal Pain, Fever, and Hypoxemia

The patient had been in his usual state of health, which included alcohol use disorder characterized by binge drinking, until 2 weeks before the current presentation, when mild, dull pain developed in the right lower abdomen and right lower back. Five days before the current presentation, the patient had body aches and subjective fever. The next day, he was evaluated in the urgent care center affiliated with his primary care physician's office. The examination was normal; laboratory test results are shown. Urinalysis was normal, and screening tests for influenza virus types A and B and severe acute respiratory syndrome coronavirus 2 were negative. Treatment with intravenous fluids and intravenous ketorolac was administered. The abdominal pain resolved, and the patient was discharged home.

Three days before the current presentation, abdominal pain recurred, and diarrhea developed. The patient took acetaminophen and ibuprofen, but the pain did not abate. One day before the current presentation, nausea with vomiting developed, and the patient was again evaluated in the same urgent care center. He reported no intake of alcohol since the previous evaluation. In addition, he reported new dyspnea and cough. The temporal temperature was 36.9°C, the pulse 115 beats per minute, the blood pressure 89/64 mm Hg, and the respiratory rate 20 breaths per minute. The oxygen saturation was 85% while the patient was breathing ambient air and increased to 98% while supplemental oxygen was delivered through a nasal cannula at a rate of 4 liters per minute. The patient was ill-appearing, with increased work of breathing and crackles over the posterior lung fields on auscultation. Scleral icterus was present. He had tenderness and guarding on palpation in the right upper abdomen. After the administration of 2 liters of intravenous fluids, the blood pressure was 78/60 mm Hg. The patient was transferred to the emergency department of this hospital for further evaluation.

Laboratory Data.

Variable	Reference Range, Adults, Urgent Care Clinic	4 Days before Current Presentation, Urgent Care Clinic	Reference Range, This Hospital†	On Current Presentation, This Hospital	15 Hours after Current Presentation, This Hospital	Day 1, This Hospital	Day 2, This Hospital
Hematocrit (%)	38.5–50.0	39.9	41–53	37.6	31.8	31.6	32.5
Hemoglobin (g/dl)	13.2–17.1	13.9	13.5–17.5	13.1	11.1	10.6	10.9
White-cell count (per μl)	3800–10,800	10,000	4500–11,000	4700	12,220	9380	7950
Differential count (per μl)							
Neutrophils	1500–7800	9090	1800–7700	4320	11,600	8600	5930
Lymphocytes	850–3900	310	1000–4800	290	420	670	1190
Monocytes	200–950	530	200–1200	40	100	330	710
Eosinophils	20–500	30	0–900	50	100	0	20
Basophils	0–200	10	0–300	10	0	90	20
Platelet count (per μl)	140,000–400,000	213,000	150,000–400,000	24,000	53,000	51,000	64,000
Alkaline phosphatase (U/liter)	53–128	71	45–115	464	221	210	203
Alanine aminotransferase (U/liter)	10–47	29	10–55	28	26	27	29
Aspartate aminotransferase (U/liter)	11–38	28	10–40	38	38	41	42
Total bilirubin (mg/dl)	0.2–1.6	1.6	0.0–1.0	3.4	2.6	3.0	1.7
Direct bilirubin (mg/dl)	—	—	0.0–0.3	3.2	2.3	2.5	1.3
Total protein (g/dl)	6.4–8.1	6.9	6.0–8.3	5.3	5.4	5.6	5.1
Albumin (g/dl)	3.3–5.5	3.6	3.3–5.0	2.4	2.3	2.5	2.3
Lipase (U/liter)	—	—	13–60	15	—	—	—
Partial thromboplastin time (sec)	—	—	24.0–37.5	27.8	30.3	28.8	29.5
International normalized ratio	—	—	0.9–1.1	1.2	1.1	1.2	1.1
Prothrombin time (sec)	—	—	10.0–13.0	13.5	12.9	13.3	12.5
Reticulocyte count (%)	—	—	0.5–2.5	0.8	—	0.5	<0.5
Lactate dehydrogenase (U/liter)	—	—	110–210	747	188	182	149
Haptoglobin (mg/dl)	—	—	30–200	226	275	278	294
Ferritin (μl/liter)	—	—	20–300	767	—	—	—
Fibrinogen (mg/dl)	—	—	200–400	727	—	962	—
D-dimer (ng/ml)	—	—	<500	>7650	—	—	—
Lactic acid (mmol/liter)	—	—	0.5–2.0	2.5	1.7	1.4	—
C-reactive protein (mg/liter)			<8	325.2			
Sodium (mmol/liter)	—	—	135–145	140	141	139	135
Potassium (mmol/liter)	—	—	3.4–5.0	3.0	3.5	3.0	3.5
Chloride (mmol/liter)	—	—	98–108	109	110	105	103
Carbon dioxide (mmol/liter)	—	—	23–32	18	21	22	25
Urea nitrogen (mg/dl)	—	—	8–25	23	17	13	12
Creatinine (mg/dl)	—	—	0.60–1.50	0.98	0.86	0.88	0.62

Arterial blood gases before and after O2 administration?

In the emergency department, the patient reported that intermittent subjective fevers had continued after discharge from the urgent care clinic 4 days earlier. No exacerbating or relieving factors were associated with the abdominal pain. The cough was productive of tan sputum. He typically drank 4 or 5 beers nightly during the week and up to 12 beers nightly on most weekends; previous treatment for alcohol use disorder included naltrexone, which he had stopped taking 3 months before the current presentation. Additional medical history included gastroesophageal reflux disease (GERD), which was thought to have been exacerbated by his intake of alcohol and highly caffeinated beverages; a 1-month course of pantoprazole had been prescribed 8 months before the current presentation, and symptoms of GERD had resolved and not recurred. He did not take any medications, and he had no known adverse reactions to medications. The patient was born in Central America and had lived in the United States for 16 years. He worked in construction and lived in a suburb of Boston with his partner and two children. He was a lifelong nonsmoker and did not use illicit drugs. There was no known personal or family history of blood clots.

On examination, the temporal temperature was 38.6°C, the blood pressure 92/50 mm Hg, the pulse 110 beats per minute, the respiratory rate 28 breaths per minute, and the oxygen saturation 94% while supplemental oxygen was delivered through a nasal cannula at a rate of 4 liters per minute. The body-mass index (the weight in kilograms divided by the square of the height in meters) was 28.3. The patient was alert and oriented with no asterixis. The sclerae were icteric. Crackles were noted in both posterior lung fields. The patient had tenderness on palpation in the right upper abdomen; he was able to take full deep breaths without pause while the right upper abdomen was palpated, and the pain did not increase during inspiration. The mucous membranes were moist, and he had no petechiae, oral ulcers, or signs of dental infection. There was no leg edema, rash, or skin breakdown.

Two additional liters of intravenous fluids were administered, and the blood pressure increased to 116/59 mm Hg. Additional imaging studies were performed.

Computed tomography (CT) of the chest, abdomen, and pelvis was performed after the administration of intravenous contrast material with pulmonary angiography timing in the chest and with portal venous timing in the abdomen and pelvis. No evidence of pulmonary embolism was found. Multifocal patchy airspace opacities were present throughout the lungs, most of which were concentrated dependently in the posterior right upper lobe and both lower lobes; more opacities were noted in the right lower lobe than in the left lower lobe (Figure 1A). Interlobular septal thickening was present in both lungs, along with associated centrilobular ground-glass opacities and trace pleural fluid (Figure 1B). Multiple mediastinal lymph nodes were enlarged, including the right hilar, perivascular, and subcarinal nodes. The liver was enlarged with diffuse periportal edema; bile duct walls appeared to be thickened, and periportal lymphadenopathy was noted. The gallbladder was contracted, and trace pericholecystic edema was seen. A partially occlusive thrombus of the superior right renal vein extending into the inferior vena cava was present (Figure 1C). After the initial report, a secondary in-person review with the admitting team revealed additional findings, including subtle proximal thickening of the duodenal wall and mucosal hyperemia, along with a possible soft-tissue connection between the duodenum and right kidney (Figure 1D). Magnetic resonance imaging (MRI) of the abdomen was recommended.

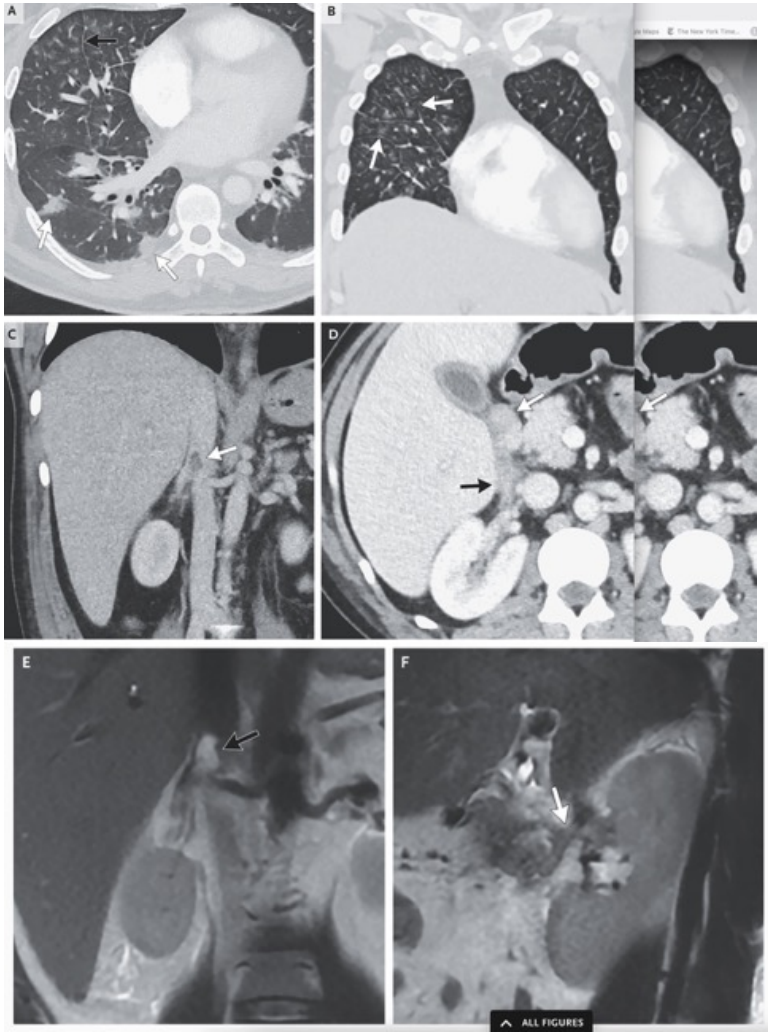

Initial Imaging Studies.

CT images of the chest were obtained after the administration of intravenous contrast material to evaluate the pulmonary arteries. An axial view (Panel A) shows multifocal patchy dependent airspace opacities (white arrows), interlobular septal thickening with centrilobular ground-glass opacities (black arrow), and trace pleural effusion on the right side. A coronal view (Panel B) also shows interlobular septal thickening with centrilobular ground-glass opacities (arrows), a finding consistent with interstitial and alveolar edema. A coronal CT image of the abdomen, obtained after the administration of intravenous contrast material (Panel C), shows a small triangular filling defect consistent with a thrombus within the superior right renal vein extending into the inferior vena cava (arrow) and an enlarged liver. An axial CT image (Panel D) shows duodenal wall thickening with an abnormal soft-tissue connection extending to the right kidney (black arrow), an enlarged periportal lymph node (white arrow), and periportal edema. A coronal image from MRI of the abdomen (Panel E), obtained after the administration of intravenous contrast material, confirms the presence of a nonenhancing ("bland") triangular thrombus in the superior right renal vein and inferior vena cava (arrow). A sagittal image (Panel F) confirms the presence of a connection between the duodenum and right kidney (arrow), which is visible only on this single image.

A nonocclusive thrombus was confirmed within the superior right renal vein that extended into the inferior vena cava and did not enhance (Figure 1E). The proximal duodenum was circumferentially thickened, with associated T2-weighted images showing hyperintensity consistent with edema. The suspected soft tissue in the anterior pararenal space between the duodenum and right renal hilum was confirmed but poorly evaluated owing to motion (Figure 1F).

On hospital day 1, the gram-positive cocci isolated in three of four blood cultures were identified as *Streptococcus anginosus*. Screening tests for human immunodeficiency virus types 1 and 2 were negative; antinuclear antibodies were not detected. Treatment with piperacillin–tazobactam, vancomycin, and acyclovir was stopped, and treatment with intravenous ceftriaxone and oral doxycycline was started. Hypotension resolved, but fever persisted with a maximum temporal temperature of 38.7°C. The platelet count had increased after platelet transfusion; the results of laboratory tests are shown. Treatment with intravenous heparin was initiated for thrombosis in the renal vein and inferior vena cava. Testing for lupus anticoagulant was positive, without evidence of IgG or IgM antibodies to β_2-glycoprotein or cardiolipin.
On hospital day 2, fever persisted. The maximum temporal temperature was 39.0°C.
A diagnostic test was performed, and management decisions were made.

Differential Diagnosis

This 36-year-old man had self-limited abdominal and back pain. Two weeks later, sepsis developed with gastrointestinal, pulmonary, hematologic, hepatic, lymphatic, and retroperitoneal abnormalities.
When considering the most likely cause of this patient's presentation, I could not identify a convincing diagnosis for the findings without selectively disregarding one or more major abnormalities — an approach that was neither logical nor defensible. I therefore adopted a strategy more suited to complex cases: constructing a causal pathway. This method organizes clinical findings in a temporal sequence of pathophysiological relationships (Figure 2).

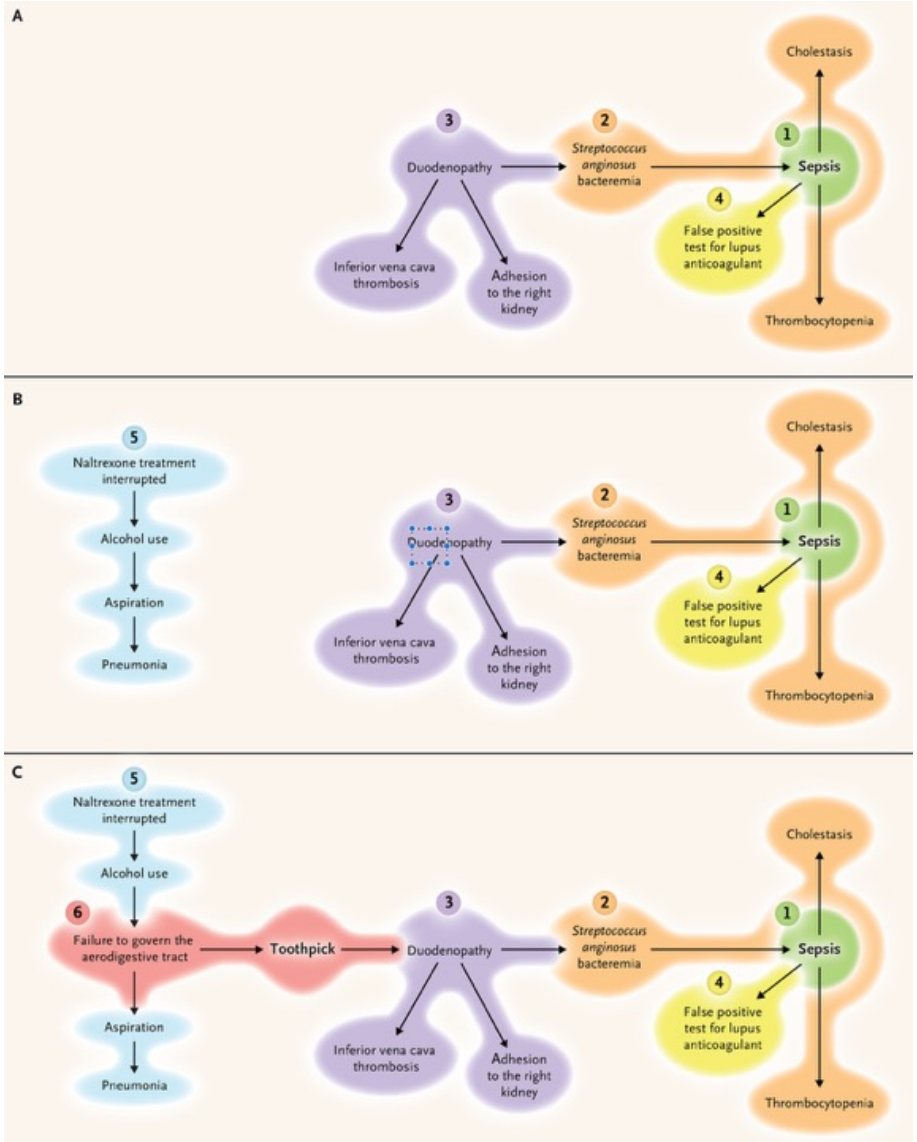

Causal Diagram.

Constructing a causal diagram forces the clinician to organize the key findings in a temporal and pathophysiological sequence that places the theory of the case in full view. The drafting of this mechanistic pathway can be a diagnostic reasoning tool, a storytelling instrument, or a cognitive scaffold for teaching. Every arrow drawn between data points requires justification and the consideration of counterfactual scenarios and must contribute to a coherent story that withstands counterarguments. Such rigor inevitably exposes knowledge gaps, inferential leaps, and unexamined assumptions. Remedying such vulnerabilities in logic sharpens clinical judgment and improves future performance, which is the ultimate purpose of these exercises. The beginning of the causal diagram (Panel A) has an undisputed clinical anchor — sepsis (highlighted in green). Multiple abnormalities associated with this patient's presentation can then be organized by causation (highlighted in orange, purple, and yellow). Shown next are two parallel pathophysiological sequences that remain unconnected (Panel B) — aspiration pneumonia linked to alcohol use (highlighted in blue) and a cascade beginning with an undefined duodenal process leading to sepsis. The causal diagram then shows how a shared antecedent — alcohol use that led to impaired aerodigestive protection and function — set off two parallel cascades (Panel C) by allowing oropharyngeal contents into the lungs and allowing a toothpick into the intestinal tract (highlighted in red), where it perforated the duodenal wall.

Diagnostic Testing

On hospital day 3, CT angiography of the abdomen showed partial resolution of duodenal inflammation, which revealed a linear hyperdense foreign body (measuring 5.2 cm in length) that was piercing through the second portion of the duodenum, tethering its posterior wall, extending through the anterior pararenal space, and penetrating the hilum and upper pole of the right kidney. There was no evidence of active extravasation or vascular injury.

The gastroenterology service was consulted for upper endoscopic evaluation of the foreign body identified on imaging. Timing of the procedure was influenced by the object type and its location within the gastrointestinal tract. Although the time of ingestion was uncertain, it was presumed to have occurred 2 weeks earlier. The object was unlikely to spontaneously pass because it was embedded within the kidney, where it had likely remained for weeks. Because of the proximity to vital organs, we proceeded with immediate intervention.

The planning of this procedure involved a multidisciplinary team, including gastroenterology, surgery, and radiology services. Owing to the complexity of the procedure and the risk of bleeding, esophagogastroduodenoscopy was performed in the operating room, with the patient in the supine position.

The endoscope was slowly advanced to the duodenum, where a foreign object was visualized that corresponded to the hyperdense object found on CT. Owing to the orientation of the object, rat-tooth forceps were used to remove it.

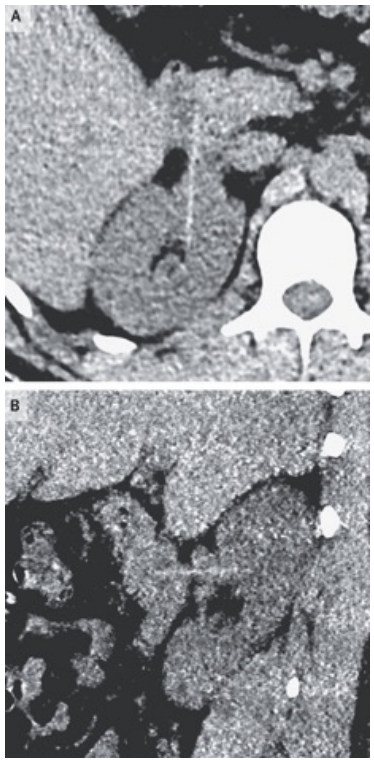

CT Angiogram of the Abdomen Performed on Hospital Day 3.

Axial (Panel A) and sagittal (Panel B) images from CT angiography of the abdomen, obtained before the administration of intravenous contrast material, show a linear hyperdense foreign body (measuring 5.2 cm) now seen piercing through the descending segment of the duodenum into the right kidney.

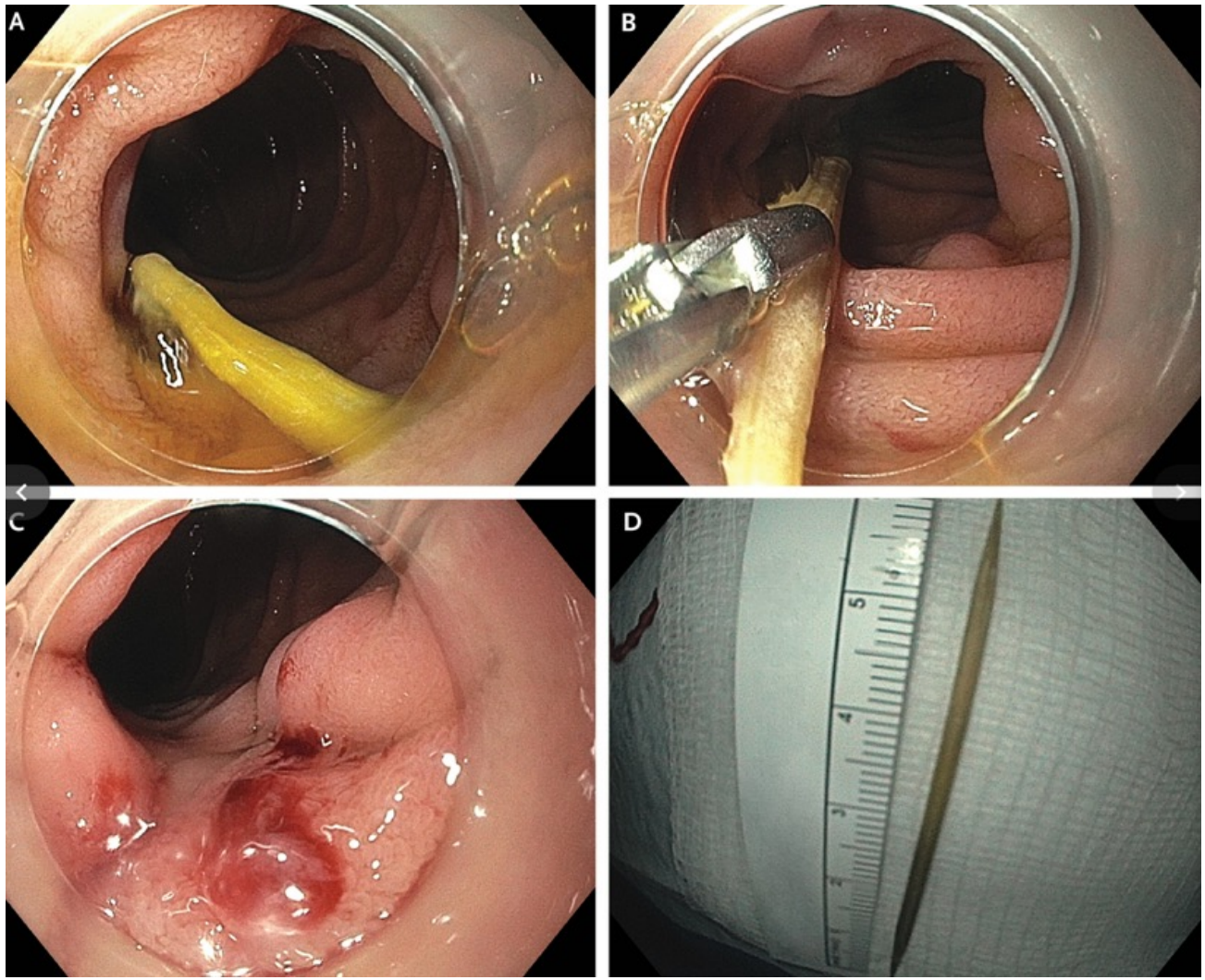

Images Obtained during Esophagogastroduodenoscopy.

During esophagogastroduodenoscopy, a foreign body was identified in the duodenum (Panel A). The foreign body was then extracted with the use of rat-tooth forceps (Panel B). After extraction, the site was monitored for bleeding (Panel C) and the toothpick was inspected and found to be intact (Panel D).

After removal of the foreign body, the gastroscope was reintroduced to assess for bleeding at the site. No bleeding was observed either during the extraction of the foreign body or for 5 to 10 minutes after extraction . The foreign body was identified as a wooden toothpick, which had been removed intact. After the procedure, the patient's condition remained stable, and he had an uneventful recovery.

Discussion of Management

This patient had a high-grade *S. anginosus* bacteremia. *S. anginosus* was identified in two of four blood cultures that had been obtained approximately 48 hours after the initiation of broad-spectrum antibacterial therapy. After 5 days of incubation, one of two blood cultures that had been obtained approximately 24 hours after admission also grew veillonella species, which are gram-negative anaerobes that inhabit the digestive tract and are known to form biofilms. The presence of this polymicrobial bacteremia was suggestive of disruption of a gut mucosal surface and prompted even greater concern about the potential bacterial seeding of the large clot in the inferior vena cava and renal vein. The patient's condition improved rapidly after the toothpick was extracted. I recommended treatment with intravenous ceftriaxone for 3 weeks, followed by 3 weeks of oral amoxicillin, given the duration of his documented bacteremia, persistence of fever, and possible septic thrombophlebitis in major vessels.

The patient received treatment with apixaban for renal-vein thrombosis. During hospitalization, the patient resumed treatment with oral naltrexone, and an extended-release formulation was administered intramuscularly before discharge. He was connected with an alcohol use disorder recovery coach and attended Alcoholics Anonymous meetings conducted in Spanish. At his most recent follow-up visit, 9 months after discharge, the patient was doing well and had remained abstinent from alcohol.

Final Diagnosis

Perforation of the duodenum by a foreign body (wooden toothpick).

Cancer is a group of diseases involving abnormal cell growth with the potential to invade or spread to other parts of the body. These contrast with benign tumors, which do not spread. Possible signs and symptoms include a lump, abnormal bleeding, prolonged cough, unexplained weight loss, and a change in bowel movements. While these symptoms may indicate cancer, they can also have other causes. Over 100 types of cancers affect humans
About 33% of deaths from cancer are caused by tobacco and alcohol consumption, obesity, lack of fruit and vegetables in diet and lack of exercise. Other factors include certain infections, exposure to ionizing radiation, and environmental pollutants.

The global, regional, and national burden of cancer, 1990–2023, with forecasts to 2050: a systematic analysis for the Global Burden of Disease Study 2023

Summary

Background Cancer is a leading cause of death globally. Accurate cancer burden information is crucial for policy planning, but many countries do not have up-to-date cancer surveillance data. To inform global cancer-control efforts, we used the Global Burden of Diseases, Injuries, and Risk Factors Study (GBD) 2023 framework to generate and analyse estimates of cancer burden for 47 cancer types or groupings by age, sex, and 204 countries and territories from 1990 to 2023, cancer burden attributable to selected risk factors from 1990 to 2023, and forecasted cancer burden up to 2050.

Methods Cancer estimation in GBD 2023 used data from population-based cancer registration systems, vital registration systems, and verbal autopsies. Cancer mortality was estimated using ensemble models, with incidence informed by mortality estimates and mortality-to-incidence ratios (MIRs). Prevalence estimates were generated from modelled survival estimates, then multiplied by disability weights to estimate years lived with disability (YLDs). Years of life lost (YLLs) were estimated by multiplying age-specific cancer deaths by the GBD standard life expectancy at the age of death. Disability-adjusted life-years (DALYs) were calculated as the sum of YLLs and YLDs. We used the GBD 2023 comparative risk assessment framework to estimate cancer burden attributable to 44 behavioural, environmental and occupational, and metabolic risk factors. To forecast cancer burden from 2024 to 2050, we used the GBD 2023 forecasting framework, which included forecasts of relevant risk factor exposures and used Socio-demographic Index as a covariate for forecasting the proportion of each cancer not affected by these risk factors. Progress towards the UN Sustainable Development Goal (SDG) target 3.4 aim to reduce non-communicable disease mortality by a third between 2015 and 2030 was estimated for cancer.

Findings In 2023, excluding non-melanoma skin cancers, there were 18·5 million (95% uncertainty interval 16·4 to 20·7) incident cases of cancer and 10·4 million (9·65 to 10·9) deaths, contributing to 271 million (255 to 285) DALYs globally. Of these, 57·9% (56·1 to 59·8) of incident cases and 65·8% (64·3 to 67·6) of cancer deaths occurred in low-income to upper-middle-income countries based on World Bank income group classifications. Cancer was the second leading cause of deaths globally in 2023 after cardiovascular diseases. There were 4·33 million (3·85 to 4·78) risk-attributable cancer deaths globally in 2023, comprising 41·7% (37·8 to 45·4) of all cancer deaths. Risk-attributable cancer deaths increased by 72·3% (57·1 to 86·8) from 1990 to 2023, whereas overall global cancer deaths increased by 74·3% (62·2 to 86·2) over the same period. The reference forecasts (the most likely future) estimate that in 2050 there will be 30·5 million (22·9 to 38·9) cases and 18·6 million (15·6 to 21·5) deaths from cancer globally, 60·7% (41·9 to 80·6) and 74·5% (50·1 to 104·2) increases from 2024, respectively. These forecasted increases in deaths are greater in low-income and middle-income countries (90·6% [61·0 to 127·0]) compared with high-income countries (42·8% [28·3 to 58·6]). Most of these increases are likely due to demographic changes, as age-standardised death rates are forecast to change by –5·6% (–12·8 to 4·6) between 2024 and 2050 globally. Between 2015 and 2030, the probability of dying due to cancer between the ages of 30 years and 70 years was forecasted to have a relative decrease of 6·5% (3·2 to 10·3).

Interpretation Cancer is a major contributor to global disease burden, with increasing numbers of cases and deaths forecasted up to 2050 and a disproportionate growth in burden in countries with scarce resources. The decline in age-standardised mortality rates from cancer is encouraging but insufficient to meet the SDG target set for 2030. Effectively and sustainably addressing cancer burden globally will require comprehensive national and international efforts that consider health systems and context in the development and implementation of cancer-control strategies across the continuum of prevention, diagnosis, and treatment.

	Global	High-income countries	Upper-middle-income countries	Lower middle-income countries	Low-income countries
Incidence					
Cases in 2023, in thousands (95% UI)	18 500 (16 400 to 20 700)	7780 (6700 to 8760)	6860 (6070 to 7760)	3190 (2850 to 3580)	698 (613 to 797)
Cases, percentage change 1990–2023 (95% UI)	105·1 (79·5 to 137·4)	67·7 (42·9 to 96·2)	117·3 (88·0 to 159·0)	219·5 (170·8 to 277·2)	194·4 (142·8 to 252·9)
Age-standardised incidence rate 2023, per 100 000 (95% UI)	205·1 (180·9 to 229·1)	303·2 (262·9 to 344·1)	182·7 (160·5 to 207·8)	125·7 (112·5 to 139·7)	166·9 (147·4 to 188·5)
Age-standardised incidence rate, percentage change 1990–2023 (95% UI)	−7·1 (−18·4 to 7·4)	−3·4 (−17·9 to 14·8)	−8·8 (−20·9 to 8·9)	28·6 (10·0 to 51·2)	23·6 (3·1 to 43·8)
Mortality					
Deaths in 2023, in thousands (95% UI)	10 400 (9650 to 10 900)	3530 (3210 to 3700)	4130 (3800 to 4440)	2240 (2060 to 2460)	455 (406 to 505)
Deaths, percentage change 1990–2023 (95% UI)	74·3 (62·2 to 86·2)	37·7 (30·2 to 42·3)	68·7 (48·7 to 87·9)	195·6 (163·7 to 234·7)	171·0 (136·8 to 209·7)
Age-standardised mortality rate 2023, per 100 000 (95% UI)	114·6 (106·5 to 121·0)	124·1 (114·5 to 129·2)	109·3 (100·7 to 117·4)	94·2 (86·4 to 103·0)	121·3 (106·1 to 134·7)
Age-standardised mortality rate, percentage change 1990–2023 (95% UI)	−23·9 (−29·1 to −19·1)	−27·3 (−30·1 to −25·5)	−33·5 (−41·4 to −25·7)	16·6 (3·9 to 32·8)	14·2 (−0·3 to 31·1)
DALYs					
DALYs in 2023, in millions (95% UI)	271 000 (255 000 to 285 000)	74 000 (69 200 to 77 000)	108 000 (100 000 to 116 000)	71 900 (66 100 to 78 200)	17 400 (15 800 to 19 400)
DALYs, percentage change 1990–2023 (95% UI)	53·4 (42·6 to 64·5)	14·7 (10·2 to 17·8)	39·2 (24·2 to 54·0)	159·2 (129·8 to 193·3)	147·8 (115·9 to 183·3)
Age-standardised DALY rate 2023, per 100 000 (95% UI)	3023·1 (2840·3 to 3177·3)	2969·7 (2806·5 to 3071·0)	2890·4 (2691·4 to 3107·3)	2727·6 (2510·9 to 2965·9)	3791·6 (3385·4 to 4200·8)
Age-standardised DALY rate, percentage change 1990–2023 (95% UI)	−26·1 (−31·1 to −20·9)	−33·0 (−35·0 to −31·5)	−37·4 (−44·1 to −30·4)	12·7 (0·3 to 27·0)	9·8 (−4·7 to 25·4)

DALYs=disability-adjusted life-years. UI=uncertainty interval.

Table 1: **Cancer incidence, death, and DALY counts and age-standardised rates in 2023 and percentage change in counts and age-standardised rates between 1990 and 2023 by World Bank income group for all ages and sexes combined**

	Incident cases, 2023, in thousands (95% UI)	Incident cases, percentage change 1990 to 2023 (95% UI)	Age-standardised incidence rate, 2023 (95% UI)	Age-standardised incidence rate, percentage change 1990 to 2023 (95% UI)	Deaths, 2023, in thousands (95% UI)	Deaths, percentage change 1990 to 2023 (95% UI)	Age-standardised death rate, 2023 (95% UI)	Age-standardised death rate, percentage change 1990 to 2023 (95% UI)	DALYs, 2023, in thousands (95% UI)	DALYs, percentage change 1990 to 2023 (95% UI)	Age-standardised DALY rate, 2023 (95% UI)	Age-standardised DALY rate, percentage change 1990 to 2023 (95% UI)
Total cancers excluding non-melanoma skin cancer	18 500 (16 400 to 20 700)	105·1 (79·5 to 137·4)	205·1 (180·9 to 229·1)	−7·1 (−18·4 to 7·4)	10 400 (9650 to 10 900)	74·3 (62·2 to 86·2)	114·6 (106·5 to 121·0)	−23·9 (−29·1 to −19·1)	271 000 (255 000 to 285 000)	53·4 (42·6 to 64·5)	3023·1 (2840·3 to 3177·3)	−26·1 (−31·1 to −20·9)
Lip and oral cavity cancer	422 (361 to 498)	145·5 (98·9 to 209·2)	4·6 (4·0 to 5·5)	11·2 (−9·8 to 39·7)	229 (197 to 267)	133·9 (89·0 to 185·4)	2·5 (2·2 to 2·9)	3·0 (−16·3 to 25·6)	6540 (5600 to 7680)	120·1 (76·4 to 170·9)	72·2 (61·7 to 84·7)	3·8 (−16·5 to 27·6)
Nasopharynx cancer	167 (130 to 218)	86·3 (34·9 to 167·9)	1·9 (1·5 to 2·4)	−7·5 (−33·4 to 32·9)	76 (63·5 to 87·9)	20·9 (−7·7 to 52·5)	0·8 (0·7 to 1·0)	−42·3 (−56·0 to −27·7)	2600 (2150 to 3050)	12·8 (−15·2 to 42·7)	29·2 (24·0 to 34·2)	−42·2 (−56·6 to −26·9)
Other pharynx cancer	191 (159 to 227)	189·2 (136·8 to 263·1)	2·1 (1·7 to 2·5)	31·0 (7·1 to 64·7)	117 (93·8 to 144)	166·2 (112·5 to 242·0)	1·3 (1·0 to 1·6)	18·9 (−4·9 to 52·3)	3420 (2680 to 4240)	151·6 (99·5 to 226·7)	37·3 (29·2 to 46·4)	17·2 (−7·2 to 51·6)
Oesophageal cancer	605 (539 to 668)	53·1 (30·9 to 82·6)	6·6 (5·9 to 7·3)	−32·8 (−42·4 to −20·4)	577 (510 to 649)	51·2 (28·1 to 79·2)	6·3 (5·6 to 7·1)	−34·6 (−44·2 to −22·4)	14 100 (12 600 to 15 800)	37·0 (16·6 to 65·2)	152·9 (136·4 to 171·7)	−38·3 (−47·4 to −25·8)
Stomach cancer	1260 (1070 to 1520)	20·0 (2·0 to 41·5)	13·8 (11·7 to 16·6)	−47·5 (−55·3 to −38·4)	935 (797 to 1060)	2·4 (−12·6 to 20·3)	10·3 (8·7 to 11·7)	−56·0 (−62·4 to −48·6)	22 500 (19 300 to 26 000)	−8·8 (−22·5 to 7·3)	246·7 (211·9 to 285·5)	−58·4 (−64·5 to −51·3)
Colon and rectum cancer	2290 (2010 to 2550)	142·7 (113·0 to 177·4)	25·1 (22·0 to 28·0)	2·1 (−10·3 to 16·2)	1110 (1000 to 1200)	90·2 (74·4 to 106·0)	12·2 (11·1 to 13·3)	−22·0 (−27·8 to −15·9)	26 200 (24 000 to 28 500)	76·3 (60·4 to 93·4)	287·4 (263·3 to 313·0)	−21·2 (−28·1 to −14·0)
Liver cancer	570 (500 to 639)	109·9 (78·4 to 144·6)	6·3 (5·5 to 7·0)	−3·4 (−17·5 to 12·3)	508 (451 to 571)	104·4 (75·4 to 138·9)	5·6 (4·9 to 6·3)	−7·6 (−20·7 to 7·6)	13 900 (12 200 to 16 100)	76·5 (48·3 to 112·0)	154·8 (135·0 to 179·6)	−13·9 (−27·7 to 3·4)
Liver cancer due to hepatitis B, Level 4	216 (188 to 249)	75·3 (44·5 to 108·8)	2·4 (2·1 to 2·7)	−16·3 (−30·7 to −0·1)	189 (162 to 221)	69·6 (41·3 to 102·9)	2·1 (1·8 to 2·4)	−20·2 (−33·4 to −4·2)	6020 (5140 to 7140)	54·2 (27·2 to 88·6)	66·9 (57·1 to 79·5)	−23·3 (−36·4 to −6·2)
Liver cancer due to hepatitis C, Level 4	169 (141 to 202)	136·8 (101·9 to 175·1)	1·9 (1·6 to 2·2)	1·6 (−13·1 to 16·9)	155 (131 to 188)	130·7 (97·8 to 168·5)	1·7 (1·4 to 2·1)	−2·8 (−16·6 to 12·5)	3390 (2810 to 4160)	101·2 (69·6 to 136·7)	37·0 (30·8 to 45·4)	−10·9 (−24·6 to 4·2)
Liver cancer due to alcohol use, Level 4	107 (85·9 to 133)	159·2 (118·2 to 202·1)	1·2 (0·9 to 1·4)	14·1 (−4·0 to 32·7)	95·2 (76·4 to 118)	150·2 (112·7 to 192·9)	1·0 (0·8 to 1·3)	8·9 (−7·1 to 26·8)	2440 (1930 to 3080)	132·1 (95·1 to 175·5)	26·5 (20·9 to 33·4)	5·5 (−11·3 to 25·2)
Liver cancer due to non-alcoholic steatohepatitis, Level 4	44·9 (34·4 to 56)	183·8 (138·2 to 238·2)	0·5 (0·4 to 0·6)	26·5 (6·2 to 50·5)	41·7 (31·2 to 52·7)	179·2 (137·1 to 233·4)	0·5 (0·3 to 0·6)	21·9 (3·7 to 45·6)	1060 (810 to 1350)	147·9 (107·0 to 201·9)	11·6 (8·9 to 14·9)	16·5 (−2·1 to 42·1)
Hepatoblastoma, Level 4	5·78 (4·33 to 7·93)	−2·2 (−31·9 to 47·7)	0·1 (0·1 to 0·1)	−8·8 (−36·7 to 38·2)	3·53 (2·28 to 5·22)	−21·5 (−50·2 to 27·6)	0·1 (0·0 to 0·1)	−25·7 (−53·0 to 21·1)	310 (200 to 460)	−21·2 (−50·0 to 27·7)	4·8 (3·1 to 7·1)	−25·3 (−52·7 to 21·5)
Liver cancer due to other causes, Level 4	27·3 (21 to 33·8)	95·9 (61·7 to 132·2)	0·3 (0·2 to 0·4)	−6·5 (−21·9 to 11·3)	23·6 (18·3 to 29·5)	89·6 (62·2 to 123·2)	0·3 (0·2 to 0·3)	−11·5 (−23·4 to 4·5)	711 (554 to 886)	65·3 (38·8 to 101·8)	8·0 (6·2 to 9·9)	−16·3 (−29·6 to 1·9)
Gallbladder and biliary tract cancer	227 (197 to 263)	103·4 (82·3 to 128·3)	2·5 (2·2 to 2·9)	−15·4 (−24·1 to −5·2)	185 (161 to 218)	82·8 (63·1 to 103·2)	2·0 (1·8 to 2·4)	−25·2 (−33·2 to −17·1)	4040 (3480 to 4830)	68·7 (49·4 to 89·9)	44·0 (38·0 to 52·7)	−26·5 (−34·6 to −17·5)
Pancreatic cancer	574 (518 to 609)	152·8 (132·9 to 172·5)	6·3 (5·7 to 6·7)	6·3 (−1·4 to 14·6)	552 (504 to 587)	150·5 (133·0 to 169·6)	6·0 (5·5 to 6·4)	3·6 (−3·0 to 10·9)	12 300 (11 500 to 13 000)	125·8 (108·5 to 145·9)	133·3 (124·4 to 141·8)	−0·6 (−7·9 to 7·9)
Larynx cancer	234 (197 to 281)	82·8 (44·8 to 121·9)	2·5 (2·1 to 3·0)	−19·2 (−35·7 to −2·1)	132 (113 to 159)	63·1 (33·6 to 94·9)	1·4 (1·2 to 1·7)	−29·1 (−41·8 to −15·2)	3610 (3000 to 4400)	54·6 (25·2 to 86·8)	39·1 (32·5 to 47·7)	−29·8 (−43·2 to −15·3)
Tracheal, bronchus, and lung cancer	2300 (2080 to 2530)	96·0 (77·8 to 117·1)	24·9 (22·5 to 27·4)	−15·0 (−22·8 to −5·9)	2040 (1840 to 2210)	85·8 (68·6 to 100·6)	22·2 (19·9 to 24·1)	−20·3 (−27·7 to −14·1)	46 700 (42 200 to 50 900)	62·0 (47·6 to 75·1)	504·9 (455·7 to 550·0)	−27·5 (−34·0 to −21·6)

(Table 2 continues on next page)

	Incident cases, 2023, in thousands (95% UI)	Incident cases, percentage change 1990 to 2023 (95% UI)	Age-standardised incidence rate, 2023 (95% UI)	Age-standardised incidence rate, percentage change 1990 to 2023 (95% UI)	Deaths, 2023, in thousands (95% UI)	Deaths, percentage change 1990 to 2023 (95% UI)	Age-standardised death rate, 2023 (95% UI)	Age-standardised death rate, percentage change 1990 to 2023 (95% UI)	DALYs, 2023, in thousands (95% UI)	DALYs, percentage change 1990 to 2023 (95% UI)	Age-standardised DALY rate, 2023 (95% UI)	Age-standardised DALY rate, percentage change 1990 to 2023 (95% UI)
(Continued from previous page)												
Malignant skin melanoma	322 (253 to 397)	150·1 (86·8 to 236·8)	3·6 (2·8 to 4·4)	17·5 (−11·9 to 57·1)	66·2 (59·6 to 75·2)	104·5 (88·0 to 118·6)	0·7 (0·7 to 0·8)	−10·3 (−17·6 to −3·9)	1810 (1590 to 2120)	74·6 (56·1 to 89·1)	20·3 (17·7 to 23·8)	−15·4 (−24·3 to −8·0)
Soft tissue and other extraosseous sarcomas	137 (107 to 171)	111·6 (51·3 to 185·1)	1·6 (1·2 to 2·0)	11·0 (−19·5 to 47·3)	60·8 (49 to 75·7)	89·1 (33·7 to 142·8)	0·7 (0·6 to 0·9)	−4·5 (−31·2 to 21·9)	2210 (1720 to 2880)	57·8 (5·0 to 110·2)	26·6 (20·4 to 34·9)	−5·1 (−35·6 to 26·2)
Malignant neoplasm of bone and articular cartilage	109 (81·4 to 157)	86·4 (23·5 to 196·2)	1·3 (1·0 to 1·9)	8·7 (−27·9 to 72·9)	76·3 (59·9 to 96·3)	88·1 (41·7 to 147·7)	0·9 (0·7 to 1·1)	−0·8 (−24·1 to 29·2)	2990 (2260 to 3890)	58·3 (13·1 to 114·4)	35·9 (26·8 to 47·0)	−1·3 (−29·0 to 33·2)
Breast cancer	2300 (2030 to 2610)	146·0 (111·0 to 187·8)	25·5 (22·4 to 29·0)	12·8 (−3·3 to 32·0)	778 (683 to 870)	111·1 (85·4 to 139·2)	8·7 (7·6 to 9·7)	−7·8 (−18·7 to 4·5)	24 500 (21 500 to 27 800)	107·7 (77·7 to 139·9)	274·4 (239·7 to 311·4)	−1·0 (−14·8 to 14·5)
Cervical cancer	867 (676 to 1140)	86·2 (40·3 to 152·6)	9·9 (7·7 to 13·0)	−4·4 (−27·7 to 29·0)	368 (290 to 476)	70·9 (32·3 to 133·0)	4·1 (3·2 to 5·3)	−19·6 (−37·7 to 8·8)	13 200 (10 200 to 17 300)	70·1 (29·1 to 136·0)	149·7 (114·8 to 197·1)	−13·3 (−34·2 to 19·8)
Uterine cancer	519 (440 to 617)	157·8 (107·2 to 223·6)	5·6 (4·8 to 6·7)	14·6 (−7·4 to 43·4)	108 (93 to 126)	85·4 (56·5 to 117·4)	1·2 (1·0 to 1·4)	−21·9 (−33·9 to −9·1)	2900 (2450 to 3370)	76·8 (44·6 to 113·0)	31·6 (26·7 to 36·8)	−20·0 (−34·4 to −4·1)
Ovarian cancer	331 (284 to 394)	109·2 (74·6 to 146·0)	3·7 (3·1 to 4·4)	−2·1 (−17·8 to 15·1)	221 (190 to 254)	108·1 (77·4 to 141·0)	2·4 (2·1 to 2·8)	−9·3 (−22·4 to 4·7)	6480 (5450 to 7650)	104·9 (67·5 to 142·9)	72·0 (60·4 to 85·0)	−2·9 (−20·5 to 15·1)
Prostate cancer	1410 (1190 to 1630)	168·7 (117·1 to 239·2)	15·2 (12·9 to 17·6)	8·8 (−11·7 to 36·6)	469 (413 to 526)	118·2 (95·9 to 148·3)	5·2 (4·6 to 5·9)	−17·2 (−25·6 to −6·1)	8850 (7790 to 9960)	108·1 (84·9 to 137·8)	96·7 (84·9 to 108·7)	−16·2 (−25·4 to −4·5)
Testicular cancer	97·6 (73·4 to 128)	122·5 (50·9 to 225·8)	1·2 (0·9 to 1·5)	40·4 (−4·6 to 104·9)	11·8 (9·56 to 14·5)	54·1 (11·5 to 94·6)	0·1 (0·1 to 0·2)	−12·1 (−36·1 to 10·9)	584 (469 to 730)	48·0 (5·8 to 91·1)	7·1 (5·7 to 8·9)	−6·3 (−32·9 to 20·7)
Kidney cancer	397 (346 to 460)	132·8 (97·7 to 173·9)	4·4 (3·8 to 5·1)	8·3 (−7·4 to 26·7)	165 (147 to 180)	106·1 (90·5 to 122·2)	1·8 (1·6 to 2·0)	−11·0 (−17·9 to −4·5)	4050 (3590 to 4500)	73·7 (58·2 to 88·6)	45·4 (40·1 to 50·3)	−16·4 (−23·8 to −8·7)
Bladder cancer	569 (499 to 643)	105·5 (75·5 to 143·7)	6·2 (5·5 to 7·1)	−13·9 (−26·1 to 1·4)	234 (209 to 258)	91·5 (74·1 to 112·0)	2·6 (2·3 to 2·9)	−24·0 (−30·3 to −16·2)	4630 (4210 to 5140)	68·6 (53·7 to 89·9)	50·7 (46·2 to 56·3)	−28·2 (−34·3 to −19·1)
Brain and central nervous system cancer	377 (315 to 466)	86·4 (50·8 to 131·6)	4·3 (3·6 to 5·4)	0·9 (−18·1 to 25·2)	263 (230 to 311)	82·9 (61·9 to 100·1)	3·0 (2·6 to 3·5)	−6·4 (−16·8 to 1·9)	9110 (7920 to 10 900)	41·7 (23·5 to 57·9)	107·4 (93·1 to 128·5)	−16·1 (−26·7 to −7·4)
Eye cancer	20·9 (15·4 to 29·4)	34·4 (−8·4 to 102·3)	0·3 (0·2 to 0·4)	−19·8 (−42·0 to 15·5)	10·1 (7·22 to 14·2)	8·3 (−46·1 to 88·5)	0·1 (0·1 to 0·2)	−34·5 (−65·2 to 13·2)	489 (294 to 810)	−12·7 (−65·5 to 102·8)	6·7 (3·7 to 11·7)	−33·8 (−73·9 to 53·9)
Retinoblastoma, Level 4	5·4 (3·02 to 9·58)	−2·9 (−65·7 to 184·0)	0·1 (0·0 to 0·1)	−9·6 (−68·1 to 164·2)	3·25 (1·28 to 7·1)	−31·6 (−80·6 to 155·9)	0·0 (0·0 to 0·1)	−36·3 (−82·0 to 138·5)	285 (113 to 622)	−31·2 (−80·5 to 156·8)	4·4 (1·7 to 9·5)	−35·9 (−81·8 to 139·6)
Other eye cancers, Level 4	15·5 (11·5 to 22·6)	55·2 (3·2 to 144·6)	0·2 (0·1 to 0·3)	−23·8 (−49·0 to 19·4)	6·81 (5·39 to 8·81)	50·1 (21·5 to 79·6)	0·1 (0·1 to 0·1)	−33·3 (−45·4 to −21·0)	204 (156 to 279)	40·1 (9·9 to 68·0)	2·3 (1·8 to 3·2)	−29·5 (−45·0 to −15·9)
Neuroblastoma and other peripheral nervous cell tumours	20·9 (13·9 to 30·1)	67·9 (0·2 to 202·3)	0·3 (0·2 to 0·4)	33·5 (−21·5 to 137·4)	5·99 (5·01 to 7·6)	68·8 (33·0 to 111·1)	0·1 (0·1 to 0·1)	13·0 (−10·9 to 41·8)	332 (266 to 441)	35·2 (2·8 to 75·1)	4·5 (3·6 to 6·1)	6·2 (−19·6 to 36·6)
Thyroid cancer	297 (220 to 373)	191·4 (104·9 to 327·0)	3·4 (2·5 to 4·2)	46·5 (3·4 to 114·0)	52·5 (44·8 to 61·1)	120·6 (84·5 to 170·1)	0·6 (0·5 to 0·7)	−3·8 (−19·6 to 18·2)	1560 (1310 to 1880)	112·1 (73·1 to 167·9)	17·6 (14·8 to 21·3)	4·4 (−14·9 to 31·5)
Mesothelioma	29·2 (25·7 to 32·2)	99·3 (71·9 to 126·8)	0·3 (0·3 to 0·4)	−14·2 (−26·0 to −2·6)	27·9 (24·6 to 30·8)	105·4 (79·6 to 132·9)	0·3 (0·3 to 0·3)	−13·0 (−23·6 to −1·6)	623 (550 to 691)	80·9 (56·5 to 109·6)	6·9 (6·0 to 7·6)	−18·3 (−29·5 to −5·3)

(Table 2 continues on next page)

	Incident cases, 2023, in thousands (95% UI)	Incident cases, percentage change 1990 to 2023 (95% UI)	Age-standardised incidence rate, 2023 (95% UI)	Age-standardised incidence rate, percentage change 1990 to 2023 (95% UI)	Deaths, 2023, in thousands (95% UI)	Deaths, percentage change 1990 to 2023 (95% UI)	Age-standardised death rate, 2023 (95% UI)	Age-standardised death rate, percentage change 1990 to 2023 (95% UI)	DALYs, 2023, in thousands (95% UI)	DALYs, percentage change 1990 to 2023 (95% UI)	Age-standardised DALY rate, 2023 (95% UI)	Age-standardised DALY rate, percentage change 1990 to 2023 (95% UI)
(Continued from previous page)												
Hodgkin lymphoma	68·7 (55·8 to 84·3)	15·0 (−7·4 to 36·3)	0·8 (0·7 to 1·0)	−32·8 (−45·7 to −20·3)	27·1 (20·8 to 34·9)	−9·9 (−30·7 to 9·0)	0·3 (0·2 to 0·4)	−51·1 (−62·0 to −41·3)	1180 (866 to 1560)	−16·0 (−38·5 to 4·1)	14·3 (10·4 to 19·0)	−47·4 (−61·9 to −34·9)
Non-Hodgkin lymphoma	632 (468 to 849)	142·9 (68·8 to 256·1)	7·1 (5·3 to 9·6)	17·1 (−18·6 to 70·8)	282 (246 to 319)	90·9 (61·0 to 126·3)	3·2 (2·8 to 3·6)	−11·8 (−25·4 to 4·4)	8290 (7080 to 9590)	58·3 (29·6 to 93·0)	96·2 (81·3 to 111·9)	−14·3 (−29·7 to 3·8)
Burkitt lymphoma, Level 4	15·9 (9·67 to 26)	99·9 (6·0 to 280·5)	0·2 (0·1 to 0·3)	34·1 (−30·1 to 152·5)	6·68 (5·04 to 9·56)	57·6 (11·4 to 138·2)	0·1 (0·1 to 0·1)	2·0 (−28·5 to 53·4)	369 (260 to 566)	33·3 (−13·2 to 112·2)	4·8 (3·4 to 7·5)	−0·6 (−35·1 to 59·3)
Other non-Hodgkin lymphoma, Level 4	616 (457 to 825)	144·3 (70·2 to 256·3)	6·9 (5·1 to 9·3)	16·7 (−18·7 to 69·9)	276 (240 to 312)	91·9 (62·2 to 127·8)	3·1 (2·7 to 3·5)	−12·2 (−25·4 to 4·2)	7920 (6800 to 9160)	59·7 (31·2 to 94·8)	91·4 (77·8 to 106·4)	−14·9 (−30·0 to 3·5)
Multiple myeloma	176 (142 to 222)	188·2 (122·3 to 288·7)	1·9 (1·6 to 2·4)	21·1 (−6·4 to 62·8)	125 (112 to 138)	156·9 (130·5 to 186·7)	1·4 (1·2 to 1·5)	5·0 (−5·7 to 16·9)	2820 (2520 to 3130)	141·3 (114·2 to 174·6)	30·7 (27·5 to 34·1)	5·2 (−6·6 to 19·5)
Leukaemia	573 (447 to 736)	42·0 (6·0 to 100·7)	6·7 (5·2 to 8·7)	−22·7 (−42·7 to 8·6)	341 (307 to 384)	26·5 (10·5 to 44·7)	3·9 (3·5 to 4·4)	−33·5 (−41·4 to −24·4)	12 100 (10 700 to 14 000)	−7·5 (−20·9 to 9·3)	147·9 (130·3 to 171·4)	−40·8 (−49·3 to −30·5)
Acute lymphoid leukaemia, Level 4	128 (91·7 to 181)	−3·2 (−30·3 to 48·9)	1·7 (1·2 to 2·4)	−29·6 (−49·6 to 9·2)	76·9 (53·7 to 98·4)	−15·5 (−32·0 to 6·6)	1·0 (0·7 to 1·2)	−42·7 (−53·7 to −27·7)	4350 (3120 to 5470)	−29·5 (−43·6 to −10·7)	57·1 (41·3 to 71·9)	−46·4 (−56·9 to −32·2)
Chronic lymphoid leukaemia, Level 4	128 (101 to 157)	88·8 (44·1 to 149·7)	1·4 (1·1 to 1·7)	−19·1 (−37·8 to 6·8)	44·9 (39·9 to 51·9)	45·2 (27·2 to 65·4)	0·5 (0·4 to 0·6)	−41·6 (−48·3 to −33·9)	985 (863 to 1190)	23·5 (4·6 to 47·9)	10·9 (9·5 to 13·1)	−44·4 (−52·5 to −34·0)
Acute myeloid leukaemia, Level 4	183 (135 to 258)	90·5 (36·9 to 178·9)	2·1 (1·5 to 3·0)	0·4 (−29·4 to 48·4)	131 (113 to 152)	71·8 (45·4 to 103·6)	1·5 (1·3 to 1·7)	−12·0 (−24·1 to 1·7)	4190 (3420 to 5190)	20·3 (−2·0 to 50·1)	49·8 (40·2 to 62·3)	−26·3 (−40·0 to −9·3)
Chronic myeloid leukaemia, Level 4	56·8 (37·7 to 80·2)	−10·6 (−43·4 to 47·7)	0·6 (0·4 to 0·9)	−56·0 (−71·9 to −27·1)	26·4 (21·1 to 32·8)	−26·7 (−43·8 to −4·1)	0·3 (0·2 to 0·4)	−65·7 (−73·1 to −55·3)	797 (600 to 1070)	−39·8 (−55·9 to −15·6)	9·3 (6·9 to 12·5)	−67·0 (−75·7 to −54·3)
Other leukaemia, Level 4	76·8 (61·7 to 96·6)	75·4 (35·2 to 128·7)	0·9 (0·7 to 1·1)	−12·0 (−31·0 to 14·3)	61·7 (49·2 to 77·3)	75·3 (37·4 to 133·1)	0·7 (0·6 to 0·9)	−16·8 (−33·7 to 9·1)	1810 (1400 to 2380)	35·1 (1·5 to 89·1)	20·8 (16·1 to 27·4)	−25·8 (−44·3 to 2·5)
Other malignant neoplasms	454 (388 to 530)	78·3 (43·7 to 122·2)	5·1 (4·4 to 6·0)	−12·0 (−28·7 to 9·3)	226 (197 to 252)	46·9 (21·4 to 72·3)	2·6 (2·2 to 2·9)	−30·6 (−42·2 to −19·3)	6690 (5730 to 7680)	14·3 (−8·1 to 38·9)	78·5 (66·9 to 90·5)	−35·7 (−48·2 to −22·3)

DALYs=disability-adjusted life-years. UI=uncertainty interval.

Table 2: Global cancer incidence, death, and DALY counts and age-standardised rates in 2023 and percentage change in counts and age-standardised rates between 1990 and 2023 for all ages and sexes combined

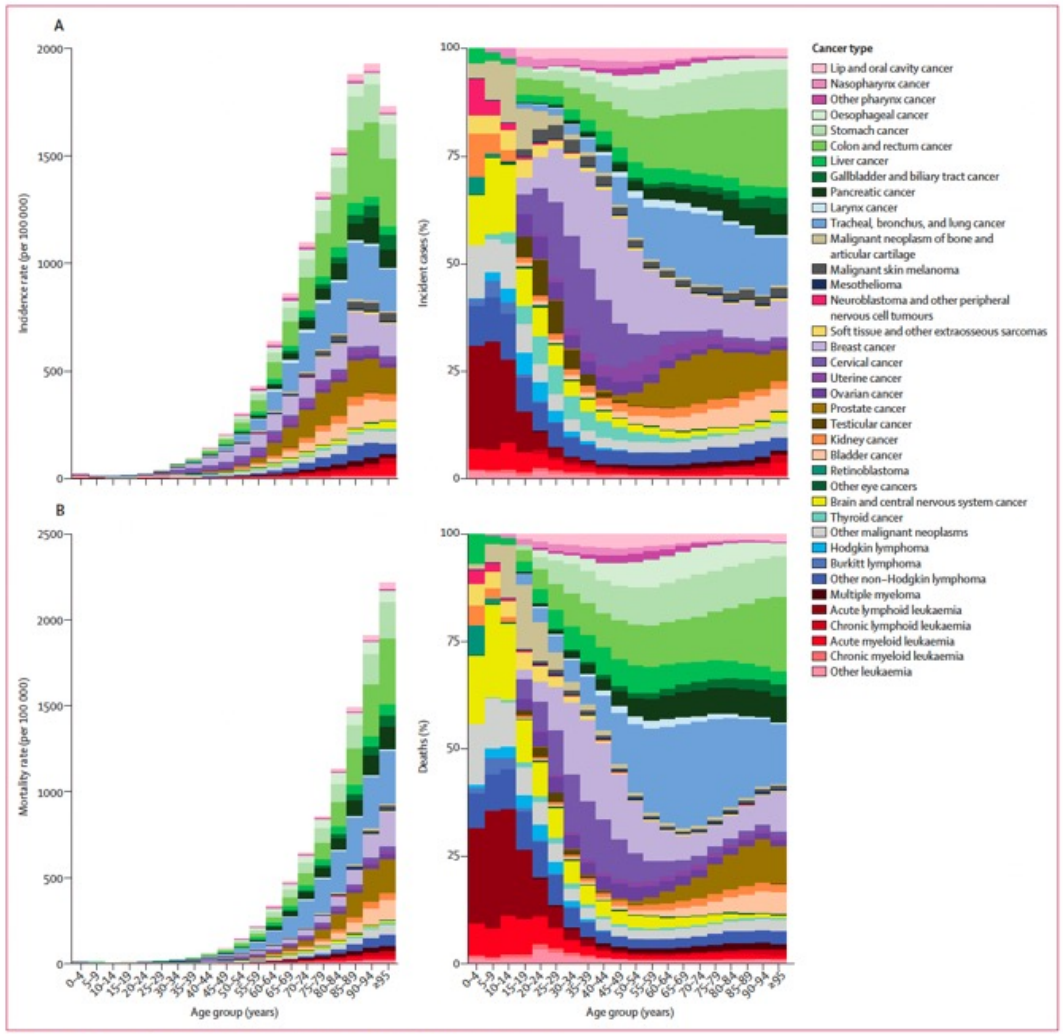

Figure 1: **Global age-specific cancer (A) incidence and (B) mortality in 2023 for all sexes combined**
Results are presented by 5-year age group. Left panels present age-specific incidence and mortality rates. Right panels present age-specific new case and death proportions. Several causes are not presented to not duplicate burden: eye cancer (Level 3); non-Hodgkin lymphoma (Level 3); leukaemia (Level 3); and liver cancer due to hepatitis B, liver cancer due to hepatitis C, liver cancer due to alcohol use, liver cancer due to non-alcoholic steatohepatitis, liver cancer due to other causes, and hepatoblastoma (Level 4).

	Total risk attributable DALYs, % (95% UI)	Tobacco attributable DALYs, % (95% UI)	Dietary risk attributable DALYs, % (95% UI)	High alcohol use attributable DALYs, % (95% UI)	Unsafe sex attributable DALYs, % (95% UI)	Other risk attributable DALYs, % (95% UI)
Total cancers excluding non-melanoma skin cancer	40·3 (36·4 to 43·9)	19·9 (17·5 to 22·5)	6·6 (2·2 to 11·0)	3·6 (2·0 to 5·4)	4·9 (3·8 to 6·2)	14·7 (12·3 to 17·6)
Lip and oral cavity cancer	39·4 (32·2 to 47·0)	35·4 (28·2 to 43·3)	NA	6·8 (1·9 to 11·8)	NA	NA
Nasopharynx cancer	21·9 (17·2 to 27·2)	21·0 (16·4 to 26·2)	NA	NA	NA	1·0 (0·7 to 1·4)
Other pharynx cancer	51·9 (44·7 to 59·1)	43·2 (35·9 to 51·3)	NA	16·5 (13·9 to 18·9)	NA	NA
Oesophageal cancer	56·9 (42·0 to 70·0)	38·1 (32·0 to 44·6)	14·3 (–2·7 to 29·5)	19·6 (–0·8 to 43·3)	NA	NA
Stomach cancer	18·9 (10·3 to 48·7)	11·2 (9·1 to 13·8)	7·2 (0·0 to 40·8)	1·7 (–0·7 to 3·5)	NA	NA
Colon and rectum cancer	55·5 (41·3 to 67·2)	4·8 (3·0 to 6·9)	37·1 (18·2 to 53·4)	5·2 (2·2 to 8·9)	NA	23·8 (18·5 to 29·2)
Liver cancer	46·4 (40·4 to 53·1)	10·8 (3·6 to 18·8)	NA	19·8 (15·8 to 25·9)	NA	24·8 (18·1 to 31·2)
Gallbladder and biliary tract cancer	11·9 (7·7 to 15·7)	NA	NA	NA	NA	11·9 (7·7 to 15·7)
Pancreatic cancer	38·6 (33·7 to 44·6)	15·6 (13·8 to 17·4)	NA	2·1 (0·4 to 2·9)	NA	26·1 (19·4 to 33·5)
Larynx cancer	72·9 (67·1 to 78·0)	68·3 (62·9 to 73·6)	NA	12·5 (3·0 to 23·0)	NA	5·7 (3·4 to 8·7)
Tracheal, bronchus, and lung cancer	77·0 (73·7 to 80·4)	62·9 (59·0 to 66·7)	4·7 (2·3 to 7·4)	NA	NA	39·5 (29·9 to 49·1)
Breast cancer	28·1 (16·5 to 38·8)	7·5 (5·2 to 9·9)	10·8 (0·0 to 23·4)	2·2 (1·1 to 3·5)	NA	11·7 (7·3 to 16·1)
Cervical cancer	100·0 (100·0 to 100·0)	5·9 (3·2 to 9·3)	NA	NA	100·0 (100·0 to 100·0)	NA
Uterine cancer	33·7 (24·2 to 42·3)	NA	NA	NA	NA	33·7 (24·2 to 42·3)
Ovarian cancer	9·9 (4·4 to 15·6)	NA	NA	NA	NA	10·1 (4·5 to 15·8)
Prostate cancer	1·6 (–5·6 to 6·8)	3·6 (1·6 to 5·9)	–3·7 (–10·2 to 2·0)	1·6 (0·1 to 3·6)	NA	NA
Kidney cancer	27·1 (17·0 to 36·7)	9·4 (5·9 to 13·4)	NA	NA	NA	19·7 (8·6 to 29·6)
Bladder cancer	34·6 (29·7 to 39·8)	27·3 (23·1 to 31·2)	NA	NA	NA	10·2 (6·1 to 15·1)
Thyroid cancer	11·4 (7·9 to 15·8)	NA	NA	NA	NA	11·4 (7·9 to 15·8)
Mesothelioma	84·9 (81·5 to 88·2)	NA	NA	NA	NA	84·9 (81·5 to 88·2)
Non-Hodgkin lymphoma	4·3 (1·4 to 7·1)	NA	NA	NA	NA	4·3 (1·4 to 7·1)
Multiple myeloma	7·6 (–3·4 to 17·4)	NA	NA	NA	NA	7·6 (–3·4 to 17·4)
Leukaemia	13·3 (9·5 to 17·8)	6·5 (2·3 to 11·0)	NA	NA	NA	7·6 (5·5 to 10·0)

The leading four Level 2 risk factors contributing to cancer DALYs for both sexes combined in 2023 are separately reported. The remainder of risk factors are presented in the "other risk-attributable DALYs" column. Causes without any risk-attributable DALYs include malignant skin melanoma; soft tissue and other extraosseous sarcomas; malignant neoplasm of bone and articular cartilage; testicular cancer; brain and CNS cancer; eye cancer; neuroblastoma and other peripheral nervous cell tumours; Hodgkin lymphoma; other malignant neoplasms; and other neoplasms. Details on risk-attributable burden estimation are available in the Methods section of this Article and in other publications.[23] The total column value might be smaller than the sum of the risk factor columns because it accounts for overlapping risk exposures when applicable (including when the "Other" column contains multiple risk factors, such as for ovarian cancer). Negative values in this table can occur when risk factors are protective. DALYs=disability-adjusted life-years. UI=uncertainty interval. NA=not applicable, because GBD 2023 does not estimate these risk factor–cancer combinations.

Table 3: **Global proportion of DALYs attributable to risk factors by cancer cause for all ages and sexes combined**

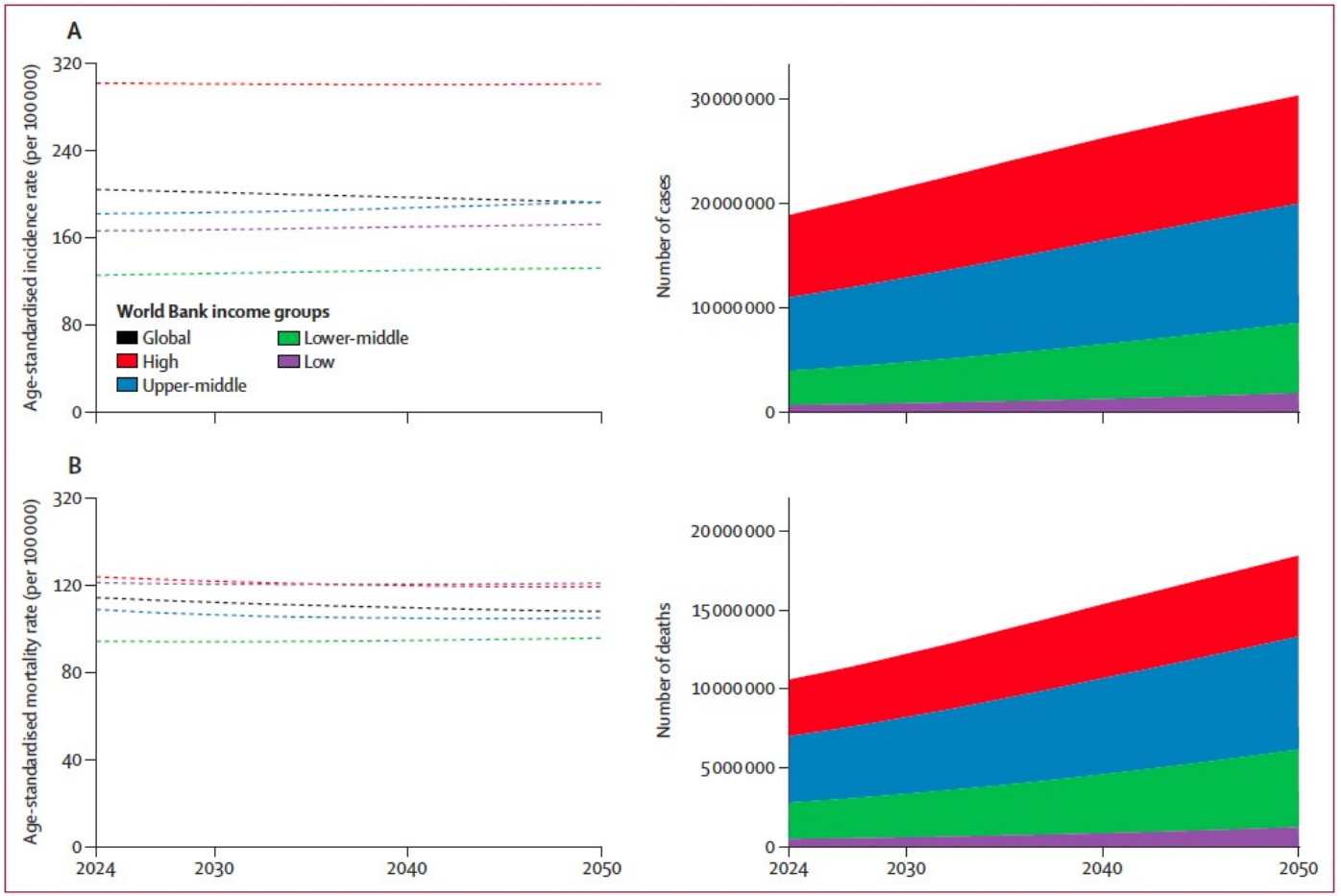

Figure 2: Cancer (A) incidence and (B) mortality in age-standardised rates and counts between 2024 and 2050 globally and by World Bank income group for all ages and sexes combined

Research in context

Evidence before this study

The Global Burden of Diseases, Injuries, and Risk Factors Study (GBD) has produced estimates of cancer burden since its inception in 1993. Over time, additional cancer types have been separately estimated, with additional years of estimates produced for cancer incidence, mortality, years of life lost (YLLs), years lived with disability, and disability-adjusted life-years (DALYs) across global, regional, national, and select subnational geographies. For relevant cancer types, the burden attributable to potentially modifiable risk factors has also been estimated across time and geography. Another source of cancer estimates is the Global Cancer Observatory (GLOBOCAN) study from the International Agency for Research on Cancer, which generates estimates for cancer incidence and mortality in single years, with the most recent iteration providing estimates for 36 cancers for 2022. Cancer burden attributable to individual risk factors or groups of risk factors (eg, obesity, alcohol, and infections) are also produced for single years, although not in each GLOBOCAN round. In the current GLOBOCAN round, forecasts of cancer incidence and mortality are provided up to 2050. However, no other research enterprise besides GBD produces, on a regular basis, global estimates of cancer DALYs—a comprehensive measure that accounts for both the mortality and morbidity of cancers—or generates estimates for other disease groups (eg, cardiovascular diseases, respiratory infections, and tuberculosis) with consistent methodology, which allows for comparison of cancer burden to other diseases as part of policy and resource priority setting. For GBD 2023, we estimated cancer burden for 55 cancer types or groupings (47 of which are reported in this Article) from 1990 to 2023; generated estimates of risk-attributable cancer burden across all relevant cancer types from 1990 to 2023; and forecasted cancer deaths, YLLs, and DALYs up to 2050.

Added value of this study

Our GBD 2023 study updates previous GBD round estimates of cancer burden and includes additional data and improvements in methods. We separately report for the first time comprehensive burden estimates for nine new cancer types: soft tissue and other extraosseous sarcomas, malignant neoplasms of the bone and articular cartilage, Burkitt lymphoma, other non-Hodgkin lymphoma, eye cancers (including separate estimates for retinoblastoma and other eye cancers), neuroblastoma and other malignant peripheral nervous cell tumours, and hepatoblastoma. Also, for the first time, we present forecasts of the trajectory of cancer burden up to 2050. These estimates can inform ongoing and future cancer-control efforts to address the growing challenge of cancer globally.

Implications of all the available evidence

Cancer is a major contributor to global disease burden, with inequitable burden weighing on low-income and lower-middle-income countries as their populations age. A substantial proportion of global cancer burden is attributable to known risk factors, which have the opportunity for mitigation through prevention efforts. Cancer burden continues to grow globally, and increasing cancer cases and deaths are expected in the coming decades. Addressing the continued and inequitable growth of cancer globally will require comprehensive and sustainable national and international efforts that consider the unique aspects of health systems and context in the development and implementation of cancer-control strategies.

C3 glomerulonephritis (C3GN) is a rare kidney disease caused by the overactivation of the complement system, leading to the deposition of complement protein C3 in the kidneys' filtering units (glomeruli). It is a type of C3 glomerulopathy (C3G) and often presents with symptoms like blood in the urine (hematuria), excess protein in the urine (proteinuria), fatigue, and swelling. The condition can be caused by genetic factors or acquired issues, such as autoantibodies.

Alternative pathway:
C3GN is caused by uncontrolled activation of the alternative pathway of the complement system.

Acquired factors:
The most common cause is acquired, often due to C3 nephritic factors (autoantibodies that stabilize a key enzyme in the complement cascade).

Genetic factors:
In about 25% of cases, genetic mutations in genes related to the complement system can be the cause.

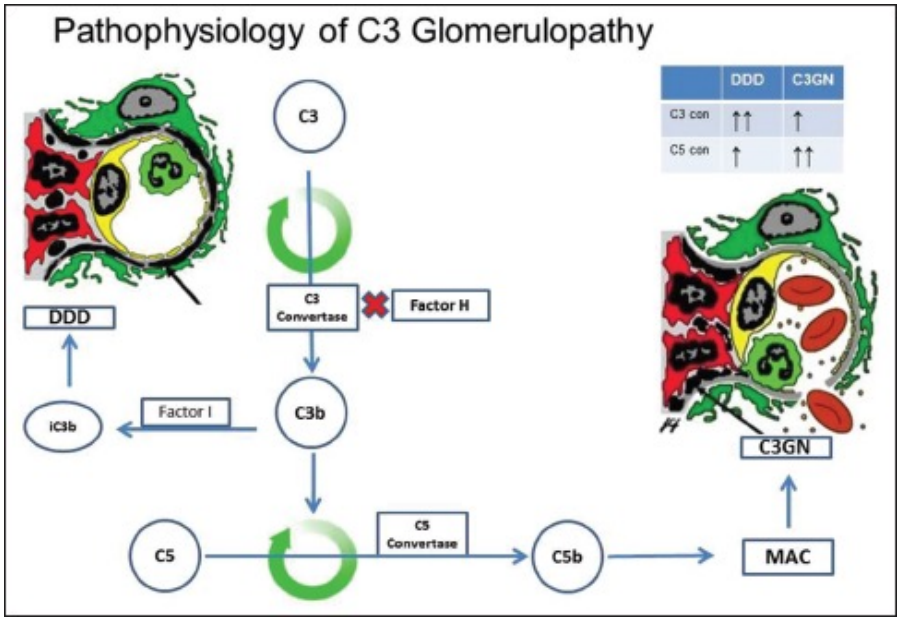

Iptacopan ist ein oral einzunehmendes Medikament, das zur Behandlung von paroxysmaler nächtlicher Hämoglobinurie (PNH) und C3-Glomerulopathie (C3G) verwendet wird. Es wirkt als Hemmer des Komplementfaktors B, wodurch die Hämolyse (der Abbau roter Blutkörperchen) bei PNH reduziert und die Proteinurie bei C3G verringert wird. Iptacopan wird unter dem Markennamen Fabhalta vertrieben und erfordert eine Impfung gegen bekapselte Bakterien, da es das Infektionsrisiko erhöhen kann.

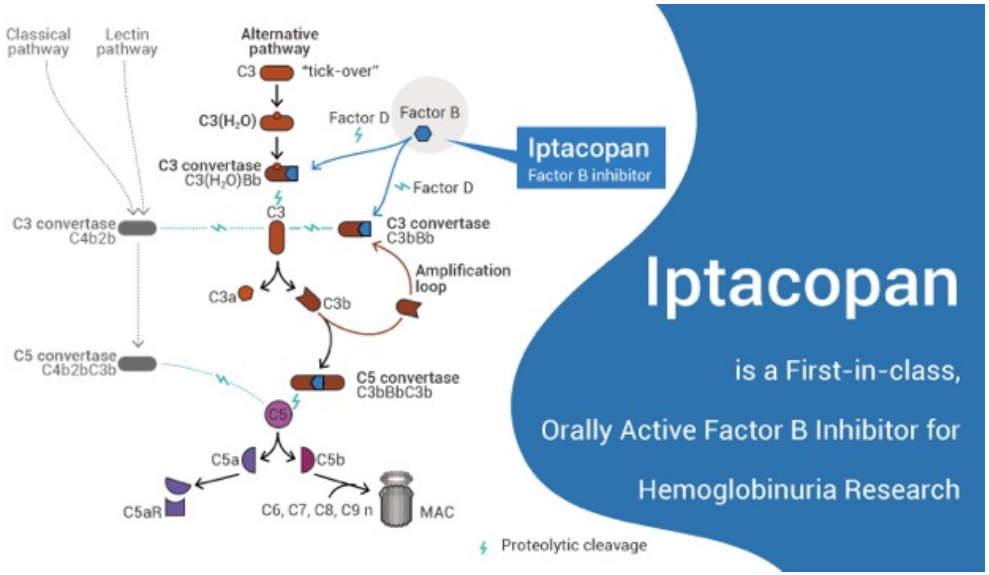

Oral iptacopan therapy in patients with C3 glomerulopathy: a randomised, double-blind, parallel group, multicentre, placebo-controlled, phase 3 study

Summary

Background C3 glomerulopathy is an ultra-rare, severe form of glomerulonephritis caused by overactivation of the alternative complement pathway. We aimed to assess efficacy and safety of iptacopan (LNP023), an oral, proximal complement inhibitor that targets factor B to selectively inhibit the alternative pathway of the complement cascade.

Methods APPEAR-C3G was a multicentre, randomised, double-blind, placebo-controlled, phase 3 study of iptacopan versus placebo (both in addition to supportive care [renin–angiotensin–aldosterone system (RAAS) inhibitors] and immunosuppression). Adult participants (aged 18–60 years) with biopsy-confirmed C3 glomerulopathy were enrolled from 35 hospitals or medical centres in 18 countries. Inclusion criteria included reduced serum C3 concentration (ie, <77 mg/dL [defined as <0·85×lower limit of the central laboratory normal range]) at screening, urine protein–creatinine ratio (UPCR) of 1·0 g/g or higher at day –75 and day –15 before randomisation, estimated glomerular filtration rate (eGFR) of 30 mL/min per 1·73 m^2 or higher at screening and day –15, and vaccination against *Neisseria meningitidis* and *Streptococcus pneumoniae*. All eligible participants were randomised 1:1 via interactive response technology to either the iptacopan or the placebo group, stratified by treatment with corticosteroids, mycophenolic acid, or both (yes or no). During the 6-month double-blind period, participants orally received either iptacopan 200 mg twice daily or placebo; this was followed by a 6-month open-label period in which all participants received iptacopan 200 mg twice daily. The primary endpoint was relative reduction in proteinuria (measured by log-transformed ratio to baseline in UPCR sampled from a 24-h urine collection) at 6 months. The primary analyses were done in the full analysis set (ie, all participants to whom study treatment was assigned by randomisation); all participants who received at least one dose of study treatment were included in the safety analysis. This trial was registered with ClinicalTrials.gov (NCT04817618) and the adult cohort has been completed.

Findings Between July 28, 2021, and Feb 15, 2023, 132 participants were screened, of whom 58 did not complete the screening period and 74 (64% male; 69% White) were randomised 1:1 to receive either iptacopan (n=38) or placebo (n=36). One participant in the placebo group discontinued treatment during the open-label period. The 24-h UPCR percentage change relative to baseline at 6 months was –30·2% (95% CI –42·8 to –14·8) in the iptacopan group and 7·6% (–11·9 to 31·3) in the placebo group. In the iptacopan group, the geometric mean of 24-h UPCR was 3·33 g/g (95% CI 2·79 to 3·97) at baseline and 2·17 g/g (1·62 to 2·91) at 6 months; in the placebo group, this was 2·58 g/g (2·18 to 3·05) at baseline and 2·80 g/g (2·37 to 3·30) at 6 months. The primary endpoint was met with a relative reduction in 24-h UPCR at 6 months for iptacopan versus placebo of 35·1% (13·8 to 51·1; p=0·0014). 30 (79%) of 38 participants in the iptacopan group had treatment-emergent adverse events, compared with 24 (67%) of 36 participants in the placebo group; most of these were of mild or moderate severity. There were no deaths, no treatment discontinuations due to treatment-emergent adverse events, and no meningococcal infections. Serious adverse events were reported in three (8%) participants in the iptacopan group and one (3%) participant in the placebo group.

Interpretation Iptacopan showed a statistically significant, clinically meaningful proteinuria reduction in addition to RAAS inhibitors and immunosuppression at 6 months. Iptacopan was well tolerated with an acceptable safety profile in patients with C3 glomerulopathy.

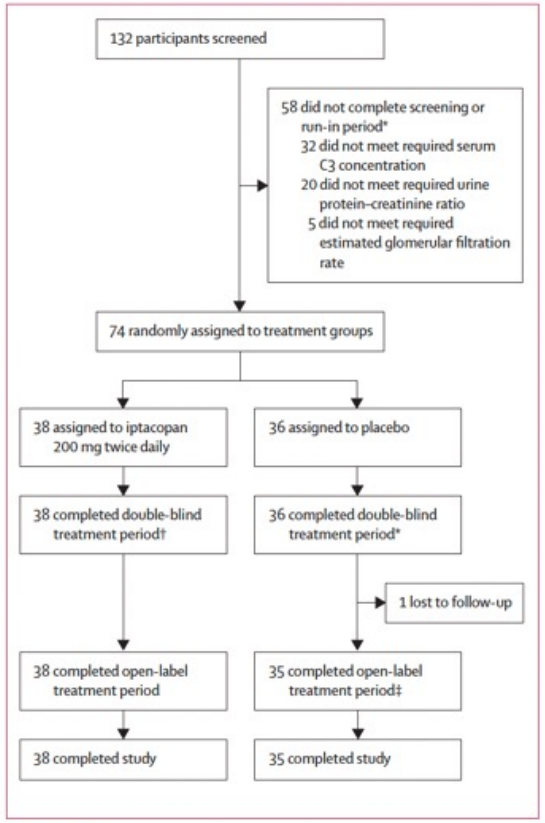

Figure 1: **Trial profile**
Data are presented for the full analysis set (ie, all participants to whom study treatment was assigned by randomisation). *Some participants did not complete screening or run-in period for more than one reason, the full list includes: did not meet blood pressure criteria; had active hepatitis or abnormal liver function tests; unable to communicate with investigator or comply with study requirements; did not have diagnosis confirmed on renal biopsy within 12 months; was not on stable dose of antiproteinuric medications for 90 or more days; and participant decision †Two participants randomly allocated to receive iptacopan discontinued treatment in the double-blind period but completed the open-label treatment and the study. ‡One participant randomly allocated to receive placebo discontinued treatment in the open-label period and was lost to follow-up.

Research in context

Evidence before this study

C3 glomerulopathy is an ultra-rare, progressive kidney disease that is caused by overactivation of the complement alternative pathway. There were no targeted treatments before iptacopan (LNP023), which was approved for the treatment of adult patients with C3 glomerulopathy by both the US Food and Drug Administration and the European Medicines Agency in 2025. Current guideline recommendations rely on supportive care (ie, blockade of the renin–angiotensin–aldosterone system with angiotensin-converting enzyme inhibitors or AT1 receptor blockers) with or without immunosuppression (eg, mycophenolic mofetil or corticosteroids), which has limited benefits and often considerable side-effects. Iptacopan is an oral complement inhibitor that targets factor B and selectively inhibits the alternative pathway by blocking C3 convertase activity and inhibiting the alternative pathway amplification loop, thus preventing downstream generation of alternative pathway C5 convertase, C3a and C5a anaphylatoxins, and the membrane attack complex. Iptacopan is also approved for the treatment of adults with paroxysmal nocturnal haemoglobinuria and for the reduction of proteinuria in adults with primary IgA nephropathy. In a phase 2 study, 12-week iptacopan treatment resulted in proteinuria reduction and stabilisation of estimated glomerular filtration rate (eGFR) in patients with C3 glomerulopathy. These effects persisted 9 months later, when assessed as part of the extension study. The improvements in kidney function were associated with substantial inhibition of the alternative pathway, thus confirming the mechanism of action of iptacopan.

Added value of this study

Selectively targeting the alternative pathway is considered the optimal approach for modifying the disease course and improving outcomes in patients with C3 glomerulopathy. To the best of our knowledge, APPEAR-C3G is the first randomised phase 3 clinical trial in C3 glomerulopathy, conducted to evaluate the efficacy, safety, and tolerability of iptacopan compared with placebo in addition to supportive care, with or without background immunosuppression in patients with native C3 glomerulopathy. The study aimed to reinforce the positive results from the phase 2 study and the longer-term roll-over extension study.

Implications of all the available evidence

The study results show that iptacopan targets the underlying cause of C3 glomerulopathy by correcting the overactivation of the alternative pathway, decreasing C3 deposition in the kidneys, and demonstrating a clinically meaningful reduction in proteinuria and eGFR stabilisation. Iptacopan showed a rapid onset of action, and the efficacy was sustained to 12 months. Based on real-world evidence, the level of proteinuria reduction and eGFR stabilisation observed with iptacopan in APPEAR-C3G would be expected to decrease the risk of kidney failure in the long term. Based on these efficacy results and acceptable safety profile, iptacopan has the potential to fulfil the unmet need for a targeted treatment for C3 glomerulopathy.

	Iptacopan 200 mg (n=38)	Placebo (n=36)
Age (years), mean (SD)	26·1 (10·39)	29·8 (10·79)
Sex		
Male	27 (71%)	20 (56%)
Female	11 (29%)	16 (44%)
Race		
White	27 (71%)	24 (67%)
Black or African American	1 (3%)	1 (3%)
Asian	9 (24%)	9 (25%)
American Indian or Alaska Native	0	1 (3%)
Multiple	0	1 (3%)
Unknown	1 (3%)	0
Region		
North America	7 (18%)	8 (22%)
Europe	22 (58%)	19 (53%)
Other	9 (24%)	9 (25%)
Ethnicity		
Hispanic or Latino	1 (3%)	6 (17%)
Not Hispanic or Latino	34 (89%)	29 (81%)
Not reported	2 (5%)	0
Unknown	1 (3%)	1 (3%)
Baseline 24-h UPCR (g/g), geometric mean (95% CI)	3·33 (2·79–3·97)	2·58 (2·18–3·05)
Baseline 24-h UPCR (3 g/g)		
<339 g/mol	17 (45%)	25 (69%)
≥339 g/mol	21 (55%)	11 (31%)
Baseline 24-h total urinary protein (3 g/day)		
<3000 mg/day	11 (29%)	15 (42%)
≥3000 mg/day	27 (71%)	21 (58%)
Baseline eGFR (mL/min per 1·73 m²), mean (SD)	89·3 (35·20)	99·2 (26·88)
Baseline eGFR		
<60 mL/min per 1·73 m²	10 (26%)	4 (11%)
≥60 mL/min per 1·73 m²	28 (74%)	32 (89%)

(Table 1 continues in next column)

(Continued from previous column)

	Iptacopan 200 mg (n=38)	Placebo (n=36)
Baseline eGFR		
<90 mL/min per 1·73 m²	19 (50%)	12 (33%)
≥90 mL/min per 1·73 m²	19 (50%)	24 (67%)
Has hypertension	23 (61%)	18 (50%)
Sitting systolic blood pressure (mm Hg), mean (SD)	125·8 (13·30)	122·6 (11·43)
Sitting diastolic blood pressure (mmHg), mean (SD)	77·7 (8·77)	77·7 (8·47)
Baseline C3 (mg/L), mean (SD)	316·8 (243·41)	339·3 (227·96)
Age at C3 glomerulopathy diagnosis (years), mean (SD)	22·0 (10·88)	25·3 (10·80)
Years since C3 glomerulopathy diagnosis		
<2 years	15 (39%)	15 (42%)
≥2 years	23 (61%)	21 (58%)
C3 glomerulopathy subtype at diagnosis		
C3 glomerulonephritis	26 (68%)	32 (89%)
Dense deposit disease	9 (24%)	1 (3%)
Mixed C3 glomerulonephritis and dense deposit disease	2 (5%)	2 (6%)
Unknown	1 (3%)	1 (3%)
Corticosteroid treatment, mycophenolic acid treatment, or both, at time of random allocation	16 (42%)	17 (47%)

Data are n (%) unless otherwise indicated. Baseline 24-h UPCR refers to UPCR as measured by the geometric mean of two 24-h urine collections at baseline. Baseline 24-h total urinary protein refers to total urinary protein as measured by the geometric mean of two 24-h urine collections at baseline. Baseline eGFR was defined as the arithmetic mean of two eGFR values at the day −15 visit (before randomisation) and the day 1 visit. Hypertension is defined based on hypertension at diagnosis, as reported by the investigator on the C3 glomerulopathy medical history case report form and the pre-defined hypertension terms taken from patient medical history. eGFR=estimated glomerular filtration rate. UPCR=urine protein–creatinine ratio.

Table 1: **Baseline characteristics**

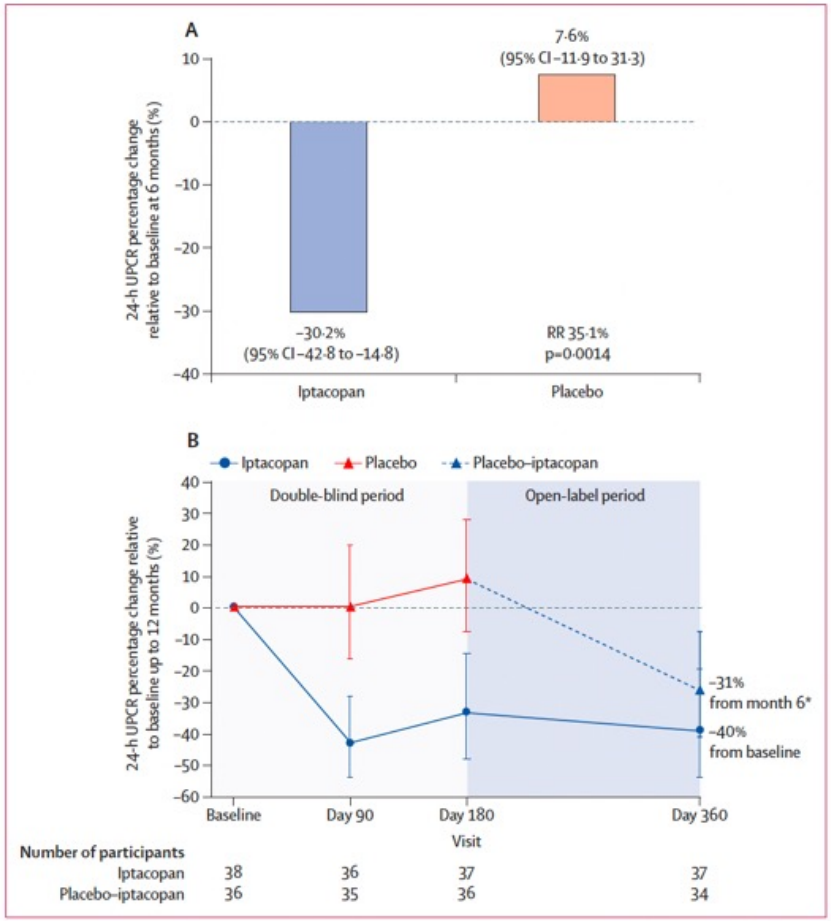

***Figure 2*: Percentage change in proteinuria (24-h UPCR) following treatment of iptacopan or placebo relative to baseline at 6 months (A) and up to 12 months (B)**

Data are presented for the full analysis set (ie, all participants to whom study treatment was assigned by randomisation). (A) The model estimated geometric mean of the ratio to baseline in percentage change (95% CI) of UPCR 24 h (g/g) at month 6 by treatment group (full analysis set). (B) Plot of percentage change (95% CI) of 24 h UPCR (g/g), up to month 12 by treatment group (full analysis set). RR=relative reduction. UPCR=urine protein–creatinine ratio. *Based on the analysis using the combined full analysis set (ie, all participants to whom study treatment was assigned by randomisation).

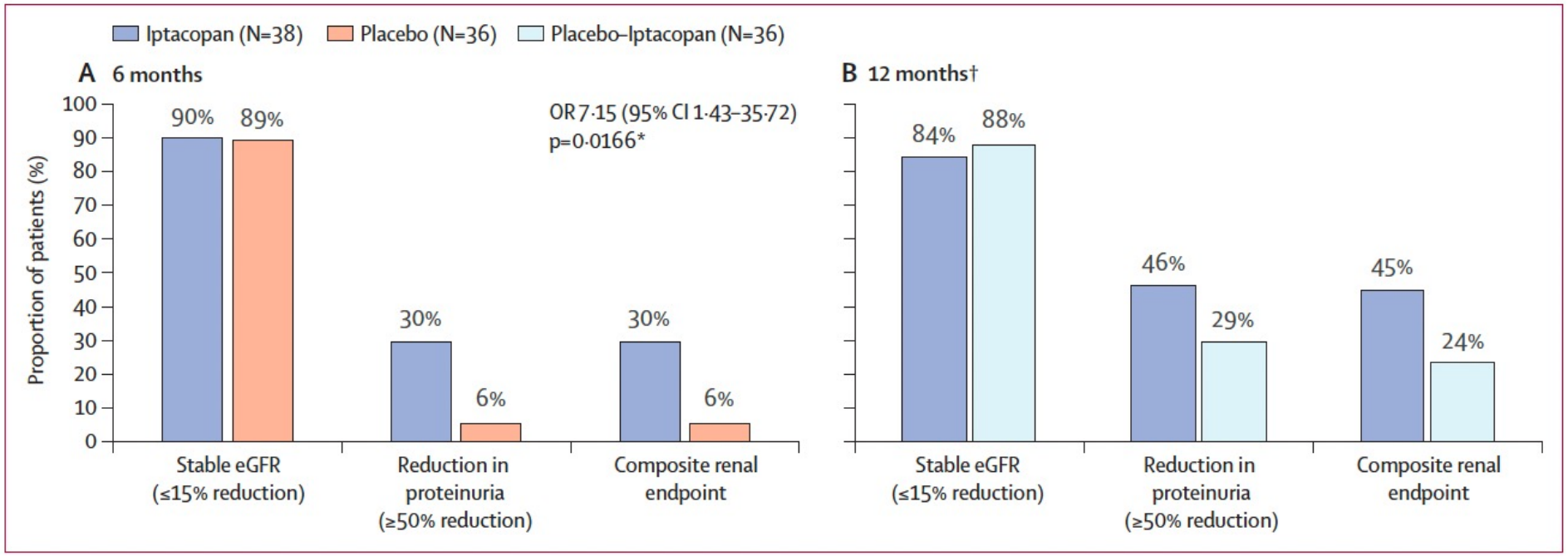

Figure 3: **The proportion of patients that achieved the composite renal endpoint (ie, ≥50% reduction UPCR and ≤15% reduction in eGFR) at 6 months (A) and 12 months (B)**

Data are presented for the full analysis set (ie, all participants to whom study treatment was assigned by randomisation). eGFR=estimated glomerular filtration rate. OR=odds ratio. UPCR=urine protein–creatinine ratio. *Statistically significant after adjustment for multiple testing. †12 months of treatment in those randomised initially to iptacopan and 6 months iptacopan treatment in those randomised initially to placebo.

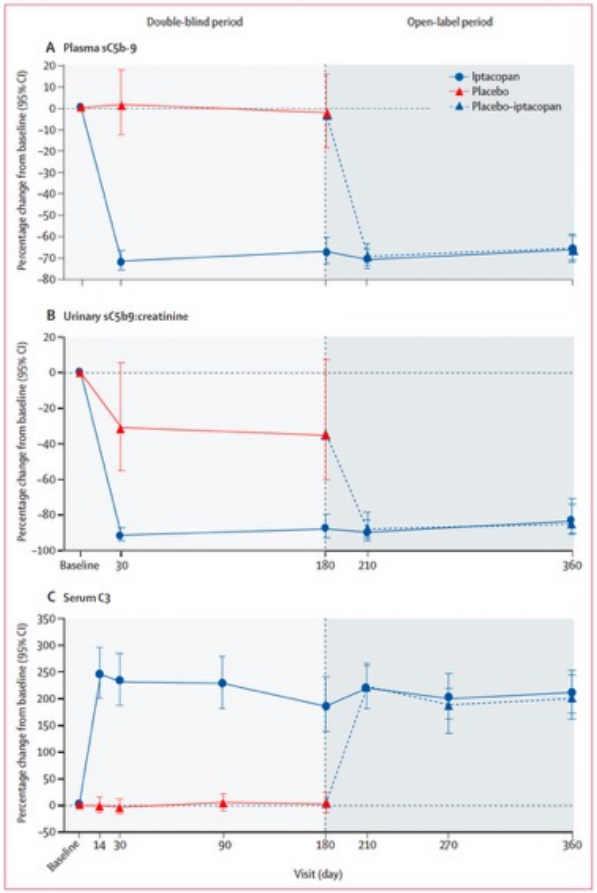

Figure 5: **Effect of iptacopan 200 mg twice daily versus placebo on concentrations of plasma sC5b-9 (A), urine sC5b-9:creatinine (B), and serum C3 (C) up to month 12 by treatment group**
Data are presented for the full analysis set (ie, all participants to whom study treatment was assigned by randomisation). Percentage change is supplied as the model estimated geometric mean of the ratio to baseline in percentage change of each complement biomarker at designated timepoints by treatment group.

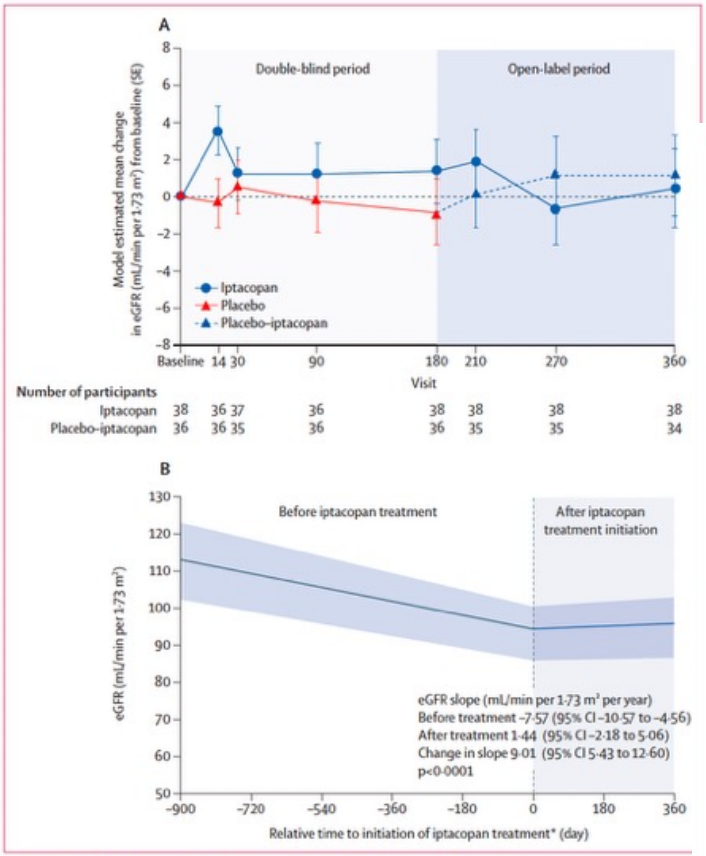

Figure 4: **Effect of iptacopan 200 mg twice daily versus placebo on eGFR (N=74)**
(A) Model estimated mean change from baseline (±SE) of eGFR (mL/min per 1·73 m²) by treatment up to month 12. (B) Annualised eGFR slope change for all patients. Data are presented for the full analysis set (ie, all participants to whom study treatment was assigned by randomisation). The thick line represents the mean value and the shaded area represents the 95% CI. Historical data were collected up to 2 years before the start of randomisation. eGFR=estimated glomerular filtration rate. *Treatment initiation occurred on day 0.

	Iptacopan 200 mg (n=38)	Placebo (n=36)
Number of participants with at least one treatment-emergent adverse event	30 (79%)	24 (67%)
Mild	19 (50%)	21 (58%)
Moderate	9 (24%)	2 (6%)
Severe	2 (5%)	1 (3%)
Suspected to be related to study medication	7 (18%)	4 (11%)
Serious adverse events	3 (8%)	1 (3%)
Blood culture positive for *Streptococcus pneumoniae*	1 (3%)	0
Infected bite	1 (3%)	0
Chest discomfort	1 (3%)	0
Acute kidney injury	0	1 (3%)
Ascites	0	1 (3%)
Adverse events leading to study drug discontinuation	0	0
Deaths	0	0

Data are n (%). All participants with non-missing baseline and covariates were included in the safety analysis. A patient with multiple occurrences for an adverse event is only counted once. Adverse events for the 12-month period are provided in the appendix (p 22).

Table 2: **Adverse events during the 6-month double-blind treatment period**

Research in context

Evidence before this study

C3 glomerulopathy is an ultra-rare, progressive kidney disease that is caused by overactivation of the complement alternative pathway. There were no targeted treatments before iptacopan (LNP023), which was approved for the treatment of adult patients with C3 glomerulopathy by both the US Food and Drug Administration and the European Medicines Agency in 2025. Current guideline recommendations rely on supportive care (ie, blockade of the renin–angiotensin–aldosterone system with angiotensin-converting enzyme inhibitors or AT1 receptor blockers) with or without immunosuppression (eg, mycophenolic mofetil or corticosteroids), which has limited benefits and often considerable side-effects. Iptacopan is an oral complement inhibitor that targets factor B and selectively inhibits the alternative pathway by blocking C3 convertase activity and inhibiting the alternative pathway amplification loop, thus preventing downstream generation of alternative pathway C5 convertase, C3a and C5a anaphylatoxins, and the membrane attack complex. Iptacopan is also approved for the treatment of adults with paroxysmal nocturnal haemoglobinuria and for the reduction of proteinuria in adults with primary IgA nephropathy. In a phase 2 study, 12-week iptacopan treatment resulted in proteinuria reduction and stabilisation of estimated glomerular filtration rate (eGFR) in patients with C3 glomerulopathy. These effects persisted 9 months later, when assessed as part of the extension study. The improvements in kidney function were associated with substantial inhibition of the alternative pathway, thus confirming the mechanism of action of iptacopan.

Added value of this study

Selectively targeting the alternative pathway is considered the optimal approach for modifying the disease course and improving outcomes in patients with C3 glomerulopathy. To the best of our knowledge, APPEAR-C3G is the first randomised phase 3 clinical trial in C3 glomerulopathy, conducted to evaluate the efficacy, safety, and tolerability of iptacopan compared with placebo in addition to supportive care, with or without background immunosuppression in patients with native C3 glomerulopathy. The study aimed to reinforce the positive results from the phase 2 study and the longer-term roll-over extension study.

Implications of all the available evidence

The study results show that iptacopan targets the underlying cause of C3 glomerulopathy by correcting the overactivation of the alternative pathway, decreasing C3 deposition in the kidneys, and demonstrating a clinically meaningful reduction in proteinuria and eGFR stabilisation. Iptacopan showed a rapid onset of action, and the efficacy was sustained to 12 months. Based on real-world evidence, the level of proteinuria reduction and eGFR stabilisation observed with iptacopan in APPEAR-C3G would be expected to decrease the risk of kidney failure in the long term. Based on these efficacy results and acceptable safety profile, iptacopan has the potential to fulfil the unmet need for a targeted treatment for C3 glomerulopathy.

C-reaktive Protein (CRP) is a protein produced by the liver in response to inflammation or infection, and a blood test for CRP measures the amount of it in your body. Elevated levels indicate inflammation, which can be acute (like from an injury) or chronic (from a long-term condition like arthritis). A CRP test helps diagnose inflammation, its severity, and monitor conditions like heart disease, infection, or autoimmune disorders.

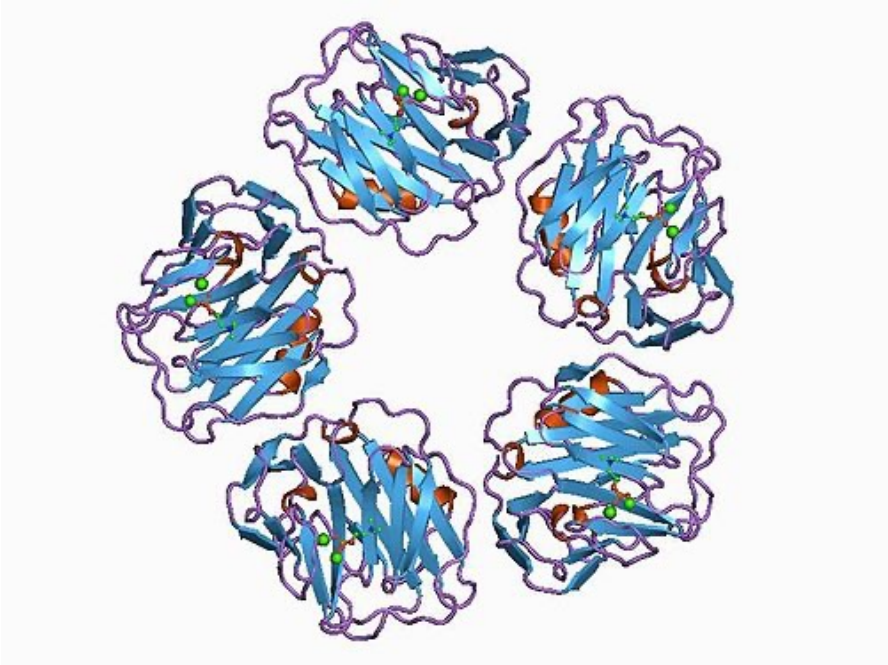

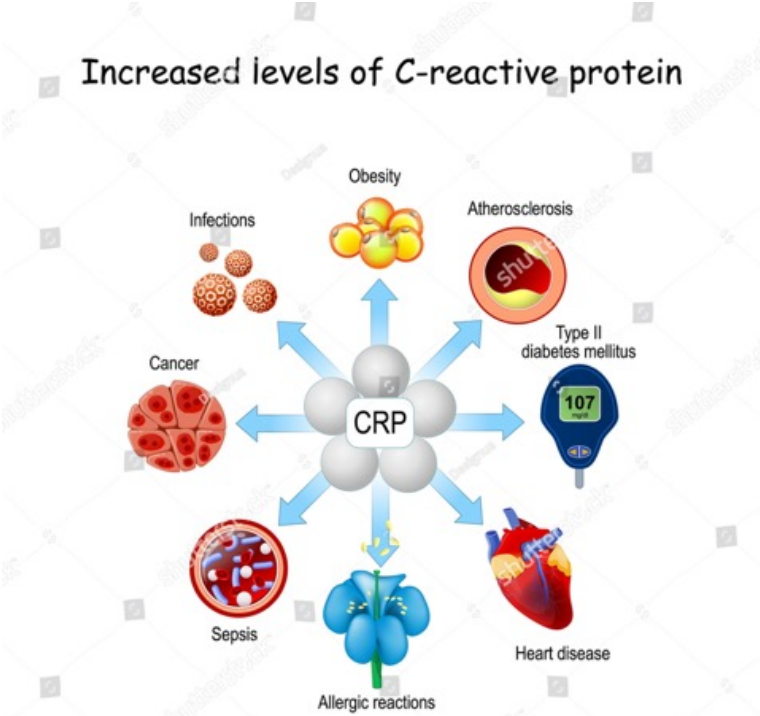

POCT CRP steht für Point-of-Care-Test für C-reaktives Protein. Es ist ein schneller Test, der zur Erstdiagnose, Behandlung und Überwachung von Entzündungen, insbesondere Infektionen, eingesetzt wird. Der Test ermöglicht es Ärzten, innerhalb von Minuten ein Ergebnis zu erhalten, anstatt auf Laboranalysen warten zu müssen. Dadurch können Entscheidungen zur Behandlung, wie die Verordnung von Antibiotika, schneller getroffen werden.

Wie funktioniert POCT CRP?

C-reaktives Protein (CRP): ist ein Akute-Phase-Protein, das in der Leber produziert wird und dessen Konzentration bei Entzündungen oder Infektionen ansteigt.

Point-of-Care-Testing (POCT): ist eine patientennahe Diagnostik, bei der der Test direkt vor Ort durchgeführt wird, beispielsweise in einer Arztpraxis oder Notaufnahme.
Das Ergebnis: liegt in der Regel innerhalb weniger Minuten vor.

Wofür wird POCT CRP verwendet?

- **Bei Infektionen der Atemwege:**

- Der Test hilft bei der Unterscheidung zwischen bakteriellen und viralen Infektionen, was wiederum die Entscheidung über die Notwendigkeit von Antibiotika beeinflusst.

- **Bei akuten Entzündungen:**

- CRP-Tests können bei der Erkennung und Beurteilung von Entzündungen, Gewebeschädigungen oder bestimmten entzündlichen Erkrankungen unterstützen.

- **Zur Überwachung:**

- Der Test kann verwendet werden, um den Verlauf einer Erkrankung zu überwachen und die Reaktion auf eine Behandlung zu beurteilen.

- **Zur Reduzierung des Antibiotikaeinsatzes:**

- Der schnelle Zugang zu CRP-Ergebnissen kann dazu beitragen, die Verschreibung von Antibiotika zu reduzieren, wenn diese nicht notwendig sind, und so die Antibiotikaresistenzbekämpfen.

A clinical decision tool including a decision tree, point-of-care testing of CRP, and safety-netting advice to guide antibiotic prescribing in acutely ill children in primary care in Belgium (ARON): a pragmatic, cluster-randomised, controlled trial

Summary

Background Antimicrobial resistance is a global health threat. Many children with acute illness in ambulatory care are unnecessarily prescribed antibiotics. We assessed the clinical effectiveness of a clinical decision tool for these children, including a validated decision tree, guided point-of-care C-reactive protein testing (POCT of CRP), and safety-netting advice.

Methods ARON was a multicentre, unblinded, pragmatic, cluster-randomised, controlled trial conducted at eligibile Belgian general practitioner and community paediatrician practices able to recruit children with acute illness consecutively, and not already doing POCT of CRP. Practices were allocated (1:1) with equal size (n=4) block randomisation to the clinical decision tool or usual care, stratified by recruiting academic centre. Children with acute illness aged 6 months to 12 years were recruited and followed up for 30 days. The coprimary outcomes were antibiotic prescribing at the index consultation (tested for superiority), as well as recovery time, additional testing, follow-up visits, and antibiotic prescribing after index consultation (all tested for non-inferiority with margins of 1 day, 3%, 4%, and 2%, respectively). Coprimary outcomes were analysed with logistic regression, accounting for practice clustering, study arm, and age in the intention-to-treat population, except recovery time, which was analysed with Cox regression adjusting for the same covariates. Safety was assessed in the intention-to-treat population. This trial is registered with ClinicalTrials.gov (NCT04470518) and is completed.

Findings Of 171 eligible practices, we randomly allocated 82 to the intervention group and 89 to the usual care group. Between Feb 24, 2021, and Dec 29, 2023, 7049 participants were screened, of whom 6760 were deemed eligible. Five patients in each study arm were excluded, so we analysed data from 6750 participants (2988 in the intervention group and 3762 in the control group; 3447 [51%] boys, 3302 [49%] girls, one [<1%] did not specify). The intervention significantly reduced antibiotic prescribing at the index consultation (466 [16%] *vs* 817 [22%], adjusted odds ratio 0·72 [95% CI 0·55–0·94]; p=0·017). Recovery time (adjusted mean difference –0·1 day [95% CI –0·5 to 0·3]), additional testing (adjusted absolute risk reduction [aARR] 2·0% [–1·7 to 5·0]), follow-up visits (aARR 2·8% [–0·9 to 6·1]), and antibiotic prescribing after index consultation (aARR 2·4% [0·2 to 4·2]) were all non-inferior in the intervention group versus the control group. 90 (88%) of 102 adverse events were serious (30 [1%] in the intervention group and 60 [2%] in the control group); none were deemed related to the study procedures. No child died throughout the trial.

Interpretation The clinical decision tool reduced antibiotic prescribing in children without causing harm. Our results support its broader dissemination and implementation to improve the management of acutely ill children in ambulatory care.

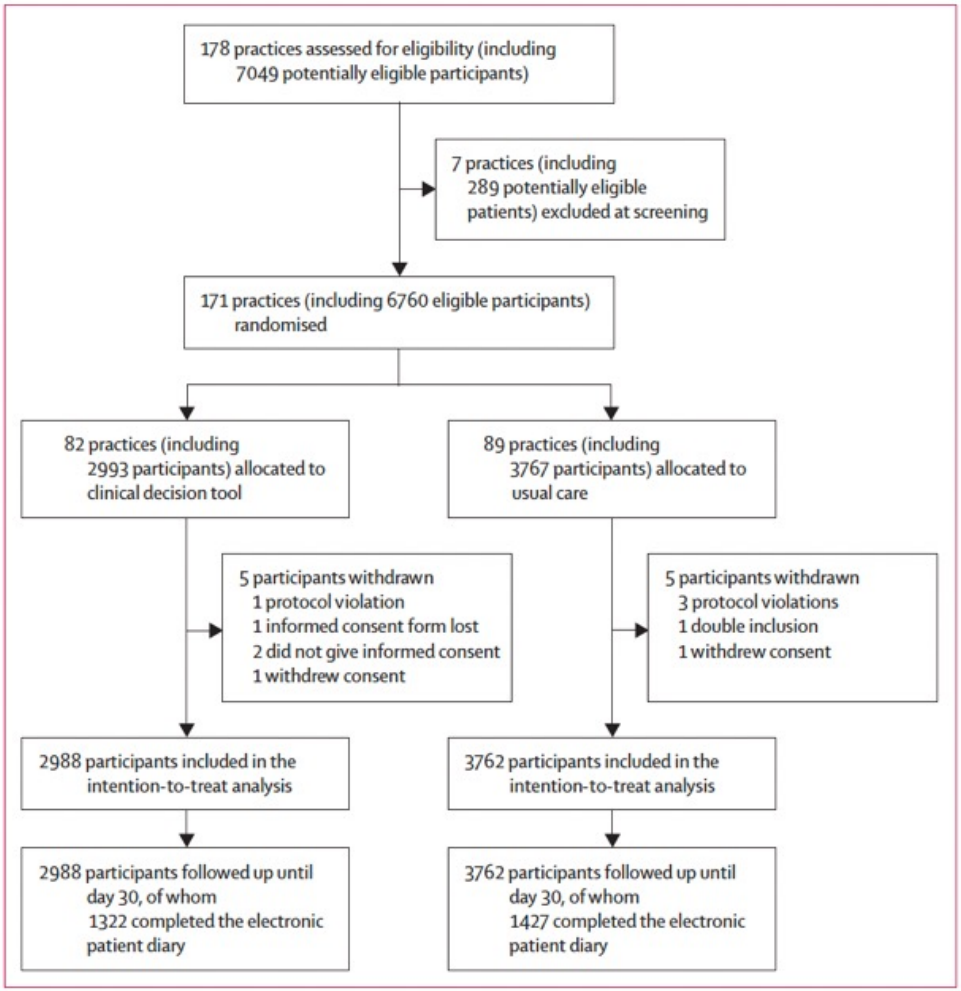

Figure 1: Trial profile

	Intervention (n=2988)	Control (n=3762)
Age		
Median, years	3·7 (1·6-7·1)	3·9 (1·8-7·2)
Age category		
0-5-1	924 (31%)	1030 (27%)
2-6	1290 (43%)	1729 (46%)
7-12	774 (26%)	1003 (27%)
Gender		
Boy	1566 (52%)	1881 (50%)
Girl	1421 (48%)	1881 (50%)
X	0	0
Prefer not to say	1 (<1%)	0
Medical specialty of recruitment		
General practitioner	2719 (91%)	3459 (92%)
Community-based paediatrician	269 (9%)	303 (8%)
Body temperature on patient history, °C	39·0 (38·5-39·5)	39·0 (38·5-39·5)
Body temperature on physical examination, °C	37·0 (36·5-37·7)	36·9 (36·5-37·5)
Bodyweight, kg	15·3 (10·7-23·0)	16·1 (11·2-24·5)
Illness duration, days	2·5 (1·3-4·0)	2·2 (1·0-4·0)
Illness severity as indicated by the physician during the index consultation		
Mild	1771 (59%)	2449 (65%)
Moderate	1146 (38%)	1238 (33%)
Severe	69 (2%)	75 (2%)
Child's illness deemed different from previous episodes by parents		
Yes	587 (20%)	730 (19%)
No	2397 (80%)	3031 (81%)
Responses to the three decision-tree questions		
Clinician gut feeling that something is wrong		
Yes	275 (9%)	290 (8%)
No	2708 (91%)	3446 (92%)
Dyspnoea		
Yes	80 (3%)	110 (3%)
No	2904 (97%)	3627 (96%)
Highest measured body temperature ≥40°C (history or at examination)		
Yes	218 (7%)	261 (7%)
No	2761 (92%)	3473 (92%)
Illness diagnoses by ICPC-2 code		
R74—acute upper respiratory infection	1084 (36%)	1373 (36%)
H71—acute otitis media or myringitis	298 (10%)	439 (12%)
A77—viral disease other or NOS	232 (8%)	241 (6%)
R78—acute bronchitis or bronchiolitis	219 (7%)	253 (7%)
R76—acute tonsillitis	157 (5%)	198 (5%)
R80—influenza or possible COVID-19	166 (6%)	178 (5%)
D73—gastroenteritis presumed infection	134 (4%)	187 (5%)
D70—gastrointestinal infection	125 (4%)	124 (3%)
R81—pneumonia	71 (2%)	85 (2%)
A03—fever	55 (2%)	64 (2%)
R77—laryngitis, acute tracheitis, or proven COVID-19	68 (2%)	110 (3%)
Other	379 (13%)	510 (14%)
Children with a secondary diagnosis during index consultation	399 (13%)	507 (13%)

Data are n (%) or median (IQR). ICPC-2=International Classification of Primary Care, second edition. NOS=not otherwise specified.

Table 1: Baseline characteristics

	Intervention (n=2988)	Control (n=3762)	aOR or aHR* (95% CI)	aARR or aMD* (95% CI)	p value
Co-primary endpoints†					
Antibiotic prescribing at the index consultation (immediate or delayed)	466 (16%)	817 (22%)	0·72 (0·55–0·94)	5·1% (1·0 to 8·5)	0·017
Duration until full clinical recovery, days	4·6 (3·5)	4·7 (3·6)	1·03 (0·96–1·09)	−0·1 (−0·5 to 0·3)	NA
Additional testing‡ from the index consultation to day 30	335 (11%)	517 (14%)	0·83 (0·60–1·15)	2·0% (−1·7 to 5·0)	NA
Follow-up visits with their physician from the index consultation to day 30	770 (26%)	968 (26%)	0·86 (0·70–1·05)	2·8% (−0·9 to 6·1)	NA
Antibiotic prescribing after the consultation to day 30	291 (10%)	429 (11%)	0·77 (0·61–0·98)	2·4% (0·2 to 4·2)	NA
Exploratory endpoints					
Additional testing‡ at the index consultation	249 (8%)	400 (11%)	0·86 (0·86–0·86)	1·4% (1·4 to 1·4)	NA
Additional testing‡ day 1–30	111 (4%)	149 (4%)	0·87 (0·62–1·23)	0·5% (−0·9 to 1·5)	NA
Referral to hospital at the index consultation	24 (1%)	13 (<1%)	2·52 (1·03–6·19)	−0·5% (−1·8 to −0·0)	NA
Referral to hospital day 1–30	79 (3%)	84 (2%)	1·14 (0·76–1·71)	−0·3% (−1·5 to 0·5)	NA
Admission to hospital at the index consultation	7 (<1%)	11 (<1%)	0·80 (0·23–2·78)	0·1% (−0·5 to 0·2)	NA
Admission to hospital day 1–30	25 (1%)	53 (1%)	0·57 (0·35–0·92)	−0·6% (−0·9 to −0·1)	NA
Mortality at the index consultation	0	0	NA	NA	NA
Mortality day 1–30	0	0	NA	NA	NA
Full clinical recovery at day 7	2539 (85%)	3200 (85%)	1·01 (0·97–1·03)	0·1% (−0·4 to 0·4)	NA
Full clinical recovery at day 30	2967 (99%)	3747 (>99%)	1·00 (0·97–1·03)	0·0% (−0·0 to 0·0)	NA
Physician's adherence to the clinical decision tool					
Self-reported adherence	2826/2986 (95%)	NA	NA	NA	NA
Did not prescribe an antibiotic when the decision tree was scored negative and they were not considering antibiotics	2104/2126 (99%)	NA	NA	NA	NA
Did not prescribe an antibiotic when the decision tree was scored negative, they were considering antibiotics, and the POCT of CRP result was ≤5 mg/L	39/54 (72%)	NA	NA	NA	NA
Performed a CRP test when at least one of the questions in the decision tree was scored positive	429/495 (87%)	NA	NA	NA	NA
Performed a CRP test when the decision tree was scored negative and they were considering antibiotics	304/354 (86%)	NA	NA	NA	NA

Data are n (%), or mean (pooled SD), or n/N (%). aHR=adjusted hazard ratio. aMD=adjusted mean difference. aOR=adjusted odds ratio. aARR=adjusted absolute risk reduction. CRP=C-reactive protein. NA=not applicable. POCT=point-of-care testing. *aOR and aARR are used with binary outcomes, aHR and aMD are used with the time-to-event outcome. †Non-inferiority margins for coprimary endpoints tested for non-inferiority are 1 day for duration until clinical recovery, 3% for additional investigations from the index consultation to day 30, 4% for follow-up visits with their physician from the index consultation to day 30, and 2% for antibiotic prescribing after the index consultation to day 30. ‡Including, but not limited to, x-ray, blood tests, and urine tests.

Table 2: **Coprimary and exploratory outcomes**

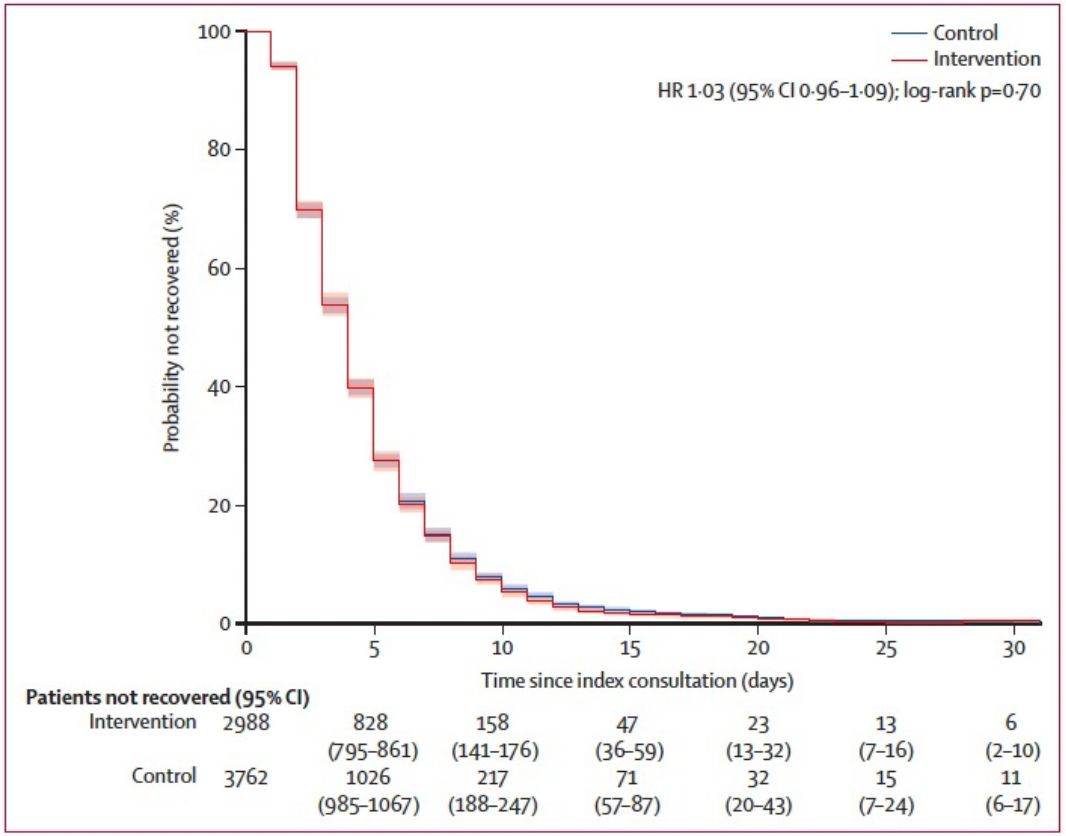

Figure 2: **Kaplan–Meier curves for the survival distributions over time for the control and the intervention group with full clinical recovery as the event of interest**

The red shaded area represents the 95% CI for the intervention group, and the blue shaded area represents the 95% CI for the control group. The numbers of patients not recovered between brackets under the figure also represent the 95% CIs. No data in this analysis were censored.

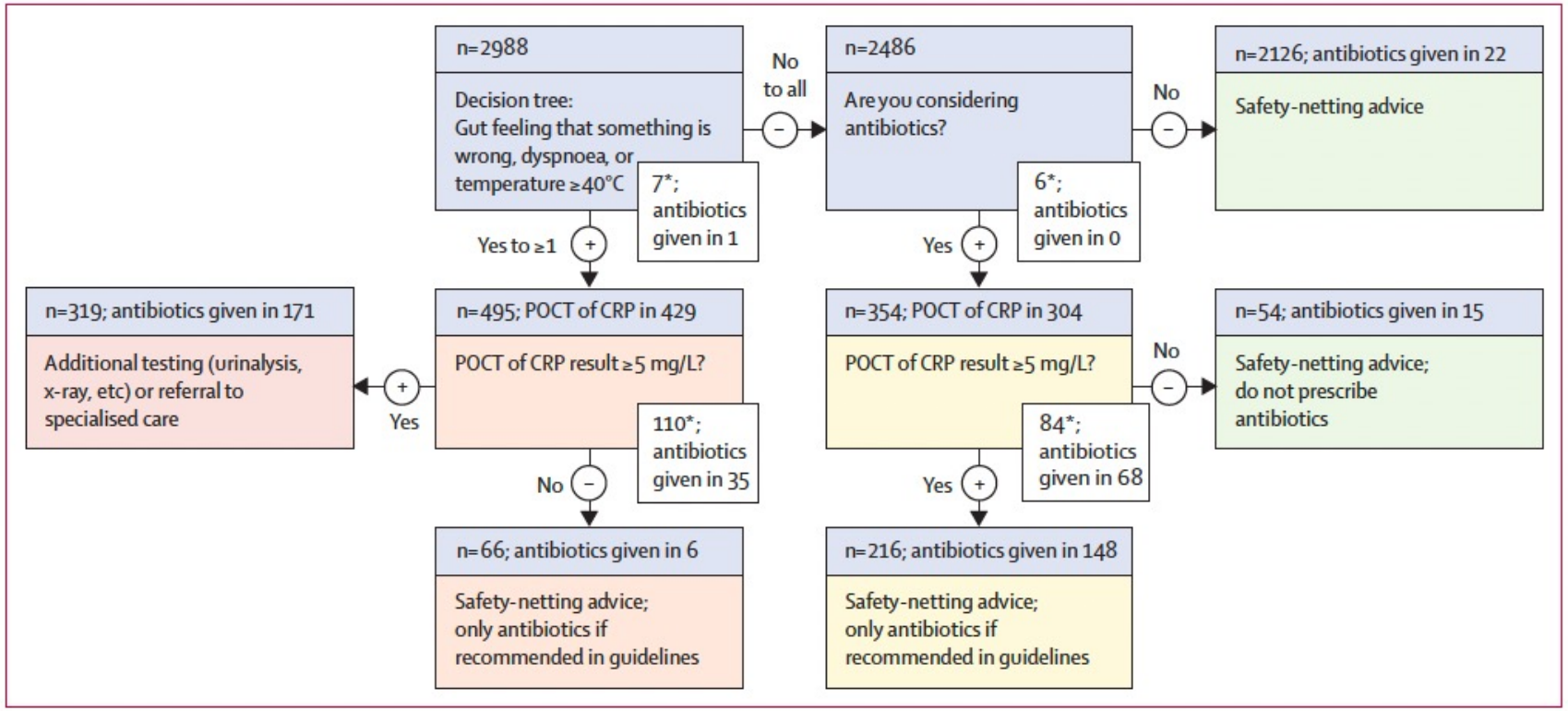

***Figure 3*: Clinical decision tool showing the number of children at each step, the number who received POCT of CRP, and the number receiving antibiotics at the final step**

POCT=point-of-care testing. CRP=C-reactive protein. *Number of children with missing or incomplete data.

Research in context

Evidence before this study

In 2019, approximately 604 000 deaths were associated with antimicrobial resistance in high-income countries alone, with 141 000 directly attributable to antimicrobial resistance. The European Centre for Disease Prevention and Control (ECDC) reports that over 800 000 infections caused by antibiotic-resistant bacteria occurred in the European Economic Area in 2020, resulting in more than 35 000 deaths directly linked to these infections, similar to the health burden of influenza, tuberculosis, and HIV combined. The 2022 WHO and ECDC report on antimicrobial resistance surveillance in Europe states that antimicrobial resistance remains a health threat in Europe and that robust investments in interventions to address antimicrobial resistance are urgently needed and would substantially positively impact population health and future health-care expenditures. The strong relationship between antibiotic consumption in the community and the proliferation of antimicrobial resistance has been established, and children are at particularly high risk of unwarranted antibiotic prescribing. We systematically searched Ovid MEDLINE, Embase, Cochrane Database of Systematic Reviews, Cochrane CENTRAL, Database of Abstracts of Reviews of Effects, and Science Citation Index for controlled studies published in all languages from database inception to March 21, 2017, assessing the impact of point-of-care testing (POCT) of C-reactive protein (CRP) on clinical care for adults and children in ambulatory settings. The search terms are listed in the appendix (pp 3–5). All 19 included studies had a high risk of performance and selection bias. POCT of CRP significantly reduced immediate antibiotic prescribing in children only when guidance on antibiotic prescribing relative to CRP concentrations was provided. No significant effect was found on patient satisfaction, clinical recovery, follow-up visits, further testing, or hospital admission. These results were supported by a 2022 Cochrane systematic review update, which found that POCT of CRP likely reduces antibiotic prescribing for respiratory tract infections (RTIs) in children, from 51% to 37%. The authors recommend additional research on children, including establishing CRP cutoff values for withholding antibiotics and validating CRP decision algorithms. Two recent UK-based cluster-randomised controlled trials showed no evidence that multifaceted interventions could reduce antibiotic prescribing rates for children with RTIs presenting to primary care. However, these interventions were not first externally validated. Qualitative research revealed that interventions aimed at reducing unnecessary antibiotic prescriptions for children with RTIs should focus on boosting clinicians' confidence in the safety of withholding prescriptions. Likewise, interventions to decrease consultations for RTIs should work on enhancing parents' confidence in their ability to discern between self-limiting illnesses and those that might require medical management, treatment, or both.

Added value of this study

By addressing these issues, the ARON trial showed that a multifaceted clinical decision tool consisting of a validated decision tree, guided POCT of CRP, and safety-netting advice can safely reduce antibiotic prescribing for acutely ill children in primary care. Importantly, this reduction in antibiotic prescribing is not associated with worse clinical outcomes in terms of illness duration, additional testing, number of follow-up visits, or antibiotic prescribing after the index consultation.

Implications of all the available evidence

Our findings support dissemination of the ARON trial's multifaceted clinical decision tool, which combines an externally validated decision tree, guided interpretation of CRP testing, and safety-netting advice. Unlike earlier studies that examined CRP testing in isolation, this trial shows that integrating these components can safely reduce inappropriate antibiotic prescribing for children with acute illness without without compromising child safety or recovery.

Simvastatin has been investigated for multiple sclerosis (MS), showing potential for slowing brain atrophy in a phase 2 trial, but a later phase 3 trial indicated it did not slow disability progression in secondary progressive MS (SPMS). While simvastatin did reduce brain tissue loss, it did not provide a clinically significant benefit for disability. Simvastatin's safety profile at an 80mg dose was confirmed, but its lack of efficacy for disability progression in the phase 3 trial means it is not being recommended as a treatment for SPMS.

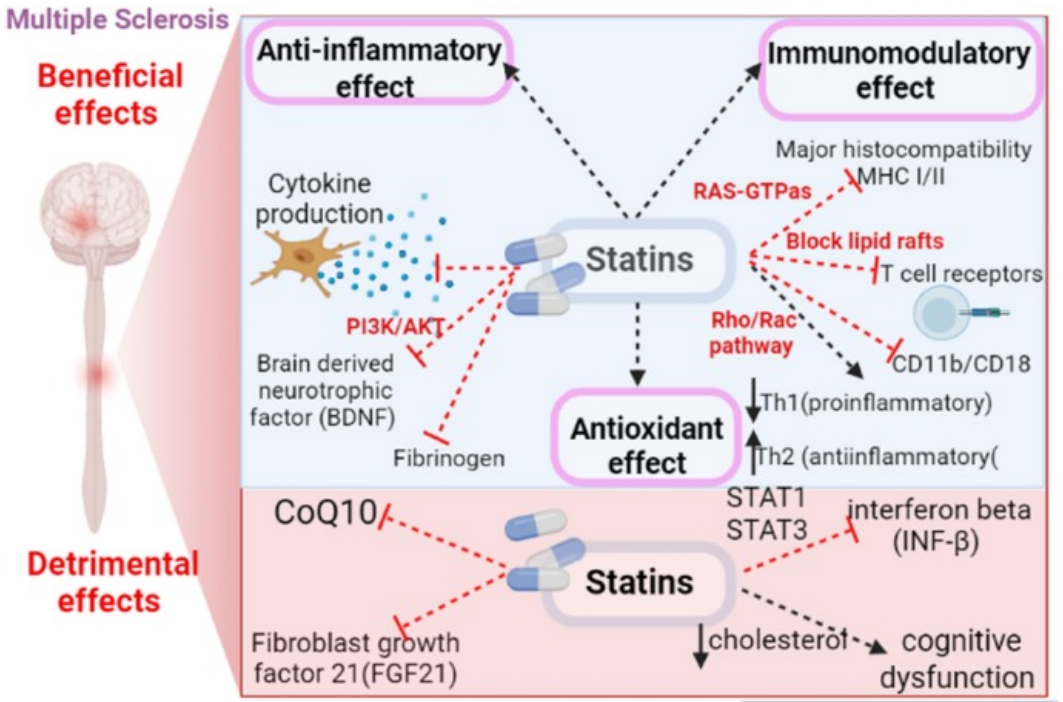

Effect of repurposed simvastatin on disability progression in secondary progressive multiple sclerosis (MS-STAT2): a phase 3, randomised, double-blind, placebo-controlled trial

Summary

Background Despite the success of immune modulation in the treatment of relapsing multiple sclerosis, disability progression is a major problem driven by multiple mechanisms. Comorbidities (eg, vascular risk) and ageing are thought to augment these neurodegenerative pathologies. In the phase 2b MS-STAT trial of simvastatin (80 mg) versus placebo in secondary progressive multiple sclerosis (SPMS), the adjusted difference in brain atrophy rate between groups was –0·254% per year: a 43% reduction. In this phase 3 MS-STAT2 trial, we aimed to assess the efficacy of simvastatin versus placebo in slowing the progression of disability in SPMS.

Methods This phase 3, randomised, double-blind, parallel group, placebo-controlled clinical trial was conducted at 31 neuroscience centres and district general hospitals in the UK. Participants aged 18–65 years with a diagnosis of SPMS and an Expanded Disability Status Scale (EDSS) of between 4·0 and 6·5 were eligible and randomly assigned (1:1) to oral simvastatin (80 mg) or matched placebo for up to 4·5 years, based on a minimisation algorithm within an independent and secure online randomisation service. All participants, site investigators, and the trial coordinating team were masked to treatment allocation. The primary outcome was time to 6-month EDSS confirmed disability progression (an increase of at least 1 point if EDSS score at baseline visit was less than 6·0 or an increase of 0·5 point if EDSS score at baseline visit was 6·0 or more) assessed in all randomly assigned participants (intention-to-treat analysis) without imputation. This study is registered with ClinicalTrials.gov (NCT03387670) and is on the ISRCTN registry (ISRCTN82598726). The study is completed.

Findings Between May 10, 2018, and July 26, 2024, 1079 patients were screened for eligibility and 964 participants were randomly assigned, with 482 (50%) in the placebo group and 482 (50%) in the simvastatin group. Of all 964 participants, 704 (73%) were female and 260 (27%) were male, with a mean age of 54 years (SD 7). 173 (36%) of 482 participants in the placebo group and 192 (40%) of 482 participants in the simvastatin group had 6-month confirmed disability progression (adjusted hazard ratio 1·13 [95% CI 0·91 to 1·39], p=0·26). Although no emergent safety issues were seen, there was one serious adverse reaction (rhabdomyolysis) in the simvastatin group. 12 (2%) of 482 participants in the placebo group and five (1%) of 482 participants in the simvastatin group had a cardiovascular serious adverse event.

Interpretation The MS-STAT2 trial did not show a treatment effect of simvastatin in slowing disability progression in SPMS. Simvastatin use in multiple sclerosis should be confined to existing vascular indications.

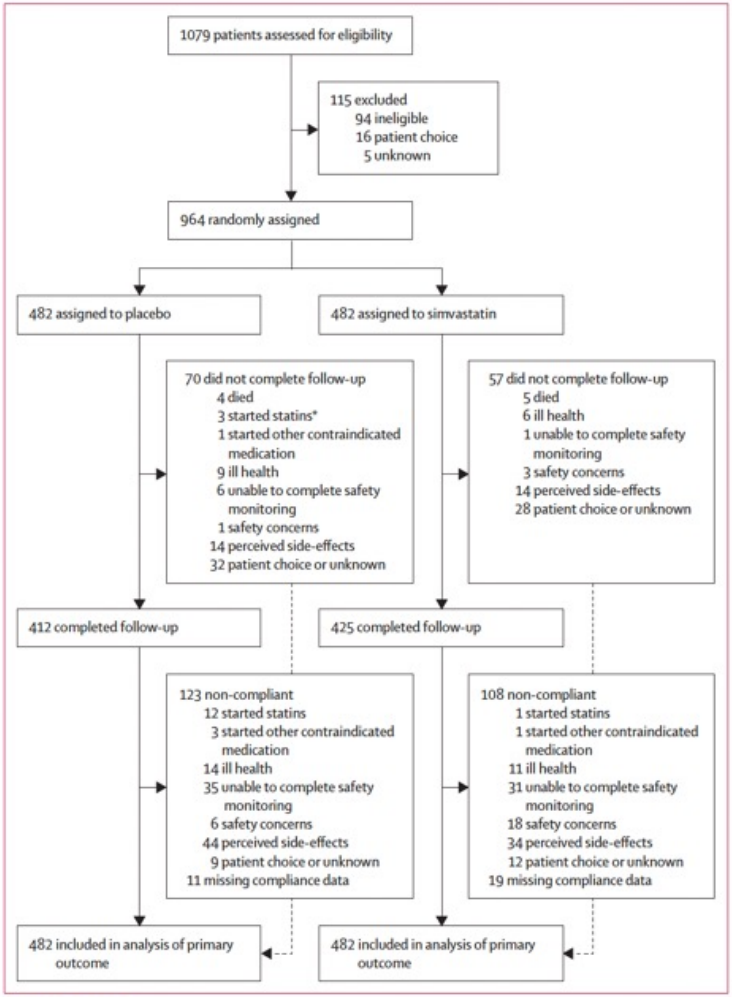

Figure 1: **Trial profile**
Compliance assessed over the first 3 years of follow-up, or until date of confirmed progression, death, or withdrawal if these happened before 3 years. *Of the three participants who withdrew from the placebo group due to starting statins, one participant was also counted as non-compliant as they had already discontinued the trial medication.

	Placebo (n=482)	Simvastatin (n=482)
Age (years)	54·4 (6·8)	54·2 (6·8)
Sex		
Female	351 (73%)	353 (73%)
Male	131 (27%)	129 (27%)
Ethnic origin		
White	466 (97%)	463 (96%)
Asian or Asian British	9 (2%)	12 (2%)
Black or Black British	3 (1%)	1 (<1%)
Mixed	3 (1%)	6 (1%)
Unknown	1 (<1%)	0
Multiple sclerosis duration (years)	23·4 (9·3)	22·3 (9·4)
Secondary progressive multiple sclerosis duration (years)	7·2 (5·0)	7·0 (4·7)
Relapse in past 12 months	24 (5%)	25 (5%)
Total cholesterol (mmol/L)	5·4 (1·1), n=478	5·4 (1·1), n=479
Expanded Disability Status Scale step score		
4–5·5	135 (28%)	140 (29%)
6	177 (37%)	177 (37%)
6·5	170 (35%)	165 (34%)
Timed 25-foot walk speed (feet per s)	2·2 (1·2), n=476	2·2 (1·2), n=477
9-hole peg test speed ($s^{-1} \times 100$)	3·4 (1·0)	3·3 (1·0)
Symbol Digit Modalities Test Z score ≤–1·5	253/470 (54%)	270/474 (57%)
California Verbal Learning Test-II Z score ≤–1·5	176/470 (37%)	171/473 (36%)
Brief Visuospatial Memory Test-Revised Z score ≤–1·5	57/458 (12%)	55/470 (12%)
SLCVA 100% contrast (out of 60)	51·1 (10·4), n=468	51·3 (10·1), n=472
SLCVA 2·5% contrast (out of 60)	25·9 (13·2), n=465	26·3 (13·0), n=463
SLCVA 1·25% contrast (out of 60)	13·7 (12·2), n=457	13·7 (12·1), n=458
MSIS-29 version 2 physical (out of 100)	54·6 (19·2), n=458	54·3 (19·4), n=469
MSIS-29 version 2 psychological (out of 100)	40·2 (22·5), n=476	38·4 (21·6), n=477
Multiple Sclerosis Walking Scale-12 version 2 (out of 100)	66·7 (18·4), n=455	67·9 (18·0), n=458
Modified Fatigue Impact Scale 21 (out of 100)	57·0 (19·5), n=440	57·5 (19·2), n=444
Chalder Fatigue Questionnaire (out of 100)	52·3 (19·0), n=477	52·8 (18·6), n=475
On siponimod treatment	0	1 (<1%)

Data are mean (SD), n (%), or n/N (%). Patient numbers are shown if group size was less than 482. SLCVA=Sloan low contrast visual acuity. MSIS=Multiple Sclerosis Impact Scale.

Table 1: **Baseline characteristics of the intention-to-treat population**

	Placebo	Simvastatin	Hazard ratio (95% CI)	Odds ratio (95% CI)	p value
Primary analysis, confirmed disability progression on EDSS	173/482 (36%)	192/482 (40%)	1·13 (0·91–1·39)	..	0·26
Sensitivity analysis, unconfirmed events	210/482 (44%)	227/482 (47%)	1·10 (0·91–1·33)	..	0·32
Sensitivity analysis, COVID-19*	98/300 (33%)	105/315 (33%)	..	1·03 (0·73–1·45)	0·85
Per-protocol analysis, high dose	125/316 (40%)	139/330 (42%)	1·12 (0·87–1·43)	..	0·38
Per-protocol analysis, high or low dose	129/331 (39%)	145/350 (41%)	1·12 (0·88–1·42)	..	0·37

Data are n/N (%), unless otherwise specified. Sensitivity analysis for unconfirmed events includes both confirmed progression and unconfirmed progression, in which the participant ended follow-up before the event could be confirmed (ie, not known whether initial progression event was confirmed or not). Sensitivity analysis for COVID-19 examined unconfirmed EDSS progression between baseline and the 3-year visit in participants who had EDSS assessed at an in-person baseline visit before March 16, 2020, and at an in-person 3-year visit after July 19, 2021 (ie, during time periods when COVID-19 related public health restrictions were not in force; appendix pp 110–13). EDSS=Expanded Disability Status Scale. *Odds ratio and its 95% CI are given for this analysis.

Table 2: **Effect of simvastatin treatment on the primary outcome, confirmed disability progression on EDSS, and sensitivity and per-protocol analyses**

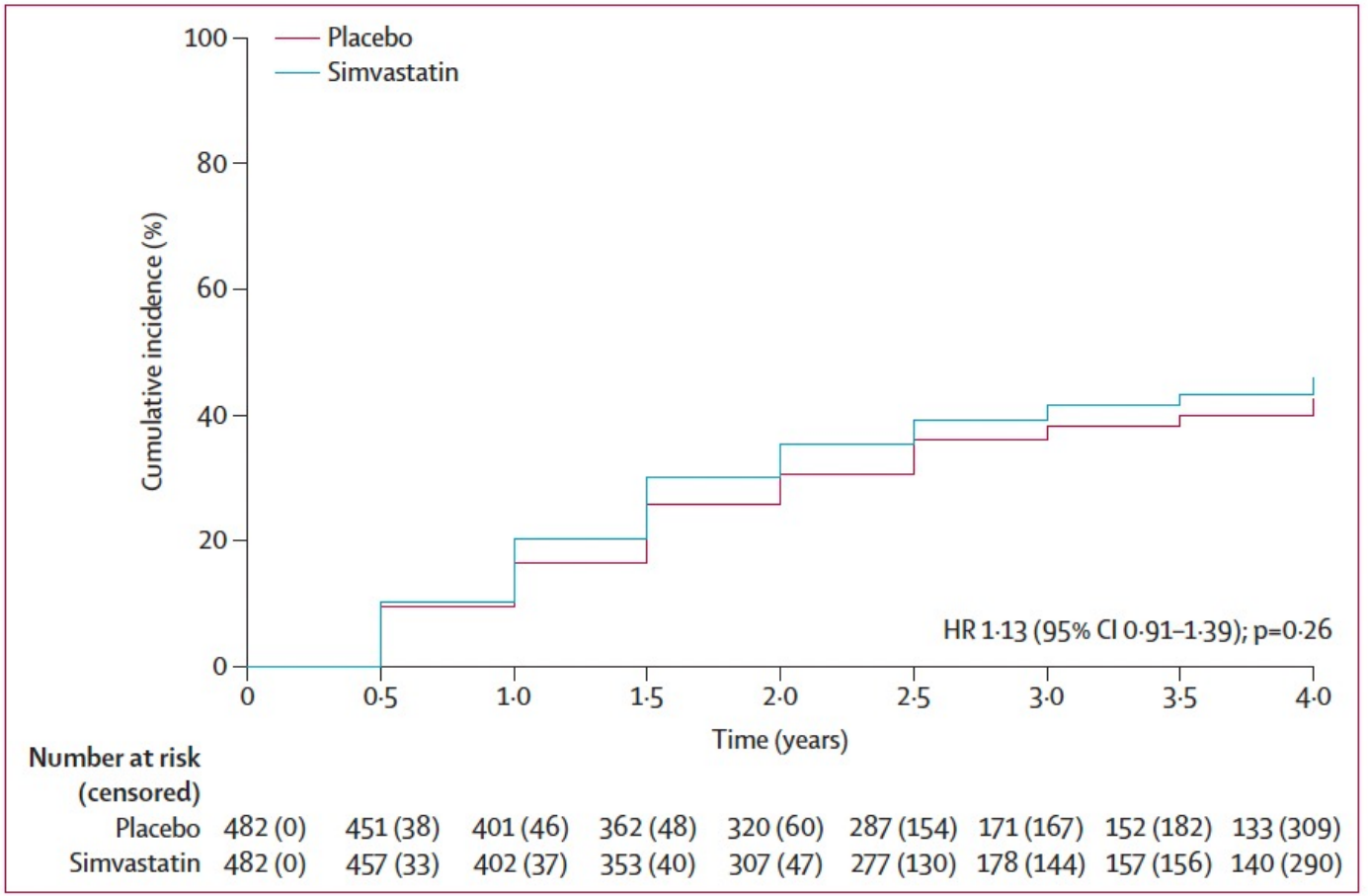

Figure 2: **Kaplan–Meier estimate of cumulative proportion with confirmed EDSS progression in each treatment group**

EDSS=Expanded Disability Status Scale. HR=hazard ratio.

	Placebo	Simvastatin	Adjusted odds ratio (95% CI)	Adjusted mean difference (95% CI)	Adjusted incidence rate ratio (95% CI)	p value
Multicomponent disability progression	242/442 (55%)	261/446 (59%)	1·17 (0·89 to 1·53)	..	..	0·26
Expanded Disability Status Scale	150/442 (34%)	166/446 (37%)	1·15 (0·87 to 1·52)	..	..	0·34
T25FW	145/442 (33%)	158/446 (35%)	1·14 (0·85 to 1·52)	..	..	0·39
9HPT	32/442 (7%)	51/446 (11%)	1·68 (1·05 to 2·69)	..	..	0·031
Modified Rankin Scale	148/393 (38%)	165/413 (40%)	1·10 (0·82 to 1·47)	..	..	0·53
MSFC						
Z score	−0·3 (1·2), n=383	−0·3 (1·2), n=402	..	0·02 (−0·09 to 0·14)	..	*
T25FW (feet per s)	1·9 (1·3), n=373	1·9 (1·2), n=389	..	−0·01 (−0·12 to 0·10)	..	0·88
9HPT (s^{-1} × 100)	3·3 (1·1), n=383	3·3 (1·1), n=401	..	0·03 (−0·05 to 0·12)	..	0·48
Symbol Digit Modalities Test score (out of 110)	43·8 (13·7), n=377	43·3 (13·9), n=397	..	−0·10 (−1·25 to 1·06)	..	0·87
SLCVA (out of 60)						
100% contrast	50·0 (10·7), n=369	50·5 (9·5), n=389	..	0·08 (−1·01 to 1·16)	..	*
2·5% contrast	24·5 (12·2), n=366	25·6 (12·6), n=388	..	0·59 (−0·79 to 1·81)	..	*
1·25% contrast	12·8 (11·1), n=362	12·7 (11·8), n=376	..	−0·49 (−1·80 to 0·76)	..	*
Brief International Cognitive Assessment for Multiple Sclerosis						
California Verbal Learning Test-II score (out of 80)	47·0 (13·3), n=378	46·8 (13·0), n=399	..	−0·04 (−1·32 to 1·24)	..	0·95
Brief Visuospatial Memory Test-Revised score (out of 36)	20·3 (9·3), n=366	20·2 (8·7). N=386	..	0·27 (−0·67 to 1·22)	..	0·57
Multiple Sclerosis Impact Scale-29 version 2 (out of 100)						
Total score	50·5 (20·4), n=387	51·1 (19·7), n=397	..	1·57 (−0·55 to 3·68)	..	0·15
Physical score	55·3 (21·3), n=389	56·8 (21·2), n=401	..	1·97 (−0·28 to 4·22)	..	0·085
Psychological score	39·8 (23·8), n=405	39·1 (22·8), n=411	..	0·88 (−1·57 to 3·32)	..	0·48
MSWS version 2 (out of 100)	69·0 (20·9), n=386	68·3 (21·0), n=394	..	−1·38 (−3·61 to 0·74)	..	*
Modified Fatigue Impact Scale 21 (out of 100)	54·7 (21·7), n=377	56·2 (20·9), n=391	..	0·96 (−1·31 to 3·23)	..	0·41
Chalder Fatigue Questionnaire (out of 100)	49·0 (18·1), n=398	50·4 (18·2), n=403	..	1·22 (−1·04 to 3·48)	..	0·29
Relapse rate per person-year	68/1348 (0·05), n=482	98/1362 (0·07), n=482	..	..	1·43 (1·01 to 2·01)	0·044

Data are n/N (%), mean (SD), or number of relapses/person-years (incidence rate per person-year), unless otherwise stated. Patient numbers are shown if group size was less than 482. Adjusted mean difference is shown for simvastatin relative to placebo. For the following outcomes a positive mean difference favours simvastatin: MSFC, SLCVA, and Brief International Cognitive Assessment for Multiple Sclerosis. For the following outcomes a negative mean difference favours simvastatin: Multiple Sclerosis Impact Scale-29 version 2, MSWS version 2, Modified Fatigue Impact Scale 21, Chalder Fatigue Questionnaire. T25FW=timed 25 foot walk. 9HPT=9-hole peg test. MSFC=Multiple Sclerosis Functional Composite. SLCVA=Sloan Low Contrast Visual Acuity. MSWS=Multiple Sclerosis Walking Scale 12. *Plots of the residuals from the model for MSFC Z score, SLCVA at all three contrast percentages, and MSWS version 2 showed marked departures from normality. Therefore, bias corrected and accelerated bootstrap 95% CIs based on 2000 replications were used for inference. p values are therefore not generated for these models, but can be inferred from the 95% CIs.

Table 3: Effect of simvastatin treatment on the secondary outcomes

	Placebo (n=482)					Simvastatin (n=482)				
	Serious adverse events	Notifiable adverse events	Adverse events (non-serious)	Serious adverse reactions	Adverse reactions (non-serious)	Serious adverse events	Notifiable adverse events	Adverse events (non-serious)	Serious adverse reactions	Adverse reactions (non-serious)
Total events (events per 100 participants)	176 (36·5)	9 (1·9)	1868 (387·6)	0 (0·0)	157 (32·6)	158 (32·8)	13 (2·7)	1965 (407·7)	1 (0·2)	167 (34·6)
Participants with one or more event	112 (23%)	8 (2%)	412 (85%)	0	100 (21%)	114 (24%)	12 (2%)	420 (87%)	1 (<1%)	97 (20%)
One event	79 (16%)	7 (1%)	65 (13%)	0	63 (13%)	80 (17%)	11 (2%)	60 (12%)	1 (<1%)	56 (12%)
Two events	18 (4%)	1 (<1%)	79 (16%)	0	23 (5%)	25 (5%)	1 (<1%)	66 (14%)	0	23 (5%)
Three events	8 (2%)	0	68 (14%)	0	9 (2%)	8 (2%)	0	75 (16%)	0	9 (2%)
Four events	3 (1%)	0	43 (9%)	0	4 (1%)	1 (<1%)	0	59 (12%)	0	7 (1%)
Five events	1 (<1%)	0	32 (7%)	0	1 (<1%)	0	0	36 (7%)	0	2 (<1%)
Six events	1 (<1%)	0	41 (9%)	0	0	0	0	29 (6%)	0	0
Seven events	2 (<1%)	0	19 (4%)	0	0	0	0	20 (4%)	0	0
Eight events	0	0	18 (4%)	0	0	0	0	25 (5%)	0	0
Nine events	0	0	14 (3%)	0	0	0	0	11 (2%)	0	0
Ten events	0	0	6 (1%)	0	0	0	0	15 (3%)	0	0
11 events	0	0	6 (1%)	0	0	0	0	4 (1%)	0	0
12 events	0	0	5 (1%)	0	0	0	0	3 (1%)	0	0
13 events	0	0	3 (1%)	0	0	0	0	2 (<1%)	0	0
14 events	0	0	3 (1%)	0	0	0	0	2 (<1%)	0	0
15 or more events	0	0	10 (2%)	0	0	0	0	13 (3%)	0	0

Data are n (n per 100 participants) or n (%).

Table 4: **Adverse events by treatment group**

Research in context

Evidence before this study

When we published the phase 2b MS-STAT trial, we searched for studies in MEDLINE (from Jan 1, 1946), Embase (from Jan 1, 1974), PubMed (from Jan 1, 1996), Cochrane Database of Systematic Reviews (CDSR; from Jan 1, 1995), CENTRAL (from Jan 1, 1996), DARE (from Jan 1, 1994), and the Health Technology Assessment Database (from Jan 1, 1996) to April 8, 2013, using the keywords "multiple sclerosis" AND "statins". We included trials, observational studies, and laboratory studies in humans and animals. The book of abstracts from the meetings of the European Committee for Treatment and Research in Multiple Sclerosis for the previous 8 years was also searched (2005 to 2012). The resulting papers were examined manually. Seven randomised controlled trials were identified: one in clinically isolated syndrome (n=81), one in optic neuritis (n=64), and five in relapsing-remitting multiple sclerosis, these with statins as a randomised add-on to β-interferon (n=540; 392 assigned simvastatin and 148 assigned atorvastatin). Overall, these studies did not demonstrate a consistent benefit of statins. The phase 2b MS-STAT trial found that simvastatin reduced whole brain atrophy rate in people with secondary progressive multiple sclerosis (SPMS) and had a positive impact on some secondary disability outcomes. Our search did not identify any other trials of statins in SPMS. We updated this search in MEDLINE, Embase, PubMed, CDSR, CENTRAL, Epistemonikos, ClinicalTrials.gov, and the International Clinical Trials Registry Platform from April 8, 2013, to March 11, 2025. Two further trials in relapsing-remitting multiple sclerosis were identified, both with atorvastatin added to β-interferon (n=249), neither of which showed benefit on the primary outcome. No further trials in SPMS (or other multiple sclerosis classifications) were reported. The searches were not limited to the English language.

Added value of this study

In contrast to the previous phase 2b study, this large phase 3 randomised controlled trial did not show any evidence that simvastatin slows disability progression in SPMS. The study design was robust with appropriate performance characteristics.

Implications of all the available evidence

Combined with the overall absence of efficacy in previous relapsing-remitting cohorts, there is no place for the use of simvastatin (and probably all statins) as a disease-modifying treatment in multiple sclerosis. Statins continue to have a crucial role in primary and secondary vascular protection.

The EAT–*Lancet* Commission on healthy, sustainable, and just food systems

Key messages

- Food systems sit at the nexus of health, environment, climate, and justice. A food systems transformation is fundamental for solving crises related to the climate, biodiversity, health, and justice. The central position of food systems emphasises the interdependent nature of these crises, rather than each crisis separately, which highlights the need to position food systems change as a global integrator across economic, governance, and policy domains.
- The updated planetary health diet (PHD) has an appropriate energy intake; a diversity of whole or minimally processed foods that are mostly plant sourced; fats that are primarily unsaturated, with no partially hydrogenated oils; and small amounts of added sugars and salt. The diet allows flexibility and is compatible with many foods, cultures, dietary patterns, traditions, and individual preferences. The PHD also provides nutritional adequacy and diminishes the risks of non-communicable diseases. At present, all national diets deviate substantially from the PHD, but a shift to this pattern could avert approximately 15 million deaths per year (27% of total deaths worldwide). Such a transition would reduce the rates of many specific non-communicable diseases and promote healthy longevity.
- Food drives five planetary boundary transgressions, including land system change, biosphere integrity, freshwater change, biogeochemical flows, and approximately 30% of greenhouse gas emissions driving climate change. How and where food is produced, which foods are produced and consumed, and how much is lost and wasted, all contribute to planetary boundary transgressions. No safe solution to climate and biodiversity crises is possible without a global food systems transformation. Even if a global energy transition away from fossil fuels occurs, food systems will cause the world to breach the Paris Climate agreement of limiting global mean surface temperature to 1·5°C.
- Human rights related to food systems (ie, the rights to food, a healthy environment, and decent work) are not being met, with nearly half the world's population below the social foundations for these rights. Meanwhile, responsibility for planetary boundary transgressions from food systems is not equal: the diets of the richest 30% of the global population contribute to more than 70% of the environmental pressures from food systems. Just 1% of the global population is in a safe and just space. These statistics highlight the large inequalities in the distribution of both benefits and burdens of current food systems. National policies that address inequities in the distribution of benefits and burdens of current food systems would aid in ensuring food-related human rights are met.
- The PHD needs to be available, affordable, convenient, aspirational, appealing, and delicious. To increase demand for healthy sustainable diets and enable necessary dietary shifts, food environment interventions, next-generation culinary research and development, increased purchasing power, and protection and promotion of healthy traditional diets are important actions.
- A food systems transformation following recommendations from the EAT-*Lancet* Commission—which include a shift to healthy diets, improved and increased agricultural productivity, and reduced food loss and waste—would substantially reduce environmental pressures on climate, biodiversity, water, and pollution. However, no single action is sufficient to ensure a healthy, just, and sustainable food system. Comparing 2050 values with the current state (as of 2020), a shift to healthy diets in isolation could lead to a 15% reduction in agricultural emissions, compared with a 20% reduction when all three actions are implemented simultaneously with improvements in productivity and food loss and waste. Individually, all three actions modestly reduce future nitrogen and phosphorous use (ie, a 27–34% increase by 2050 with individual actions vs a 41% increase under the business-as-usual scenario); however, in combination they substantially reduce future growth in nitrogen and phosphorous use (ie, a 15% increase compared with 2020 levels of use).
- Additional environmental benefits are accrued through sustainable and ecological intensification practices. Unprecedented investments and effort in these practices could potentially result in a net-zero food system. A diversity of context-specific practices can sequester additional carbon biomass, create and connect habitats, reduce nutrient applications, and increase the interception and capture of excessive crop fertiliser before it pollutes groundwater and surface water systems. These practices can be enabled by securing equitable access to land and water resources, strengthening public advisory services, addressing structural imbalances between producers and dominant agribusinesses, and through public and private sector investments that support farmers shifting towards sustainable practices.
- A food systems transformation following recommendations from the EAT-*Lancet* Commission could lead to a less resource-intensive and labour-intensive food system that can supply a healthy diet for 9·6 billion people, with modest impacts on average food costs. However, such a transformation would have profound implications for what, how, and where food is produced, and for people involved in these processes. For example, as a part of this restructuring, some sectors would need to contract (eg, a 33% reduction in ruminant meat production) and others would need to expand (eg, a 63% increase in fruit, vegetable, and nut production) compared with 2020 production levels.

(Continues on next page)

(Key messages continued from previous page)

- Justice is needed to unlock and accelerate action for transformation. A fair distribution of opportunities and resources—such that the rights to food, a healthy environment, and decent work are met, and distribution of the responsibility to produce, distribute, and consume healthy diets within planetary boundaries is fair—are the basis of a successful food systems transformation. Power asymmetries and discriminatory social and political structures prevent these rights from being met, which results in harms to people's health, precarious livelihoods for food systems workers, and lack of voice, undermining freedom, agency, and dignity. Ensuring liveable wages and collective bargaining, while regulating and limiting market concentration and improving transparency, accountability, representation, and access to information, are all impactful actions. We emphasise the protection of basic human rights in conflict areas as a fundamental foundation of justice.
- Unprecedented levels of action are required to shift diets, improve production, and enhance justice. A just transformation requires building coalitions with actors from inside and outside the food system, identifying bundles of actions, developing national and regional roadmaps for implementation, unlocking finance for the transformation, and rapidly putting joint plans into action. Such efforts should closely align with other sustainability and health initiatives (eg, the Paris Agreement, Kunming–Montreal Global Biodiversity Framework, and nation-specific food-based dietary guidelines). These frameworks have all identified food systems actions as powerful, particularly in their capacity to integrate across goals. Mobilising and repurposing finance is essential for enabling this transformation.

Conclusions: accelerating meaningful action

This Commission calls for an urgent, comprehensive approach to food systems transformation, centred on the development of context-specific roadmaps that provide viable, evidence-based solution sets. Such roadmaps should focus on bundling actions, setting science-based targets, building inclusive coalitions, establishing and building on already existing monitoring and accountability mechanisms, and mobilising financial resources at scale. At the core of our Commission's framework are three foundational elements: (1) recommended food group intake values for the PHD to advance human health; (2) food system boundaries to achieve environmental sustainability; and (3) social foundations to guide the creation of just food systems. These values, boundaries, and foundations can guide target setting and collective action, and are adaptable across geographies and sectors.

Seeking ghosts

A Japanese botanist is revealing the secrets of plants that have given up photosynthesis

Suetsugu has become one of the world's preeminent authorities on these unusual symbiotic plants, called mycoheterotrophs. Combining dogged fieldwork with old-school taxonomic studies and modern molecular technologies, he has produced some 250 papers since 2008 that have shed new light on these plants, tiny forest floor dwellers that typically bloom for just a few days once a year. His studies have overturned conventional ideas about how mycoheterotrophic plants pollinate and reproduce. He's also helped describe 30 previously unrecognized species found in Japan and overseas. **IN ESSENCE**, mycoheterotrophic plants are thieves. Found in forests worldwide, they entwine their roots with the threadlike hyphae of soil fungi. These fungi acquire carbon from trees and shrubs while providing nutrients in a mutually beneficial exchange. The mycoheterotrophs then steal some of that carbon from the fungi, instead of relying on sunlight and chlorophyll to power photosynthesis.

More than 33,000 plant species—including certain clubmosses, ferns, liverworts, and all orchids—are known to be initially mycoheterotrophic during germination and early development. Botanists have also identified about 600 species, nearly half of which are orchids, that have fully abandoned photosynthesis and depend on fungi throughout their lives. (An unknown number of species are partially mycoheterotrophic, drawing carbon from both photosynthesis and fungi, and may represent a transitional stage toward full mycoheterotrophy.)

Evolutionary biologists have found evidence that full mycoheterotrophy has evolved independently more than 40 times. The strategy could be an adaption to surviving in dense forests where light is scarce. But how mycoheterotrophy arises and persists is still a mystery—in part because the plants can be elusive. In Japan, Suetsugu says, “There has been very little research done on mycoheterotrophic plants.” Ollerton says the same is true elsewhere in the world.

Suetsugu set out to fill that gap during his undergraduate and graduate studies at Kyoto University. A year after completing his Ph.D. in 2014, he joined Kobe University, becoming a full professor in 2022 at age 34. (He is still the youngest full professor on the university's Faculty of Science.) Today, Suetsugu's prodigious scientific output on mycoheterorophs makes him "the most productive author in the field of botany and pollination ecology," says Zong-Xin Ren, a botanist and a pollination ecologist at the Chinese Academy of Sciences's Kunming Institute of Botany.

In conversation, Suetsugu is reserved and chooses his words carefully, although he is prone to chuckle over amusing or philosophical questions. He is most at home in the field, where his "explorational" approach has enabled him to "discover things previously unknown," says Vincent Merckx, a botanist at the Naturalis Biodiversity Center.

Could a group of strangers go a month without their smartphones? Could I?

A little less than 20 years after Steve Jobs stepped onto a San Francisco stage to introduce the iPhone, the near-ubiquitous device and others like it are claiming 4½ hours of the average American's day. Over an average lifespan, that's more than 14 years — 14 years! — a number so jaw-dropping I thought I did the math wrong the first time. Plenty of studies have shown that this is too much, that round-the-clock social media access is leaving us anxious, depressed and divided. Lately a wave of resistance has been building, with the spread of phone bans in schools, the embrace of "dumbphones" (a word Merriam Webster just officially added to the dictionary) and the rise of anti-tech activists like ex-influencer August Lamm, who made a pamphlet on practicalities "for anyone who's ever wanted to throw their phone into the sea." Her social media post about it, ironically, went viral.

Everyone had their own reason for being there. Rock Harper, an unassuming celebrity chef, missed the days when people were truly present at local go-gos and sang along with all the songs. Johanna Bockman, a sociology professor, wanted to break a Facebook habit she found embarrassing. Lydia Peabody, a mental health therapist, reached for her phone when she was frustrated or stalling or having a bad day; she worried she was numbing herself. And Ali Tintera, a performance analyst for Metro and self-described chronic podcast listener, had realized something that seemed to get to the heart of it: "Since 2020, I have not heard the birds."